JASON

Technical Report
JSR-79-01

February 1980

FREE ELECTRON LASERS WITH VARIABLE PARAMETER WIGGLERS

By: N. M. Kroll
P. Morton
M. N. Rosenbluth

SRI International
1611 North Kent Street
Arlington, Virginia 22209

JASON

Technical Report
JSR-79-01

February 1980

FREE ELECTRON LASERS WITH VARIABLE PARAMETER WIGGLERS

By: Norman M. Kroll
Philip Morton
Marshall N. Rosenbluth

SRI International
1611 North Kent Street
Arlington, Virginia 22209

UNCLASSIFIED

SECURITY CLASSIFICATION OF THIS PAGE (When Data Entered)

(14)

REPORT DOCUMENTATION PAGE

READ INSTRUCTIONS BEFORE COMPLETING FORM

1. REPORT NUMBER	2. GOVT ACCESSION NO.	3. RECIPIENT'S CATALOG NUMBER
SRI-JSR-79-01	AD-A084 323	

4. TITLE (and Subtitle)

(6) Free Electron Lasers with Variable Parameter Wigglers.

5. TYPE OF REPORT & PERIOD COVERED

(9) Technical Report.

6. PERFORMING ORG. REPORT NUMBER

JSR-79-01

7. AUTHOR(s)

(10) Norman M. Kroll
Philip Morton
Marshall N. Rosenbluth

8. CONTRACT OR GRANT NUMBER(s)

(15) MDA903-78-C-0086
ARPA Order 2504

9. PERFORMING ORGANIZATION NAME AND ADDRESS

SRI International
1611 North Kent Street
Arlington, VA 22209

10. PROGRAM ELEMENT, PROJECT, TASK AREA & WORK UNIT NUMBERS

A. O. 2504, 27 & 28

11. CONTROLLING OFFICE NAME AND ADDRESS

Defense Advanced Research Projects Agency
1400 Wilson Boulevard
Arlington, VA 22209

12. REPORT DATE: August 1979

13. NO. OF PAGES: 170

14. MONITORING AGENCY NAME & ADDRESS (if diff. from Controlling Office)

(11) Feb 80

15. SECURITY CLASS. (of this report)

UNCLASSIFIED

15a. DECLASSIFICATION/DOWNGRADING SCHEDULE

16. DISTRIBUTION STATEMENT (of this report)

Cleared for open publication, distribution unlimited.

(12) 172

17. DISTRIBUTION STATEMENT (disclaimer) The views and conclusions contained in this document are those of the authors and should not be interpreted as necessarily representing the official policies, either expressed or implied, of the Advanced Research Projects Agency or the U.S. Government.

18. SUPPLEMENTARY NOTES

19. KEY WORDS (Continue on reverse side if necessary and identify by block number)

Free Electron Lasers
Ubitron
Wiggler
Phase Area Desplacement
Raman Instability

20. ABSTRACT (Continue on reverse side if necessary and identify by block number)

A general discussion of free electron lasers with variable parameter wigglers is presented with a view towards their potential for the production of high power optical radiation at reasonable efficiency. The theoretical analysis is based upon a one dimensional relativistic Hamiltonian formulation and is developed in a manner to take advantage of the analogy between the free electron laser process and radio frequency accelerators. Three promising operational modes are identified and analyzed. The first may be thought of as an electron decelerator and is thought to have the most promise for single pass devices. Both oscillator and amplifier con-

DD FORM 1 JAN 73 1473

EDITION OF 1 NOV 65 IS OBSOLETE

UNCLASSIFIED

SECURITY CLASSIFICATION OF THIS PAGE (When Data Entered)

389941

19. KEY WORDS (Continued)

20 ABSTRACT (Continued)

figurations are studied. The second is based upon adiabatic trapping and detrapping, intended to reduce the spread in electron energy typically induced by the FEL process. The third is based upon the method of phase area displacement. It has the advantage of wide gain bandwidth and small induced energy spread, and is thought to have the most promise for storage ring applications. Generally speaking, it is found that high peak power is intrinsic to these modes of operation. Potential problems from parasitic oscillations analogous to the stimulated Raman effect are analyzed, and some others arising from transverse inhomogeneity are identified.

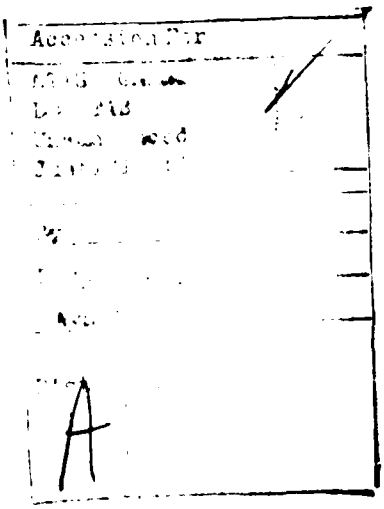

CONTENTS

LIST OF FIGURES

LIST OF FIGURES (Continued)

ABSTRACT

A general discussion of free electron lasers with variable parameter wigglers is presented with a view towards their potential for the production of high power optical radiation at reasonable efficiency. The theoretical analysis is based upon a one dimensional relativistic Hamiltonian formulation and is developed in a manner to take advantage of the analogy between the free electron laser process and radio frequency accelerators. Three promising operational modes are identified and analyzed. The first may be thought of as an electron decelerator and is thought to have the most promise for single pass devices. Both oscillator and amplifier configurations are studied. The second is based upon adiabatic trapping and detrapping, intended to reduce the spread in electron energy typically induced by the FEL process. The third is based upon the method of phase area displacement. It has the advantage of wide gain bandwidth and small induced energy spread, and is thought to have the most promise for storage ring applications. Generally speaking, it is found that high peak power is intrinsic to these modes of operation. Potential problems from parasitic oscillations analogous to the stimulated Raman effect are analyzed, and some others arising from transverse inhomogeneity are identified.

1.0 INTRODUCTION

The recent successful operation of the "free electron laser" by the group at Stanford and the availability of high power electron beams has stimulated a great deal of interest in the use of the "free electron laser" (FEL) to produce a high power tunable laser beam.[1] When an electron travels through a periodic transverse magnetic field, the electron is given a transverse velocity which allows it to either receive or give energy to the transverse electric field of a plane electromagnetic wave. If the longitudinal velocity of the electron is such that the electron slips behind the radiation wave by one radiation wave length while traveling a distance of one magnetic field period, the transverse velocity of the electron remains in phase with the electric field of the radiation. Such electrons will continue to have their energy increased or decreased, depending on their phase relative to the radiation field. Phillips investigated such a device, called the Ubitron, and used it to produce microwaves.[2] The FEL experiment by the Stanford group[3] used a helical wiggler magnet with a constant magnetic field and periodicity and produced optical radiation in a similar manner as the Ubitron. Most of the analysis of the FEL, as well as the methods envisioned for FEL operation, started with the assumption that the magnetic field and period of the wiggler are constant.[4,5] A brief review of the properties and limitations of such a device is presented in Section 3 of this paper.

The maximum fractional energy that can be extracted from a constant parameter FEL is equal to 1/2N where N is the number of wiggler periods while the resulting energy spread beam of the electrons emerging from the FEL is comparable to or greater than the mean energy loss. This places severe limitations on the overall gain, efficiency, and modes of operation for the constant parameter FEL. While there are many schemes to overcome some of the limitations of the constant parameter FEL, such as the use of transverse gradients in the magnetic field of the wiggler[6] and the coupling of the FEL with an isochronous storage ring,[7] the use of a variable parameter wiggler may be an even more attractive method to remove these limitations.

It is the purpose of this paper to discuss the operation of a variable parameter FEL and to illustrate many of the possible operational modes that may be used to overcome these limitations of the constant parameter FEL. For the case where the wiggler parameters such as magnetic field and wavelength are variable, the possible operating modes envisioned for an FEL are considerably different than those for a constant parameter wiggler; for example, it becomes possible to extract a reasonable fraction of the electron's energy with an emerging energy spread a great deal less than the mean energy loss. The method of describing the electrons' motion in this paper is similar to the treatment used by the accelerator physicist in describing the motion of charged particles in a radio frequency accelerating system.[8,9] We assume from the beginning that the magnetic field and period vary along the wiggler and derive the equations of motion for an electron passing through the FEL, from which we can obtain the

energy lost or gained by the electron. The change in the radiation field is taken to be given by the sum of the energies lost by all of the electrons which pass through the FEL.

In Section 2.1 we present the equations that define the energy and relative phase of a resonant or synchronous electron in terms of the wiggler magnetic field, the wiggler period, the optical field, and the optical wave numbers. In Section 2.2 we discuss the motion of the electrons about the synchronous energy, using the Hamiltonian formulation similar to that used in the treatment of charged particle acceleration with radio frequency fields. The summary of the "bucket" or maximum stable phase trajectories for the electrons is presented in Section 2.3. The results of Section 2 are used in Section 3.0 to briefly discuss the well-known properties of the constant parameter wiggler, both as an illustration of the use of the Hamiltonian formulation and to obtain the results in terms of notation of this paper.

In Section 4 the use of a variable parameter wiggler to trap a significant fraction of the electron beam in a decelerating bucket is discussed.[10] The wiggler parameters are varied so as to gradually reduce the resonant energy of the trapped electrons, which results in a value for the transfer of energy from the trapped electrons to the radiation approximately equal to the reduction in the resonant energy. This reduction in the resonant energy can be much larger than the energy that can be transferred in the constant parameter wiggler. The operation of a laser oscillator which utilizes this scheme is discussed in Section 4.1 where the

amplification of the radiation field in passing through the wiggler just compensates for the reflection loss. Amplifier designs for this trapping and deceleration mode of FEL operation are discussed in Section 4.2. While the trapped electrons emerge with an energy spread comparable to that of the constant parameter FEL, the mean energy loss of electrons is an order of magnitude larger than that from the constant parameter FEL.

In Section 5 a method of adiabatically capturing, deceleration, and decapture of the electrons is discussed. The purpose of this scheme is to achieve a small energy spread for the emerging beam while at the same time to obtain a significant reduction of the average electron energy. Such a scheme would be useful if the same electron beam was reaccelerated with an external source and then passed through the FEL again.

The last method of extracting energy from the electrons, discussed in Section 6, is called phase area displacement, and is one in which the initial resonant energy is below the energy of the injected electrons.[11] The wiggler parameters are varied such that the resonant energy is increased to a final value above the energy of the electrons, a process which can result in a decrease in the mean energy of the electrons while producing a rather modest increase in the energy spread of the beam. While the average energy lost by this process for mono-energetic electrons is of the same order as the energy lost from a constant parameter FEL, it has the advantage of being less sensitive to the initial energy spread of the electrons and of producing a lower energy spread in the emerging beam.

There is a possibility of an instability that can arise from the interaction between a radiation signal at a frequency shifted from the main radiation frequency by an amount equal to the oscillation frequency of the electrons in the pondermotive potential well; this instability is investigated in Section 7. The results show that the instability that must build up from noise is probably not important for the amplifier, but in the design of an oscillator some type of damping will probably need to be included.

Some related considerations are presented in the Appendices. Appendix A gives a more general derivation of the Madey Theorem[12] relating small signal energy gain and spread with application to the variable wiggler. Appendix B presents some mathematical details relating to Chapter VI. Appexdix C is concerned with the requirements on e-beam emittance. Appendix D discusses the justification at high γ for neglecting electrostatic effects. Appendix E discusses a different variable wiggler concept, the Klystron,[13] which is related to π-pulse designs,[14] in which one wiggler is used for prebunching and a second for energy extraction.

2.0 EQUATIONS OF MOTION

The equations of motion of an individual electron are determined by a Hamiltonian, $H_o(x, P_x, y, P_y, z, P_z, t)$ which satisfies a modified Hamiltonian variational principle

$$\delta \int_{t_1}^{t_2} (P_x\dot{x} + P_y\dot{y} + P_z\dot{z} - H_o)dt = 0 \tag{2.1}$$

Throughout this derivation we shall assume that the electrostatic interaction between the electrons can be neglected, deferring until later the determination of the circumstances in which this assumption is justified. With this assumption we can write

$$H_o(\underset{\sim}{r}, \underset{\sim}{P}, t) = c\sqrt{m^2c^2 + [\underset{\sim}{P} - (e/c)\,\underset{\sim}{A}(\underset{\sim}{r}, t)]^2} \tag{2.2}$$

where the total energy, E, of the electron is to be identified with the Hamiltonian, i.e. $E = H_o$. We expect many of the various parameters to vary with the longitudinal coordinate z; for this reason it is useful to identify z as the independent variable rather than the time t. We rewrite Eq. (2.1) as

$$\delta \int_{z_1}^{z_2} [P_x x' + P_y y' + (-E)t' - (-P_z)]dz = 0 \tag{2.3}$$

where we define the derivatives with respect to z with a prime, i.e. $x' = dx/dz$, etc.

It is convenient to designate the quantity $(-P_z)$ as a new Hamiltonian H_1 such that

$$H_1(x, P_x, y, P_y, (-E), t, z) = -P_z \tag{2.4}$$

where $(-E)$ plays the role of the momentum conjugate to t and z is the independent variable. The solution of Eq. (2.2) for P_z yields

$$H_1 = -\left\{(E^2/c^2 - m^2c^2) - (P_x - e/c\ A_x)^2 - (P_y - e/c\ A_y)^2\right\}^{1/2} - e/c\ A_z \tag{2.5}$$

For the vector potential we shall write

$$\underset{\sim}{A} = \underset{\sim}{A}_w + \underset{\sim}{A}_s \tag{2.6}$$

where $\underset{\sim}{A}_w$ refers to the vector potential of the wiggler field and $\underset{\sim}{A}_s$ to that of the signal (or optical) field. We assume these potentials to have the special forms

$$\underset{\sim}{A}_w = -A_w(z)\left[\hat{x}\cos\left(\int_0^z k_w(z_1)dz_1\right) + \hat{y}\sin\left(\int_0^z k_w(z_1)dz_1\right)\right] \tag{2.7}$$

$$\underset{\sim}{A}_s = A_s(z)\left[\hat{x}\cos\left(\int_0^z k_s(z_1)dz_1 - \omega_s t\right) - \hat{y}\sin\left(\int_0^z k_s(z_1)dz_1 - \omega_s t\right)\right] \tag{2.8}$$

Equation (2.7) corresponds to a circularly polarized static magnetic field of the sort used in the original Stanford FEL experiments. The assumption of no transverse variation can only be an approximation in practice, but we assume that the electrons are confined to a region in which transverse variation can be neglected. The use of a non static or linearly polarized wiggler field makes no essential difference in the theory, but the assumption of the form (2.7) allows some simplification of the exposition. A_w and k_w are both taken to be z dependent to allow for the use of specialized magnet designs. We assume A_w, k_w, A_s, k_s to be slowly varying in z in the sense that it will generally be permissible to neglect $A_w' = dA_w/dz$ as compared to $k_w A_w$, etc. The signal field has also been chosen to be circularly polarized (in the direction that is driven by the FEL amplification process).

The assumption that $\underset{\sim}{A}$ is independent of the transverse coordinate implies that $P_\perp = P_x\hat{x} + P_y\hat{y}$ is a constant of the motion. We shall, throughout most of this paper, assume this constant to be zero, an assumption which corresponds to the neglect of transverse velocities in the incoming beam before it enters the wiggler. Some aspects of the effect of non zero $P_\perp$ on operation are discussed in Appendix C and applied to a discussion of the relation of the characteristics of realizable electron beams to other design parameters.

Taking account of the above assumptions we find that the equations of motion for the energy and time can be obtained from the following Hamiltonian

$$H_1((-E),\ t,\ z) = -mc\left\{-\mu^2(z) + \gamma^2 + 2a_w a_s \cos\psi(z,\ t)\right\}^{1/2} \qquad (2.9)$$

where we have introduced the dimensionless vector potentials

$a = e\,A/mc^2$, $(mc^2/e = 1706$ gauss-cm $= .511 \times 10^6$ Volts)

$$\mu^2(z) = 1 + a_w^2(z) + a_s^2(z) \quad , \qquad (2.10)$$

$$\psi = \int_0^z (k_w + k_s)dz_1 - \omega_s t \quad \text{and} \qquad (2.11)$$

$$\gamma = E/mc^2 \qquad (2.12)$$

With the special assumptions that we have made, the problem has been reduced to a straightforward one of one dimensional relativistic motion with specified external forces. The quantity, $m\mu$ may be thought of as an effective electron mass, increased above the rest mass by the transverse kinetic energy.

From Hamilton's equations (in the context of Eq. 2.9), $\partial H_1/\partial(-E) = t'$, $\partial H_1/\partial t = -(-E')$, and the definitions of ψ and γ Eqs. (2.11) and (2.12) we obtain

$$\psi' = (k_w + k_s) + \frac{\omega_s}{mc^2}\frac{\partial H_1}{\partial \gamma} \qquad (2.13)$$

and

$$\gamma' = -\frac{\omega_s}{mc^2}\frac{\partial H_1}{\partial \psi} \qquad (2.14)$$

Strong beam-wave interaction occurs when the beam velocity is approximately matched to that of the bunching wave, in which case ψ is approximately constant. While we expect to allow the various parameters to vary with z it will still be the case that the orbits of principal interest will be those which remain in approximate velocity resonance and for which ψ is slowly varying. For this reason it proves to be more convenient to use ψ and γ as (canonical) coordinates rather than t and (-E) with z still the independent coordinate. This leads us to use the following Hamiltonian to describe the motion in the ψ, γ coordinates

$$H_2 = \gamma(k_w + k_s) - \frac{\omega_s}{c}\left|\gamma^2 - \mu^2 + 2a_w a_s \cos\psi\right|^{1/2} \tag{2.15}$$

The equations of motion for ψ and γ which follow from this new Hamiltonian are

$$\psi' = \frac{\partial H_2}{\partial \gamma} = (k_w + k_s) - \frac{\frac{\omega_s}{c}\gamma}{\sqrt{\gamma^2 - \mu^2 + 2a_w a_s \cos\psi}} \tag{2.16}$$

$$\gamma' = -\frac{\partial H_2}{\partial \psi} = -\frac{\frac{\omega_s}{c} a_w a_s \sin\psi}{\sqrt{\gamma^2 - \mu^2 + 2a_w a_s \cos\psi}} \tag{2.17}$$

which of course are the same equations that are obtained by the use of Eqs. (2.13) and (2.14) with the old Hamiltonian $H_1(-E, t, z)$.

For the applications to be discussed in this paper $\gamma^2 >> \mu^2$, $\gamma^2 >> a_w a_s$ and $a_w >> a_s$. With these approximations the Hamiltonian may be approximated by

$$H_3 = \gamma(k_w + \delta k_s) + \frac{\omega_s}{2\gamma c}(\mu^2 - 2a_w a_s \cos\psi) \tag{2.18}$$

with

$$\mu^2 = 1 + a_w^2 \quad \text{and} \quad \delta k_s = k_s - \frac{\omega_s}{c} \quad . \tag{2.19}$$

Evidently the term

$$U_p = \frac{a_w a_s \omega_s}{\gamma c} \cos\left[\int_0^z (k_s + k_w)dz_1 - \omega_s t\right] \tag{2.20}$$

plays the role of a potential (the "ponderomotive potential"). It may be thought of as providing a bunching force which moves at the resonant velocity.

$$v_r = \frac{\omega_s}{k_w + k_s} \tag{2.21}$$

The equations of motion that correspond to the approximate Hamiltonian H_3 are

$$\psi' = (k_w + \delta k_s) - \frac{\omega_s}{2\gamma^2 c}(\mu^2 - 2a_w a_s \cos\psi) \quad , \tag{2.22}$$

and

$$\gamma' = -\frac{\omega_s a_s a_w}{\gamma c} \sin\psi \tag{2.23}$$

The corresponding equations for the particle energy and phase may be written as

$$\gamma^2 = \frac{\omega_s}{2c} \frac{\mu^2 - 2a_w a_s \cos \psi}{(k_w + \delta k_s - \psi')}$$

$$\approx \frac{\omega_s \mu^2}{2c(k_w + \delta k_s - \psi')} \tag{2.24}$$

and

$$\psi'' = (k_w' + \delta k_s') - \frac{2(k_w + \delta k_s - \psi')a_w}{\mu^2}[a_w' + (2k_w + 2\delta k_s - \psi')a_s \sin \psi] \tag{2.25}$$

where we have used the approximation that $a_w >> a_s$.

The z dependence of a_w and k_w are determined by the physical design of the FEL hardware, and in subsequent sections we will discuss the design considerations upon which these specifications may be based. The optical field amplitude, and to some extent the phase, depend explicitly upon the FEL amplification process and will be affected by such additional properties as the design of the optical cavity and the design and magnitude of the electron beam. In keeping with our assumption of the absence of variation in the transverse direction we shall assume that the electron beam and optical beam overlap perfectly and that the electron beam is also uniform in electron density. Under these conditions the variation of a_s is determined by energy conservation. Thus we write

$$\frac{c}{4\pi}\left(|\underset{\sim}{E}_s \times \underset{\sim}{B}_s|_z - |\underset{\sim}{E}_s \times \underset{\sim}{B}_s|_o\right) = \frac{c}{4\pi} k_s^2 \left(\frac{mc^2}{e}\right)^2 \left(a_s^2(z) - a_s^2(0)\right)$$

$$= n_e mc^2 \left(\langle\gamma(0)\rangle - \langle\gamma(z)\rangle\right)$$

or

$$a_s^2(z) = a_s^2(0) + \frac{\omega_p^2}{\omega_s^2}\left(\langle\gamma(0)\rangle - \langle\gamma(z)\rangle\right) \tag{2.26}$$

where $\langle\ \rangle$ implies averages over initial distributions of energy and phase and $\omega_p^2 = 4\pi n_e e^2/m$ is the plasma frequency. n_e is the electron density measured in the laboratory frame, and we have assumed $v \approx c$.

An alternative derivation of Eq. (2.26) along with a determination of δk_s can be obtained from the Maxwell equation

$$\frac{\partial^2 \underset{\sim}{A}_s}{\partial z^2} - \frac{1}{c^2}\frac{\partial^2 \underset{\sim}{A}_s}{\partial t^2} = -\frac{4\pi}{c}\underset{\sim}{J}_\perp \tag{2.27}$$

Substitution of the form (2.8) yields

$$\frac{2\omega_s}{c}\,\delta k_s A_s \hat{e}_1 - 2\frac{\omega_s}{c} A_s' \hat{e}_2 = \frac{4\pi}{c}\underset{\sim}{J}_\perp \tag{2.28}$$

where $\hat{e}_1$ and $\hat{e}_2$ are defined by

$$\hat{e}_1 = \left[\hat{x}\cos\left(\int_o^z k_s(z_1)\,dz_1 - \omega_s t\right) - \hat{y}\sin\left(\int_o^z k_s(z_1)\,dz_1 - \omega_s t\right)\right]$$

$$\hat{e}_1' = k_s \hat{e}_2 \tag{2.29}$$

and we have neglected derivatives of A_s' and δk_s compared to ω_s/c . Because $\hat{e}_1$ is a unit vector and $\hat{e}_1 \cdot \hat{e}_2$ vanishes we find

$$\frac{2\omega_s}{c}\,\delta k_s A_s = \frac{4\pi}{c}\,\underset{\sim}{J}_\perp \cdot \hat{e}_1 \tag{2.30}$$

In order that the form originally chosen for $\underset{\sim}{A}_s$ be strictly correct it is necessary that the right hand side of Eq. (2.30) be time independent. In actual fact the $\underset{\sim}{J}_\perp \cdot \hat{e}_1$ generated by the assumed form for $\underset{\sim}{A}_s$ will be a periodic function of time with period $2\pi/\omega_s$. We shall eliminate the oscillating terms by carrying out a long time average of $\underset{\sim}{J}_\perp \cdot \hat{e}_1$. Such a procedure is valid[15] provided $\delta k_s \ll k_w$.

For a single electron we have

$$\underset{\sim}{J}_\perp \cdot \hat{e}_1 = e\underset{\sim}{v}_\perp \cdot \hat{e}_1 \delta(x - x_o(t))\delta(y - y_o(t))\delta(z - z(t)) \tag{2.31}$$

where

$$\underset{\sim}{v}_\perp = \underset{\sim}{\nabla}_{p_\perp} H_o\Big|_{p_\perp=0} = \frac{-e\underset{\sim}{A}}{\gamma mc} \approx \frac{-e\underset{\sim}{A}_w}{\gamma mc} \tag{2.32}$$

for $A_s \ll A_w$. Hence,

$$(\underset{\sim}{J}_\perp \cdot \hat{e}_1)_{\text{single particle}} = \frac{e^2 A_w(z)}{\gamma mc}\cos\psi\ \delta(x - x_o(t))\delta(y - y_o(t))\delta(z - z_o(t)) \tag{2.33}$$

We time average by integrating over time from $-T/2$ to $T/2$ to obtain

$$(\underset{\sim}{J}_\perp \cdot \hat{e}_1)_{\text{single particle}} = \frac{e^2 A_w(z)}{v_z T \gamma mc} \cos \psi(z)\ \delta(x - x_o(z))\ \delta(y - y_o(z))$$

$$\text{for } -T/2 < t(z) < T/2$$

$$= 0 \quad \text{otherwise.} \tag{2.34}$$

Summing over all electrons, and averaging over the beam cross section to eliminate the transverse δ functions we obtain

$$(\underset{\sim}{J}_\perp \cdot \hat{e}_1)_{\text{time average}} = \frac{n_e e^2 A_w}{mc} \quad \langle \cos \psi/\gamma \rangle \tag{2.35}$$

where again $\langle\ \rangle$ means average over initial ψ and energy. Substitution of Eq. (2.35) with Eq. (2.30) yields

$$\delta k_s = \frac{\omega_p^2}{2c\omega_s} \frac{a_w}{a_s} \quad \langle \cos \psi/\gamma \rangle \tag{2.36}$$

Again from Eq. (2.28) we find

$$2 \frac{\omega_s}{c} A_s' = - \frac{4\pi}{c} \underset{\sim}{J}_\perp \cdot \hat{e}_2$$

and proceeding in a similar manner we find

$$a_s' = \frac{\omega_p^2}{2\omega_s c} a_w \langle \sin \psi/\gamma \rangle \tag{2.37}$$

To compare Eq. (2.37) with Eq. (2.26) we note that

$$\frac{d\gamma}{dz} = \frac{1}{mc^2}\frac{\partial H_1}{\partial t} = -\frac{a_s a_w \omega_s}{c} \quad (\sin \psi/\gamma)$$

so that

$$\frac{d\langle\gamma\rangle}{dz} = -\frac{a_s a_w \omega_s}{c} \quad \langle\sin \psi/\gamma\rangle \tag{2.38}$$

The equivalence of Eq. (2.37) and Eq. (2.38) to Eq. (2.26) is apparent. From Eq. (2.36) and Eq. (2.37) we have

$$\delta k_s = \frac{a_s'}{a_s} \frac{\langle\cos \psi/\gamma\rangle}{\langle\sin \psi/\gamma\rangle} \tag{2.39}$$

so that the assumption $a_s'/a_s << k_w$ made at the outset would appear to typically imply $\delta k_s << k_w$ as well. Since we expect the particles to bunch in the $0 < \psi < \pi/2$ range, $\langle\cos \psi/\gamma\rangle$ will be positive. This implies a tendency of the electron beam to trap the optical beam and hence to counter to some extent the effects of diffraction.

The equations of motion derived above (Eqs. (2.24) and (2.25)) are valid (under the special assumptions that were made) for every electron, and given the initial conditions $\psi(o)$ and $\gamma(o)$ for every electron along with the expressions for k_w, a_w, a_s, and δk_s, these equations may be integrated to yield the values of ψ and γ as functions of the longitudinal position z. Of course, for a high gain FEL it is necessary to make sure that the signal field a_s used in the equations of motion is

also a self consistent solution to Eqs. (2.26) and (2.39); by using a computer one can solve the equations of motion for a large number of particles and obtain the final coordinates in phase space for every particle as well as the final signal field and phase. In principle this procedure could be used to choose the optimum functional form for $k_w(z)$ and $a_w(z)$. It is possible to gain physical insight into the content of these equations without the need of integrating the equations of motion for a large number of initial conditions by referring the electrons energy variable γ to the synchronous or <u>resonant</u> value γ_r . This approach is extremely useful in determining the functions $k_w(z)$ and $a_w(z)$ to be used in different modes of operation for the FEL.

2.1 Definition of Synchronous Energy and Phase

The synchronous energy, γ_r , and phase, ψ_r , are defined by

$$\gamma_r^2 = \frac{\omega_s \mu^2}{2(k_w + \delta k_s)c} \tag{2.40}$$

and

$$\frac{d\gamma_r}{dz} = - \frac{a_w a_s \omega_s}{\gamma_r c} \sin \psi_r \quad . \tag{2.41}$$

If Eq. (2.41) yields a z independent value for ψ_r , then substitution in Eqs. (2.24 & 2.25) shows that a particle with values of γ and ψ equal to γ_r and ψ_r respectively will retain these values throughout its motion through the wiggler. Such a particle may be thought of as a

synchronous particle. More generally, as will become apparent below, if $\gamma - \gamma_r$, $\psi - \psi_r$ are initially small, they tend to remain small.

It is possible to look at Eqs. (2.40) and (2.41) as definitions of γ_r and ψ_r assuming that k_w, a_w, a_s and δk_s are known functions of z . However, it is also possible to consider these as design equations where the wiggler functions k_w and a_w are to be determined to achieve the desired functions γ_r, ψ_r and a_s .

Much of the remainder of the paper will deal with different ways to choose ψ_r and γ_r and hence the wiggler parameters for various operating modes of the FEL. We first must study the motion of electrons with phase coordinates different from the synchronous values and demonstrate that for sufficiently small deviations the electrons will perform stable oscillations about the synchronous values. It must be noted that one is restricted in the choice for the functions γ_r and ψ_r ; for example ψ_r is not defined if

$$\left|\frac{d\gamma_r}{dz}\right| > \left|\frac{\omega_s a_w a_s}{c\gamma_r}\right|$$

2.2 Motion About the Synchronous Energy

In this section we study the motion of the electrons about the synchronous energy by writing

$$\gamma = \delta\gamma + \gamma_r \quad . \tag{2.42}$$

We regard $\delta\gamma$ as the new canonical momentum with a new Hamiltonian H_4 given by

$$H_4(\psi, \delta\gamma, z) = H_3(\psi, \gamma_r + \delta\gamma, z) + \psi \frac{d\gamma_r}{dz} \tag{2.43}$$

With the definitions for γ_r *and* ψ_r *as* chosen in Eqs. (2.40)and (2.41) and with the assumption of $\delta\gamma << \gamma_r$ the new Hamiltonian H_4 , which is derived from the approximate Hamiltonian H_3 Eq. (2.18), is

$$H_4 = \frac{k_w + \delta k_s}{\gamma_r} (\delta\gamma)^2 - \frac{\omega_s a_w a_s}{c\gamma_r} (\cos \psi + \psi \sin \psi_r) \tag{2.44}$$

This form for the Hamiltonian and the resulting equations of motion are very familiar to accelerator physicists. The following analysis is quite similar to their treatment of RF acceleration in standing wave linacs. In writing Eq. (2.44) we have omitted terms which are functions only of the independent variable z , since they have no effect upon the equations of motion, and it has been assumed that a value of ψ_r exists, i.e. that

$$\left| \frac{d\gamma_r}{dz} \right| < \left| \frac{\omega_s a_w a_s}{\gamma c} \right| . \tag{2.45}$$

H_4 has the form of a nonrelativistic single particle Hamiltonian with z dependent "mass" and a z dependent potential function, F, given by

$$F(\psi) = -C(\cos \psi + \psi \sin \psi_r) \tag{2.46}$$

with

$$C(z) = \frac{\omega_s a_s a_w}{\gamma_r c} \tag{2.47}$$

We assume $C > 0$ and $-\pi/2 < \psi_r < \pi/2$, so that $\psi = \psi_r$ corresponds to a minimum of the potential and $(\pi \operatorname{sgn} \psi_r - \psi_r)$ to a maximum. There are, of course, a succession of minima at $\psi = \psi_r + 2\pi n$ and maxima at $\psi = \pi - \psi_r + 2\pi n$, and one may conveniently think of the successive troughs as buckets in which particles may become trapped. $F(\psi)$ is illustrated in Fig. 2.1.

Of particular interest are design parameters chosen so that the behavior changes adiabatically with z. In that case electrons trace out trajectories in the ψ, $\delta\gamma$ phase plane given by

$$\delta\gamma(\bar{H}, \psi, z) = \mp \sqrt{\frac{\gamma_r}{k_w + \delta k_s} \left[\bar{H} - F(\psi)\right]} \tag{2.48}$$

and illustrated for $\psi_r > 0$ in Fig. 2.2 at $z = 0$. The case $\psi_r > 0$ corresponds to $d\gamma_r/dz < 0$ and therefore represents decelerating buckets. $\bar{H}(0)$ is determined by the initial values of ψ and $\delta\gamma$. The closed orbits correspond to the particles trapped in the buckets. If the change of parameters with z is adiabatic, then $\bar{H}(z)$ is determined by the requirement that the area of the closed phase curve, given by

$$J = \oint \delta\gamma d\psi \tag{2.49}$$

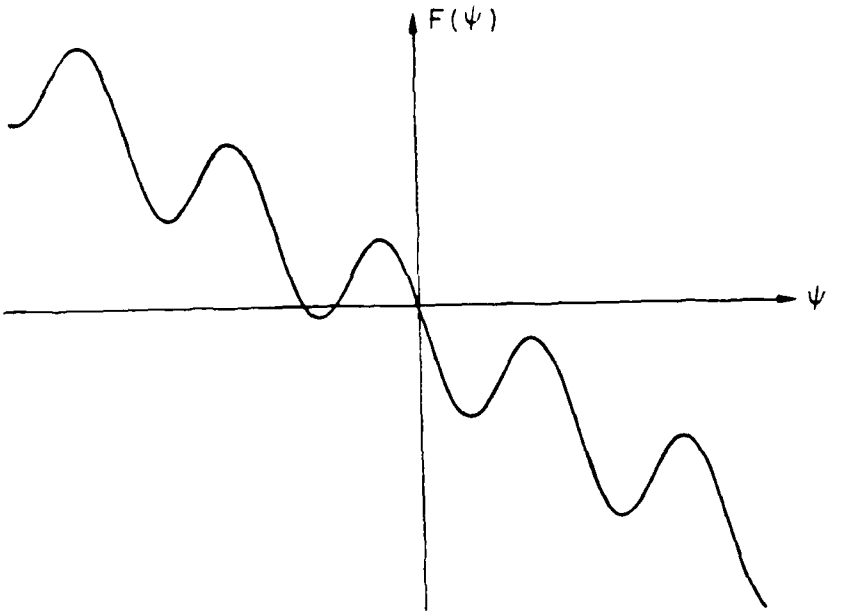

FIGURE 2.1

THE PONDEROMOTIVE POTENTIAL, F (ψ). THE CASE SHOWN IS FOR POSITIVE ψ_r CORRESPONDING TO THE CASE IN WHICH ENERGY IS EXTRACTED FROM THE ELECTRONS.

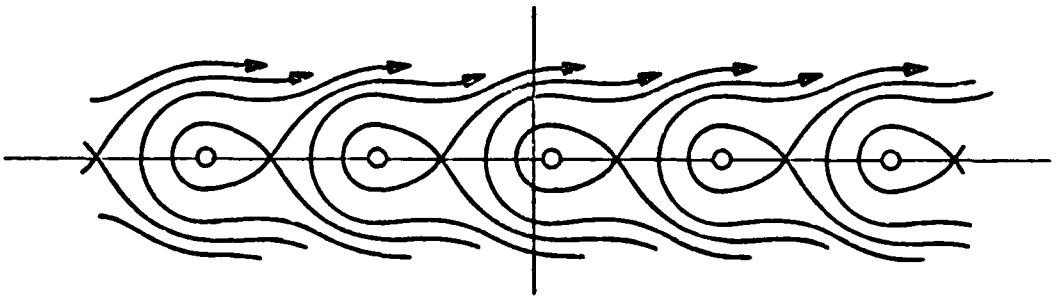

FIGURE 2.2

TRAJECTORIES IN THE ψ, $\delta\gamma$ PHASE PLANE FOR $\psi_r > 0$.

remain constant as z changes. For the unbound orbits, the representation is valid only over a range of z for which the change in parameters is small. For small oscillations about ψ_r one can expand $F(\psi)$ about ψ_r The motion for these orbits is harmonic with period of oscillation

$$Z = \frac{\pi\mu}{(k_w + \delta k_s)\sqrt{a_s a_w \cos\psi_r}} \approx \frac{\mu\lambda_w}{2\sqrt{a_s a_w \cos\psi_r}} \qquad (2.50)$$

$\left(\lambda_w \equiv 2\pi/k_w\right)$.

The period for weakly trapped particles, with large excursion in ψ, is of course larger. The parameter variation may be considered to be adiabatic if it is small over a distance of the order of the period.[16] In order that a particle be trapped in a bucket it is necessary that $|\delta\gamma| < \delta\gamma_{max}$ with

$$\frac{\delta\gamma_{max}}{\gamma_r} = \frac{2}{\mu}\sqrt{a_w a_s\left[\cos\psi_r - \left(\frac{\pi}{2}\,\mathrm{sgn}\,\psi_r - \psi_r\right)\sin\psi_r\right]} \qquad (2.51)$$

If one wishes to avoid the approximations associated with the use of Eq. (2.44) it is straightforward to base the definition of γ_r, ψ_r and J upon Eqs. (2.15 & 2.43).

2.3 Summary of Bucket Parameters

Because the pattern of the stable trajectories traced out by the electrons in the ψ, $\delta\gamma$ phase plane repeat in ψ at intervals of 2π we only

will discuss the phase motion in the interval for $-\pi < \psi < \pi$. The maximum stable phase curve or bucket is shown in Fig. 2.3 and corresponds to the trajectory given by Eq.(2.48) for

$$\bar{H} = \bar{H}_m = C\,[\cos\psi_r - (\pi \operatorname{sgn}\psi_r - \psi_r)\sin\psi_r] \tag{2.52}$$

with

$$C = \frac{\omega_s a_s a_w}{\gamma_r c} \tag{2.53}$$

The bucket intercepts of the ψ axis, designated by ψ_1 and ψ_2 in Fig. 2.3, are given by

$$\psi_2 \equiv \pi \operatorname{sgn}\psi_r - \psi_r \tag{2.54}$$

and

$$\cos\psi_1 + \psi_1 \sin\psi_r = \cos\psi_2 + \psi_2 \sin\psi_r \tag{2.55}$$

The values of ψ_1 and ψ_2 are shown as a function of ψ_r in Fig. 2.4. The maximum bucket height $\delta\gamma_{max}$ given by Eq. (2.51) can be written as

$$\frac{\delta\gamma_{max}}{\gamma} = \frac{2\sqrt{a_w a_s}}{\mu}\,\Gamma(\psi_r) \tag{2.56}$$

with

$$\Gamma(\psi_r) = \sqrt{\cos\psi_r - (\tfrac{\pi}{2}\operatorname{sgn}\psi_r - \psi_r)\sin\psi_r} \tag{2.57}$$

$\Gamma(\psi_r)$ is shown in Fig. 2.5.

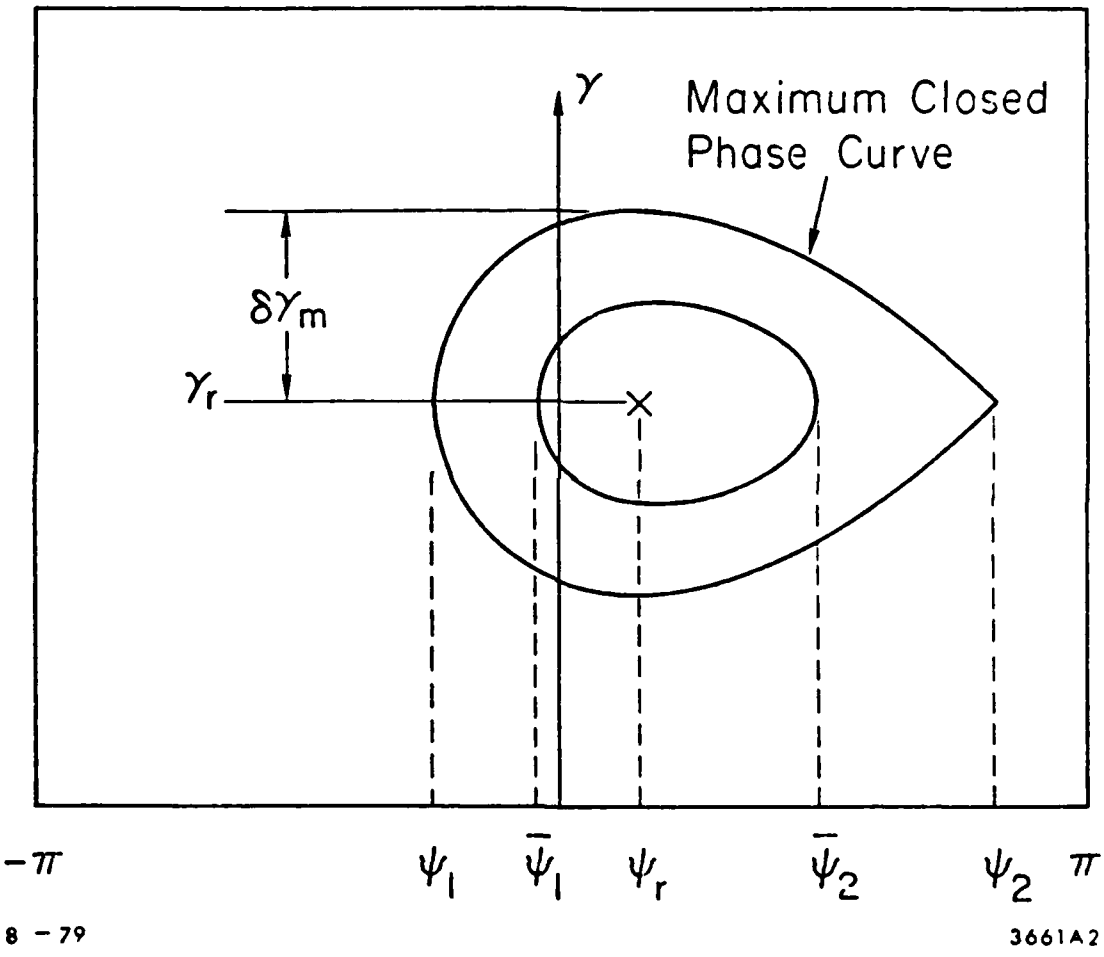

FIGURE 2.3

STABLE PHASE PLANE TRAJECTORIES

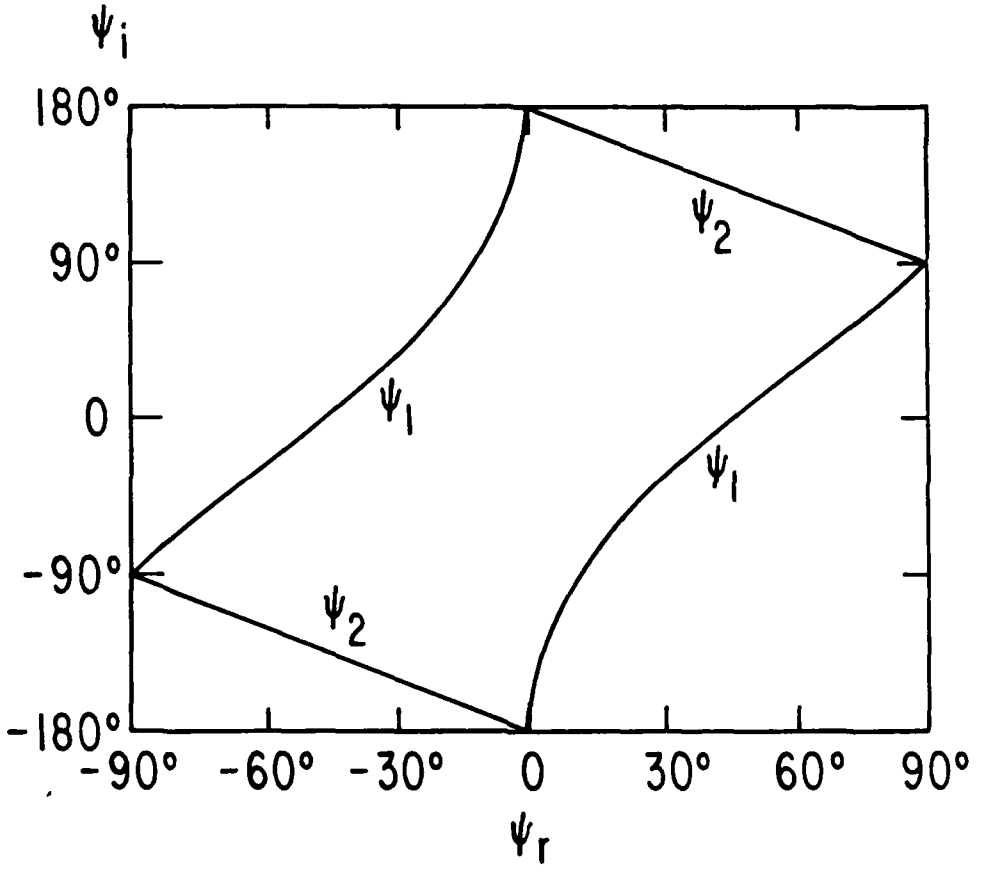

FIGURE 2.4

ψ_1, ψ_2 AS FUNCTIONS OF ψ_r

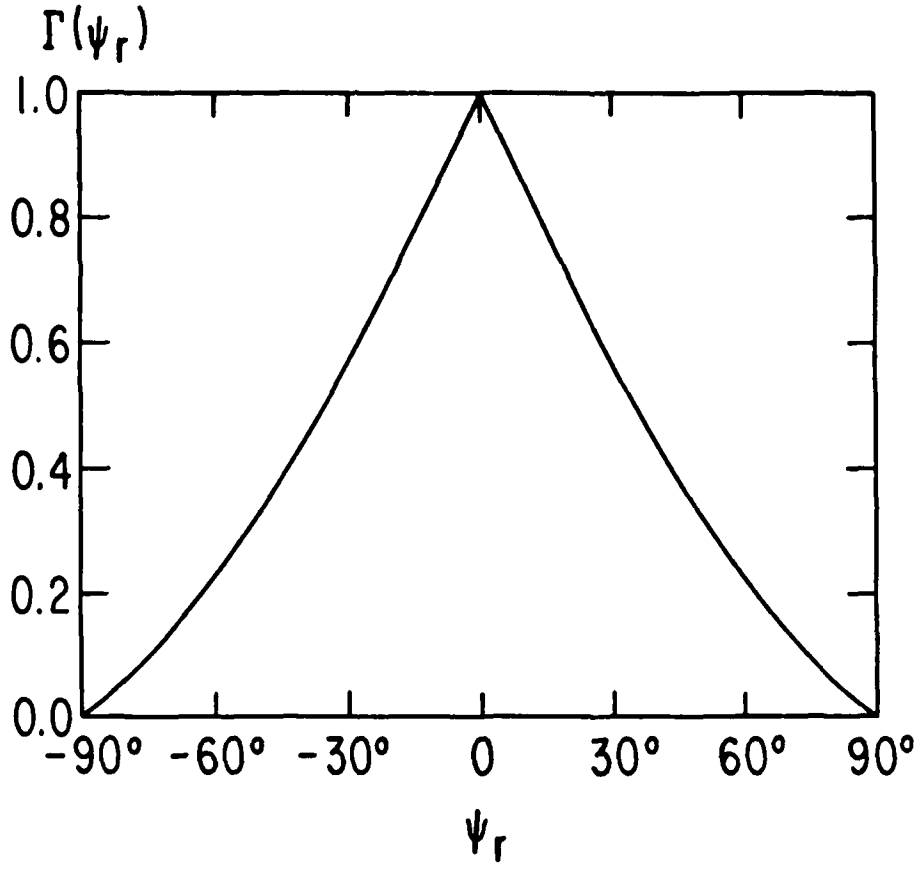

FIGURE 2.5

THE BUCKET HEIGHT FUNCTION, $\Gamma(\psi_r)$.

The area of the bucket shown in Fig. 2.3 may be obtained from Eq. (2.49) and is given by

$$J = 2 \frac{\gamma_r}{\mu} \sqrt{2a_s a_w} \int_{\psi_1}^{\psi_2} \left[\cos \psi_r + \cos \psi - (\pi - \psi_r - \psi) \sin \psi_r\right]^{\frac{1}{2}} d\psi \tag{2.58}$$

$$= \frac{16}{\mu} \frac{\gamma_r}{} \sqrt{a_s a_w} \; \alpha(\psi_r) \tag{2.59}$$

where

$$\alpha(\psi_r) = \frac{\sqrt{2}}{8} \int_{\psi_1}^{\psi_2} \left[\cos \psi_r + \cos \psi - (\pi - \psi_r - \psi) \sin \psi_r\right]^{\frac{1}{2}} d\psi \tag{2.60}$$

is the moving bucket area and is plotted in Fig. 2.6. Note that α equals one for $\psi_r = 0$ and decreases to zero for $\psi_r = \mp\pi/2$. (Eqs. (2.58) and (2.60) are for $\psi_r > 0$, For $\psi_r < 0$, use $\alpha(\psi_r) = \alpha(-\psi_r)$.)

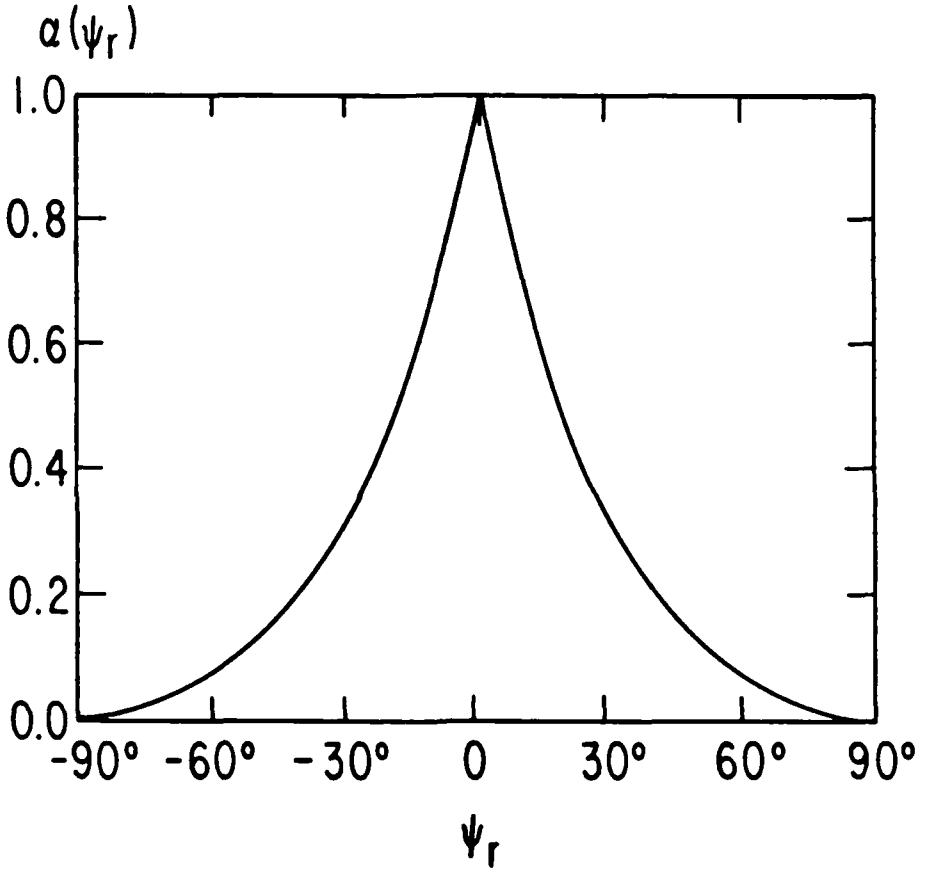

FIGURE 2.6

THE PHASE SPACE AREA FUNCTION, $\alpha(\psi_r)$.

3.0 CONSTANT PARAMETER WIGGLER

The original mode of FEL operation demonstrated[3] by Madey and co-workers utilized a wiggler with a fixed wave number k_w and field amplitude[4] a_w . For such a case the operational mode is one in which

$$\psi_r = \text{constant} = 0 \tag{3.1}$$

and

$$\gamma_r^2 = \text{constant} = \frac{\omega_s \mu^2}{2k_w c} \tag{3.2}$$

where the fact that $\delta k_s << k_w$ has been used.

The Hamiltonian[5] which describes the motion of the electrons is given by

$$H_4 = \frac{k_w}{\gamma_r} (\delta\gamma)^2 - C \cos \psi \tag{3.3}$$

where

$$C = \frac{\omega_s a_s a_w}{2\gamma_r c} \tag{3.4}$$

For this mode of operation the buckets are stationary or non-accelerating with a half-height

$$\frac{\delta\gamma_m}{\gamma_r} = \frac{2}{\mu}\sqrt{a_w a_s} \tag{3.5}$$

and the length of one synchrotron period

$$Z = \frac{\mu\lambda_w}{2\sqrt{a_w a_s}} = \frac{\lambda_w \gamma_r}{(\delta\gamma)_m} \tag{3.6}$$

The motion of the electrons in such a bucket is one in which some of the electrons gain energy while others lose energy in a manner that depends upon the total length of the FEL as well as the initial phase and energy of the electron. If the average injection energy equals the resonance energy, the average change in the electron energy will be zero, provided that the initial phase distribution is uniform. While there are modes of operation for the constant parameter wiggler which assume a non-uniform phase distribution for the injected electrons, we will consider only the case where the initial phase distribution is uniform.

Electrons that have an initial energy different from the resonant energy by an amount large compared to the maxiumum bucket height will not be appreciably affected by the FEL and hence will have only a small change in their energy (they will not be resonant with the optical wave), while electrons that are too near the resonant energy also will, on the average, have only a small energy change. The electrons with an initial energy

difference, from resonance, $(\delta\gamma)_i$ will have the largest energy change in traveling through the FEL when

$$(\delta\gamma)_i \sim (\delta\gamma_r)_m$$

Clearly, if a significant fraction of the electrons are to lose energy, it is necessary for the initial energy spread in the beam to be less than the maximum bucket height. Consider a mono-energetic beam of electrons with an initial energy difference $(\delta\gamma)_i > 0$ as shown in Fig. 3.1a. After a distance L which corresponds to approximately one-half of a synchrotron oscillation many particles will have their energy shifted below the resonant energy as shown in Fig. 3.1b. For longer distances these electrons will continue to oscillate about the resonant energy and the average energy will begin to increase back to the initial energy as shown in Fig. 3.1c.

The performance of a FEL operating with an electron beam of an initial uniform phase distribution and a constant parameter wiggler will have the following properties. First, for reasonable performance, the energy spread of the beam must not be significantly larger than the bucket height, secondly, the maximum energy loss by the beam will be of the order of the bucket height and thirdly the optimum length of the FEL is of the order of one-half of a synchrotron period. From Eqs. (3.5 & 3.6) we see that the maximum allowable energy spread, maximum energy loss, and optimum FEL length are related by

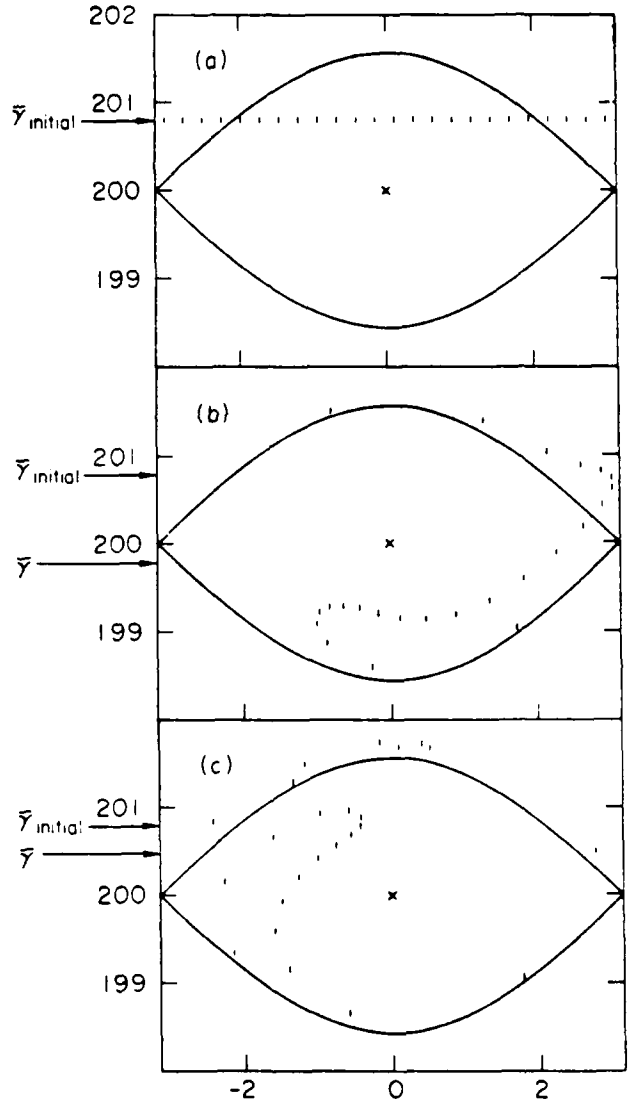

FIGURE 3.1

PHASE SPACE PLOTS FOR MONO-ENERGETIC ELECTRONS IN A CONSTANT PARAMETER WIGGLER.

a) at z = 0
b) L corresponds to ~ 1/2 synchrotron oscillation
c) L is 5/3 the value shown in b.

$$\left(\frac{\Delta\gamma}{\gamma}\right)_{\substack{\max \\ \text{spread}}} \sim \left(\frac{\Delta\gamma}{\gamma}\right)_{\substack{\max \\ \text{loss}}} \sim \left(\frac{\delta\gamma_m}{\gamma_r}\right)_{\substack{\text{bucket} \\ \text{height}}} \sim \frac{\lambda_w}{2L} \sim \frac{1}{2N} \qquad (3.7)$$

where N is the number of wiggler periods.

Another important characteristic of the constant parameter wiggler is the fact that, due to the dependence of final energy upon initial phase, electrons which enter at a particular energy emerge with an energy spread that is of the same order (typically larger) as the mean energy loss. This property is qualitatively apparent in Fig. 3.1b. As a result the energy spread in the emerging electrons tends to be increased, over that of the entering electrons, by an amount comparable to the mean energy loss. The above refers to the situation in which the signal amplitude is such that the synchrotron period is of the order of twice the length. When the signal amplitude is small compared to this characteristic amplitude, one is in the linear regime. Then the relation between energy loss and induced energy spread is governed by the Madey Theorem[12] (Appendix A)

$$\langle \gamma_f - \gamma_i \rangle = \frac{1}{2} \frac{\delta}{\delta\gamma_i} \langle (\gamma_f - \gamma_i)^2 \rangle$$

where $\langle\ \rangle$ denotes average over entry phase, and implies that the induced energy spread becomes much larger than the mean energy loss as the optical amplitude becomes small. These results have important consequences for the operation of an FEL as an oscillator in a storage ring. Renieri,[17] Deacon, et al[18] and Elias, et al[19] have shown that if one depends upon the synchrotron radiation to damp the growth of velocity spread then the

maximum signal power which can be extracted from the electrons is of the order of the product of the synchrotron radiation rate with the maximum value of the fractional energy spread that will circulate in the ring, hence of the order of 1% of the synchrotron radiation power.

4.0 IMPROVED ENERGY EXTRACTION BY MEANS OF ADIABATIC DECREASE OF THE RESONANT ENERGY

We have seen in Section 3 that the electron energy which can be extracted in passing through a fixed parameter wiggler designed to operate at some specified z independent optical power level is limited to some fraction ($\sim .5$) of the bucket height given by Eq. (2.56), so that $\left(<\delta\gamma>/\gamma_r\right)_{max} \approx \sqrt{a_w a_s}/\mu$. On the other hand, if the wiggler parameters are varied so as to gradually reduce γ_r as the bucket moves through the wiggler, electrons which remain trapped in the bucket give up an energy approximately equal to the reduction in γ_r. In this section we discuss in an exploratory way some characteristic features of this mode of operation.

4.1 Operation at Constant Signal Amplitude

A laser oscillator, fitted with an optical cavity formed of highly reflecting mirrors, operates at steady state so that the amplification of the signal field a_s in passing through the wiggler just compensates for the reflection loss. Accordingly, it is a reasonable approximation to assume that the electrons see a constant a_s. On the other hand, as we shall find that very large a_s is desirable, we may suppose that only a small portion of the resonator is occuppied with coincident electron beam and laser "micropulses". On account of Eq. (2.39), it is also a good approximation to neglect δk_s.

It is convenient for discussion and probably desirable as a design characteristic to choose γ_r so that ψ_r is constant. Then Eq. (2.41) immediately provides the relation

$$\gamma_i^2 - \gamma_f^2 = 2 \frac{\omega_s}{c} L \, a_s \bar{a}_w \sin \psi_r \tag{4.1}$$

where

$$\gamma_i \equiv \gamma_r(z = 0) \, , \quad \gamma_f \equiv \gamma_r(L) \quad \text{and}$$

$$\bar{a}_w L \equiv \int_0^L a_w(z) dz$$

The assumption of constant ψ_r together with Eqs. (2.40) and (2.41) provides a useful constraint on the wiggler design. One sees, for example, that if one chooses to keep k_w constant, then Eqs. (2.40) and (2.41) are satisfied by decreasing a_w linearly. For this choice the bucket (more accurately, the bucket minimum) moves with constant velocity; the electron energy loss comes entirely from the reduction in μ^2, the effective electron mass. Alternatively, if one keeps a_w constant then the wiggler wavelength decreases linearly with z. The effective mass remains constant, but the bucket slows down. An intermediate case is provided by keeping the wiggler field, $b_w = k_w a_w$, constant. Eq. (2.41) is again readily integrable.

Eq. (4.1) implies the inequality

$$(\gamma_i^2 - \gamma_f^2) < 2 \frac{\omega_s}{c} L\, a_s \bar{a}_w$$

which is equivalent to

$$2La_s > \frac{1}{2\bar{a}_w} \left(\frac{\mu^2(0)}{k_w(0)} - \frac{\mu^2(L)}{k_w(L)} \right) \tag{4.2}$$

Eq. (4.2) represents a constraint on the length and/or optical power density which is required to obtain a desired change in γ_r. It is probably desirable, therefore, to design the wiggler magnet so as to minimize the right hand side subject to a specified value[20] of $k_w(L)$ and bucket efficiency, which we define by $\eta_b = (\gamma_i - \gamma_f) / \gamma_i$. The required relations are easily established for the constant k_w and constant a_w cases. One obtains the following simple results:

Constant k_w case:

$$k_w L a_s > \frac{1}{2} \eta_b \frac{2 - \eta_b}{1 - \eta_b} \tag{4.3}$$

$$a_w(0) = \frac{\gamma_i}{\gamma_f} \quad , \quad a_w(L) = \frac{\gamma_f}{\gamma_i} \tag{4.4}$$

$$a_w(z) = a_w(0)(1 - z/L) + a_w(L) z/L \tag{4.5}$$

Constant a_w case

$$k_w(L)La_s > \frac{1}{2}\,\eta_b\,\frac{2-\eta_b}{(1-\eta_b)^2} \tag{4.6}$$

$$a_w = 1$$

$$\lambda_w(z) = \lambda_w(0)(1 - z/L) + \lambda_w(L)z/L \tag{4.7}$$

It is apparent from these results that the constraint becomes severe as η_b approaches unity, and that it is less severe in the constant k_w case. The constant b_w case turns out to be intermediate between the two (see Fig. 4.7). Much of the discussion for the remaining part of this section will for definiteness be with reference to the constant k_w case. The above discussion suggests that it is likely to be one of the better methods of varying γ_r. It also may offer hardware advantages.

For the system described by Eqs. (4.3) and (4.4) we have from Eq. (4.1)

$$k_w La_s = \frac{1}{2}\,\eta_b\,\frac{2-\eta_b}{1-\eta_b}\,\csc\,\psi_r \tag{4.8}$$

In the absence of prebunching, electrons will enter the wiggler at arbitrary initial phase $\psi(0)$. For electrons of energy γ_r, only those for which

$$\psi_1 < \psi(0) < \pi - \psi_r \equiv \psi_2 \tag{4.9}$$

will be trapped in the bucket, where ψ_1 is defined by Eq. (2.55). The fraction trapped in the bucket is therefore $f_b \equiv \frac{\psi_2 - \psi_1}{2\pi}$. For electrons with initial energy different from γ_r, the trapped fraction will be smaller and no electrons are trapped if the deviation exceeds $\delta\gamma_{max}$ Eq. (2.56). The product $f_b \eta_b$ can be thought of as a sort of idealized electronic efficiency. Fig. 4.1 provides a plot of f_b as a function of ψ_r. It is apparent that increases of idealized efficiency either by increasing η_b or increasing f_b drives the needed magnitude of La_s to larger values.

Although we are not carrying out any serious study of the effects of transverse variation in this paper, we do wish to take account of some obvious constraints which are thereby imposed upon operating parameters. To control the effects of transverse variation in a_w we write

$$k_w r_e = \frac{1}{3} \sigma_w \tag{4.10a}$$

The quantity σ_w is a parameter, which we shall typically set equal to one, which represents our ignorance of what it should really be. It may be dependent upon other operating parameters. In addition, we assume the oscillator to be provided with an optical resonator formed by a pair of mirrors and producing a Gaussian beam centered in the wiggler. This causes

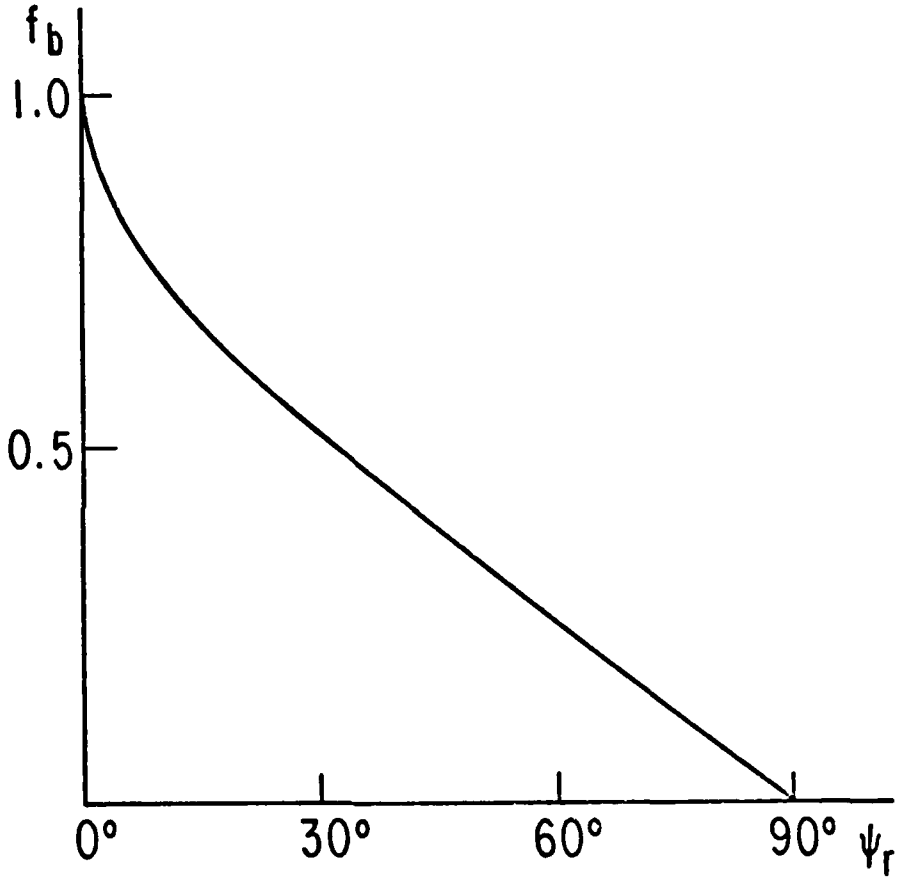

FIGURE 4.1

TRAPPING FRACTION, f_b, AS A FUNCTION OF ψ_r

an amplitude variation both transverse to and along the optical beam of the form

$$|a_s(r,z)| = |a_s(r,\tfrac{L}{2})| \frac{\exp\left[-r^2f^2/(r_s^2f^2 + d^2)\right]}{\left[1 + \frac{d^2}{f^2}\right]^{1/2}}$$

where $f = \frac{1}{2}\frac{\omega_s}{c} r_s^2$, and $d = z - L/2$. To control transverse and longitudinal variation in a_s we write

$$r_e = \frac{2}{3} r_s \sigma_e \tag{4.10b}$$

and

$$L = \frac{1}{2}\frac{\omega_s}{c} r_s^2 \sigma_L \tag{4.10c}$$

where σ_e , σ_L play a role analogous to σ_w . Combining these relations we obtain

$$k_w L a_s = \frac{1}{4} a_s r_s \frac{\omega_s}{c} \frac{\sigma_w \sigma_L}{\sigma_e} \tag{4.10d}$$

which tells us that, apart from the σ factors, the left hand side of Eq. (4.8) is proportional to the square root of the peak power circulating in the optical resonator. Returning to dimensional variables we obtain for this power

$$P = \frac{1}{2}\left(\frac{m^2c^5}{e^2}\right) \eta_b^2 \left(\frac{2 - \eta_b}{1 - \eta_b}\right)^2 \csc^2\psi_r \, \sigma_P \tag{4.11}$$

where

$$\frac{m^2c^5}{e^2} = 8.7 \text{ Gigawatts}$$

and

$$\sigma_P = \left(\frac{\sigma_e}{\sigma_w \sigma_L}\right)^2$$

Equation (4.11) provides us with some working relations which we find to be useful for further discussion. It suggests that there is a minimum circulating power required to reduce the γ of any electron by $\delta\gamma = \gamma_i \eta_b$. We call this the threshold power P_T with the working definition

$$P_T = \frac{1}{2} \frac{m^2c^5}{e^2} \eta_b^2 \left(\frac{2 - \eta_b}{1 - \eta_b}\right)^2 \qquad (4.12)$$

We also note that for fixed σ_p and idealized efficiency $\eta_i = \eta_b f_b$, it is possible to minimize the right hand side of Eq. (4.8) with respect to η_b. We define P_m as the result of this minimization, with σ_p set equal to one. This procedure provides us with a useful estimate of circulating power required for a given idealized efficiency and a reasonable basis for selection of η_b and ψ_r. Fig. 4.2a provides a plot of P_T and P_m as functions of η_b and η_i respectively. Fig. 4.2b provides a plot of the ψ_r and η_b functions of η_i which emerge from the minimization.

Computer simulation, to be described later, yields electronic efficiencies which are of the order of 80 to 90 percent of η_i. There are two reasons for departure from the ideal. First, electrons which are

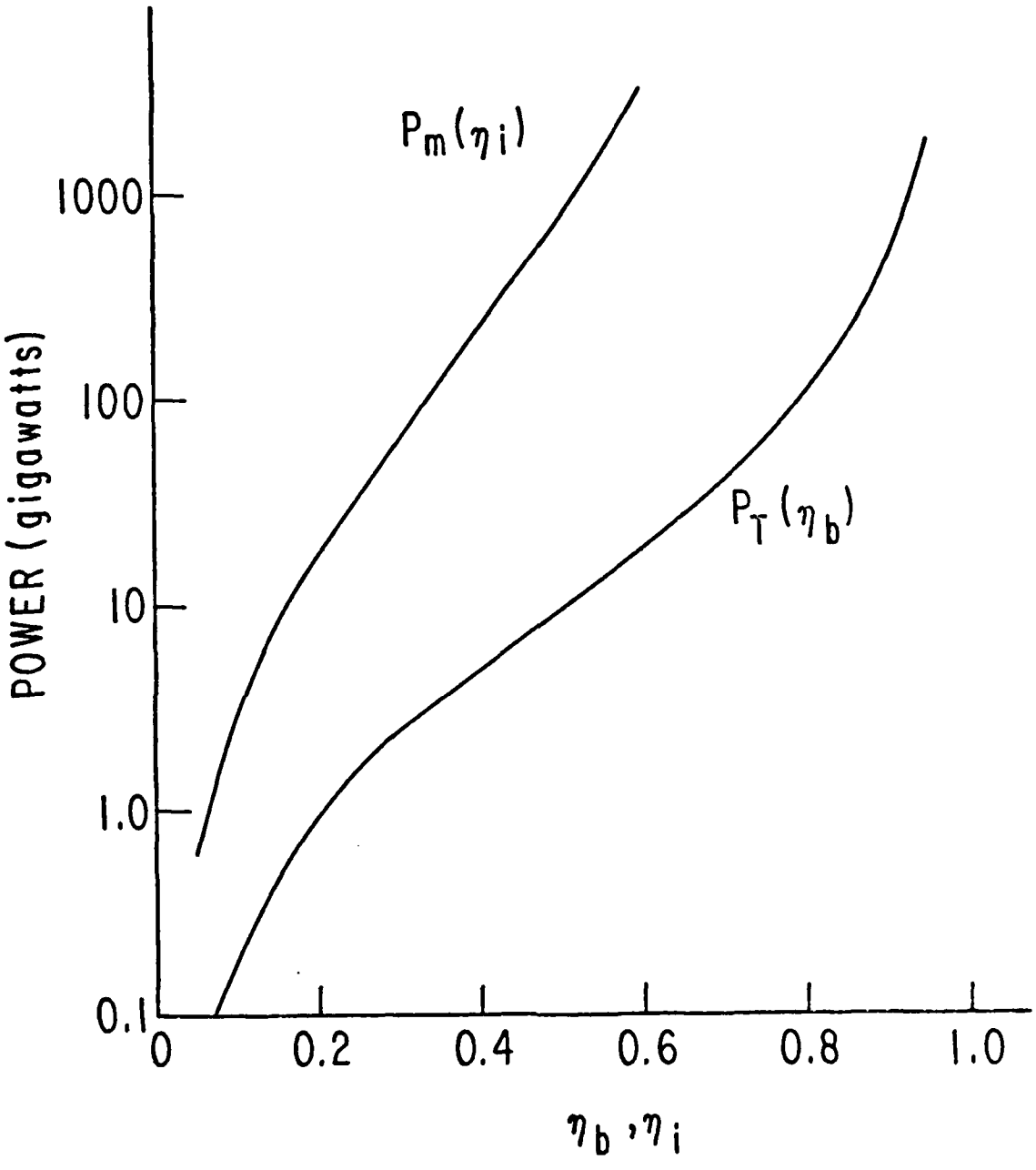

FIGURE 4.2a

THRESHHOLD POWER FOR TRAPPING, P_T , AS A FUNCTION OF BUCKET EFFICIENCY η_b .

MINIMUM REQUIRED POWER, P_m , AS A FUNCTION OF IDEAL EFFICIENCY η_i .

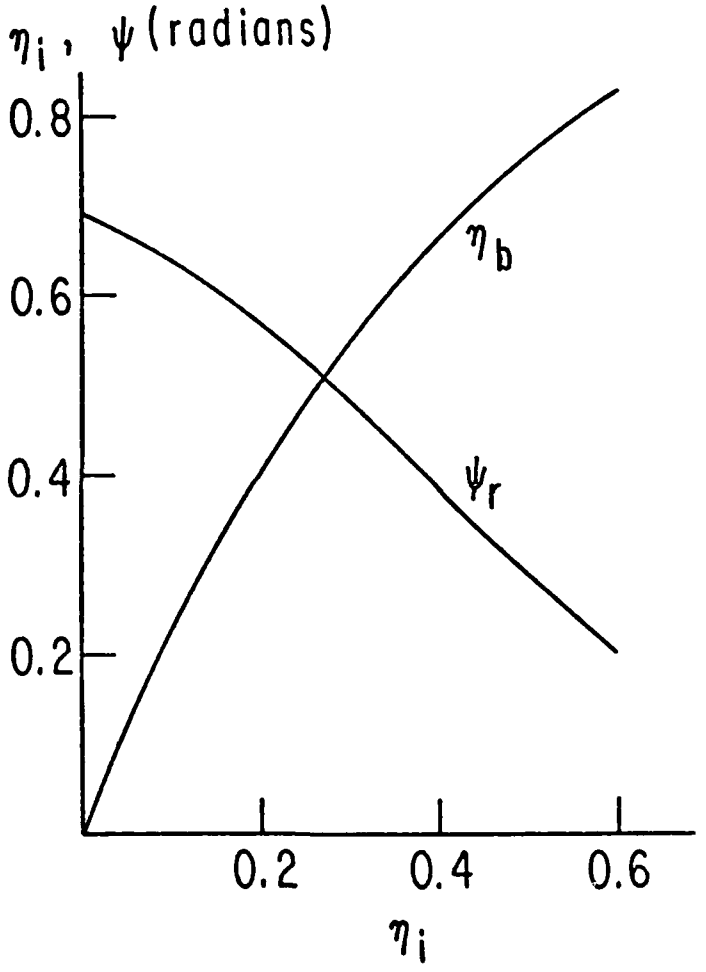

FIGURE 4.2b

VALUES OF BUCKET EFFICIENCIES η_b AND RESONANT PHASE ψ_r FOR MINIMUM POWER DESIGN AS FUNCTIONS OF IDEAL EFFICIENCY η_i.

initially trapped do not necessarily remain trapped for the entire transit through the wiggler. An electron which escapes from a bucket at some $z = z_e$ experiences a fractional energy loss of

$$\delta\gamma/\gamma = \frac{\gamma(0) - \gamma(z_e)}{\gamma(0)} < \eta_b \ .$$

Second, the electrons which are not initially trapped, i.e. those for which the initial phase is outside the $\psi_1 < \psi < \psi_2$ range, all tend to gain energy. The average gain of these electrons is of the order of $\frac{1}{2}(\delta\gamma)_{max}$; both the fact that there is an increase, and its order of magnitude can be inferred from Fig. 2.2.

Detrapping appears to be the more important of the two effects. Its occurrence can be readily related to the adiabatic invariant defined in Eq. (2.49). For an electron which enters at $\delta\gamma = 0$, $\psi = \psi_o$, we have from Eqs. (2.44), (2.46), (2.47), (2.48) and (2.49)

$$J(\psi_r, \psi_o) = 8\sqrt{\frac{2\omega_s a_w(0) a_s(0)}{c\left[k_w(0) + \delta k_w(0)\right]}}\ \bar{\alpha}(\psi_r(0), \psi_o) \qquad (4.13)$$

where

$$\bar{\alpha}(\psi_r, \psi_o) = \frac{\sqrt{2}}{8}\int_{\bar{\psi}_1}^{\bar{\psi}_2} \left[\cos\psi + \psi\sin\psi_r - \cos\psi_o + \psi_o\sin\psi_r\right]^{1/2} d\psi \qquad (4.14)$$

One of the limits is given by ψ_o and the other is related to it by (see Fig.2.3)

$$\cos \bar{\psi}_1 + \bar{\psi}_1 \sin \psi_r = \cos \bar{\psi}_2 + \bar{\psi}_2 \sin \psi_r = \cos \psi_o + \psi_o \sin \psi_r \tag{4.15}$$

In general one has

$$\psi_1 < \bar{\psi}_1 < \psi_r \quad , \quad \psi_r < \bar{\psi}_2 < \psi_2 = \pi - \psi_r$$

so that which of the two is equal to ψ_o depends upon the range in which ψ_o is located. In addition, at any z there is a maximum possible value for J which is given by

$$J_M(\psi_r, z) = 8 \sqrt{\frac{2\omega_s a_w(z) a_s(z)}{c\left(k_w(z) + \delta k_w(z)\right)}}\, \bar{\alpha}\left(\psi_r(z),\, \pi - \psi_r(z)\right) \tag{4.16}$$

The function, $\bar{\alpha}(\psi_r, \pi - \psi_r) = \alpha(\psi_r)$ is plotted as a function of ψ_r in Fig. 2.6. The value (z_e) of z at which a particle escapes from the bucket is determined by

$$J_M\left(\psi_r(z_e),\, z_e\right) = J\left(\psi_r(0),\, \psi_o\right)$$

For the oscillator problem which we have been studying, with constant a_s , ψ_r , k_w and $\delta k_s = 0$ we have

$$a_w(z_e) = a_w(0) \frac{\bar{\alpha}^{-2}(\psi_r, \psi_o)}{\alpha^2(\psi_r)} \tag{4.17}$$

and hence, from Eq. (4.4) and (4.5)

$$z_e = \frac{L}{\eta_b(2 - \eta_b)} \left(\frac{\bar{\alpha}^{-2}(\psi_r, \psi_o)}{\alpha^2(\psi_r)} - 1 \right) \tag{4.18}$$

One easily sees that for a given η_b , there is a range of ψ_o about ψ_r such that Eq. (4.18) yields values of $z_e > L$. These correspond, of course, to particles which do not detrap. Fig. 4.3 provides a family of plots of $(\bar{\alpha}^{-2}(\psi_r, \psi_o)/\alpha^2(\psi_r))$ as a function of ψ_o for various values of ψ_r , and Figs. 4.4a and 4.4b present z_e as a function of ψ_o with η_b and ψ_r as parameters. Incidentally, the adiabatic theory of detrapping typically implies an upper bound of electronic efficiency for some designs. For the constant k_w, ψ_r, a_s wiggler the bound is found to be .672. If a_w rather than k_w is held constant, the bound is reduced to .544.

A numerical simulation of the constant k_w , ψ_r , a_s case has been carried out, based upon Eq. (2.25). The solution is used to compute (L) from Eq. (2.24) as a function of ψ_o for various values of η_b and ψ_r . The results of some of these computations are shown in in Fig. 4.5

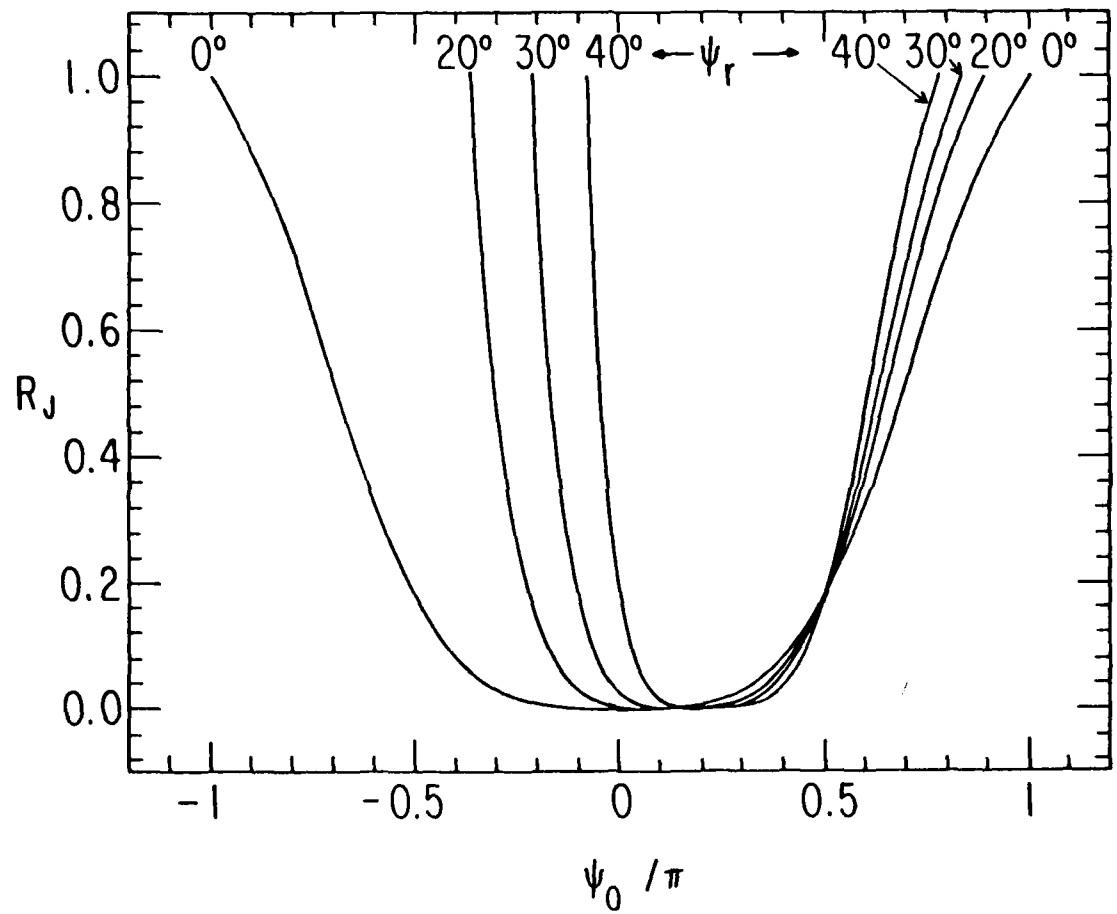

FIGURE 4.3

THE DETRAPPING FUNCTION $R_J(\psi_o, \psi_r) \equiv \bar{\alpha}^2(\psi_r, \psi_o)/\alpha^2(\psi_r)$ PLOTTED AS A FUNCTION OF INITIAL PHASE ψ_o FOR VARIOUS VALUES OF RESONANT PHASE ψ_r.

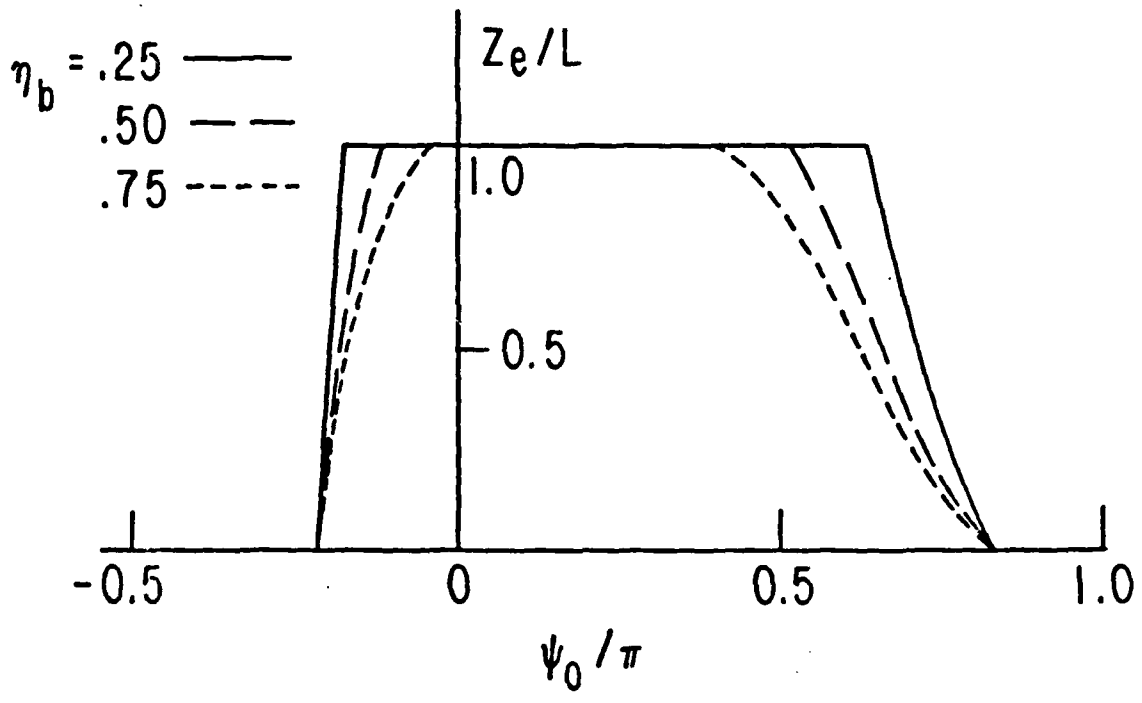

FIGURE 4.4a

DETRAPPING DISTANCE Z_e SHOWN AS A FUNCTION OF INITIAL PHASE ψ_o, WITH:

a) Bucket efficiency η_b as parameter

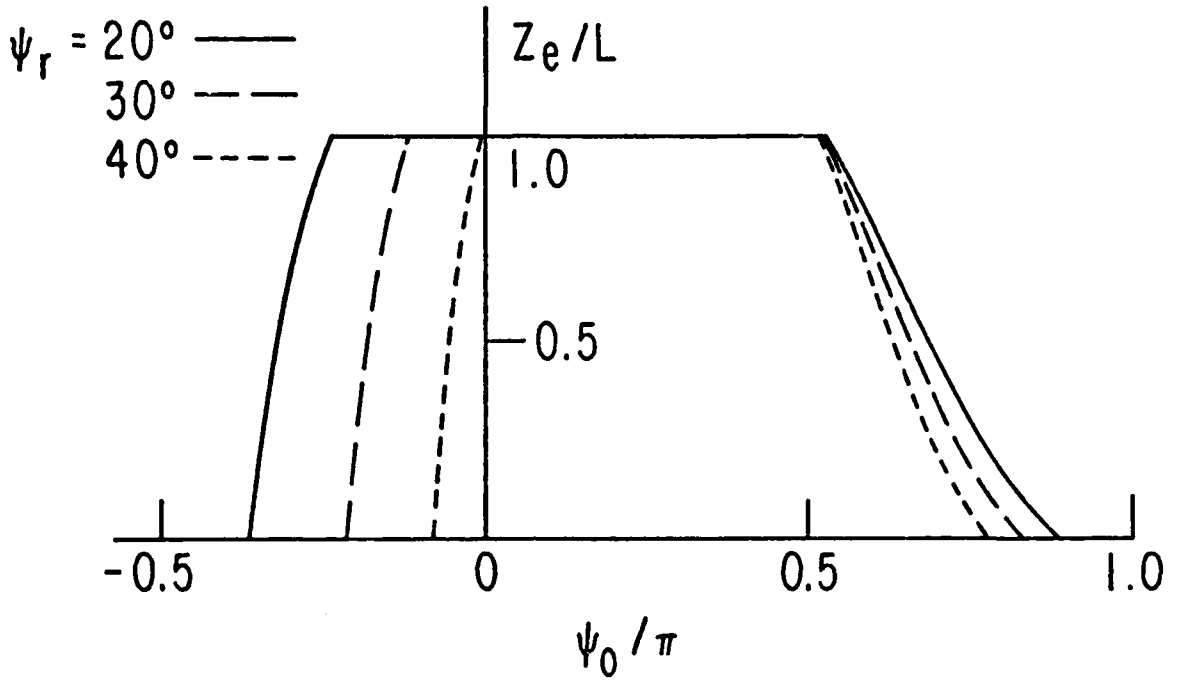

FIGURE 4.4b

DETRAPPING DISTANCE Z_e SHOWN AS A FUNCTION OF INITIAL PHASE ψ_o, WITH:

b) Resonant phase ψ_r as parameter.

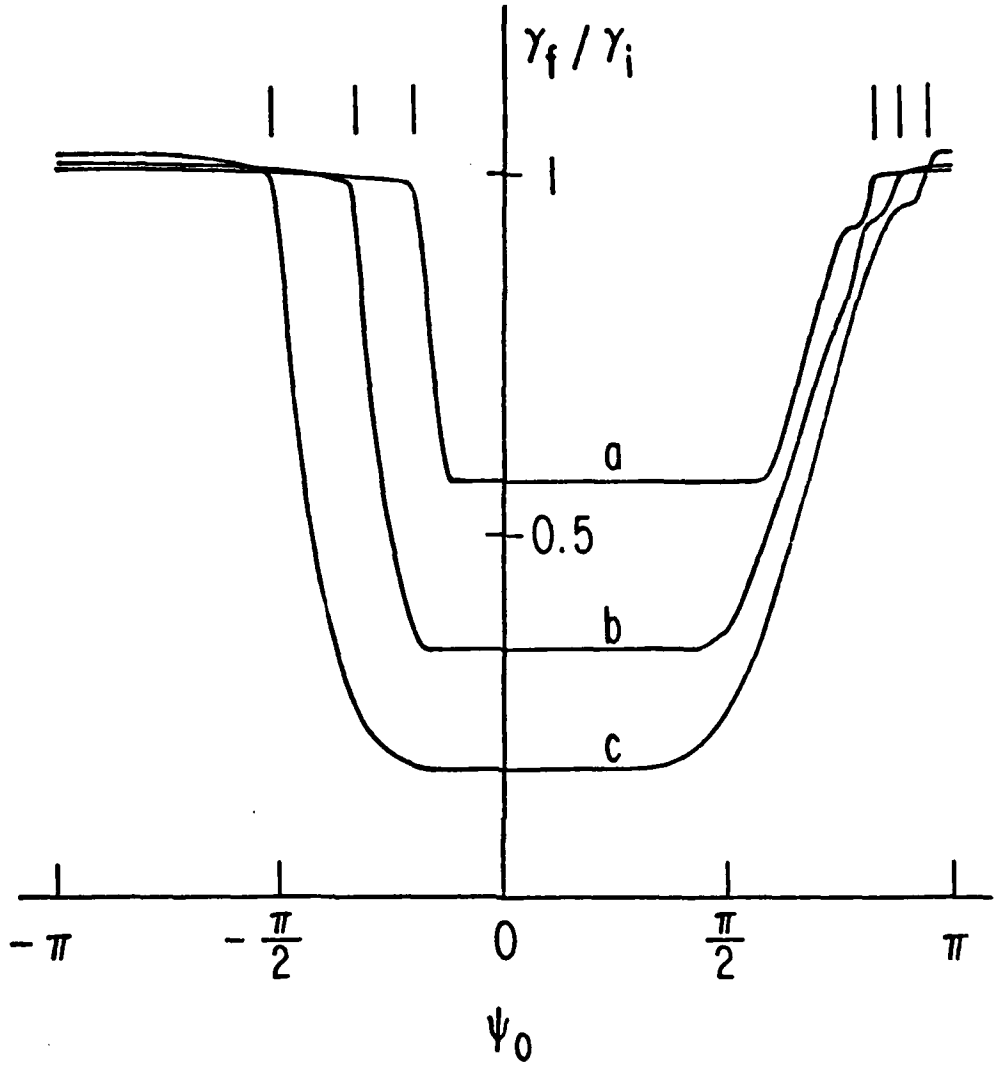

FIGURE 4.5

ENERGY SPECTRUM OF EMERGING ELECTRONS AS A FUNCTION OF ENTRY PHASE. ALL ELECTRONS ENTER WITH ENERGY EQUAL TO $\gamma_r(0)$. THE THREE CURVES REFER TO MINIMUM POWER CONFIGURATIONS OF THE SORT ILLUSTRATED IN FIGURE 4.2. THE PARAMETERS OF THE THREE CURVES ARE:

	η_b	ψ_r	η_i	η_e
a	.425	31.9°	.215	.181
b	.66	21.9°	.400	.314
c	.823	11.4°	.600	.448

THE VERTICAL LINES ABOVE THE CURVES DENOTE POSITIONS OF THE TRAPPING BOUNDARIES ψ_1 AND ψ_2.

for some of the minimum power configurations of Fig. 4.2. The flat portions at $\gamma(L)/\gamma_i = 1 - \eta_b$ corresponds to the range of ψ over which there is no detrapping.

The fact that the rapidly changing portions are not vertical is an indication that detrapping is taking place. The peculiar jog at the right hand end just before ψ_o reaches ψ_2 is due to particles which detrap after the first synchrotron oscillation. Note that untrapped particles gain energy. All of the curves shown are for $\gamma_i = \gamma_r$, with no energy spread included. They should be representative for a spread small compared to $\delta\gamma_{max}$. The numerical simulation also provides a value for the electronic efficiency η_e. Fig. 4.6 shows the extent to which η_e differs from η_i for the configurations of Fig. 4.2.

It is clear from Eq. (4.16) that detrapping can be avoided for the constant a_s case by designing the wiggler so that a_w/k_w is constant. As in the constant k_w, constant a_w, and constant b_w cases discussed previously one can use the condition of constant ψ_r and specified η_b to determine the z dependence of a_w and k_w, and the required power. The required threshold powers in the constant k_w, a_w, b_w, and a_w/k_w cases are compared in Fig. 4.7 as functions of η_b. Since the penalty due to detrapping is rather small, one actually obtains a better net efficiency from a constant k_w wiggler than from one which avoids detrapping. Some small improvement can probably be obtained over the constant k_w case by taking detrapping into account, but we have not pursued this question further. This assessment applies to the case in which the incident electron energy spread is small compared to $\delta\gamma_{max}$. When they are comparable, as is likely to be the case in practice, the penalty imposed by

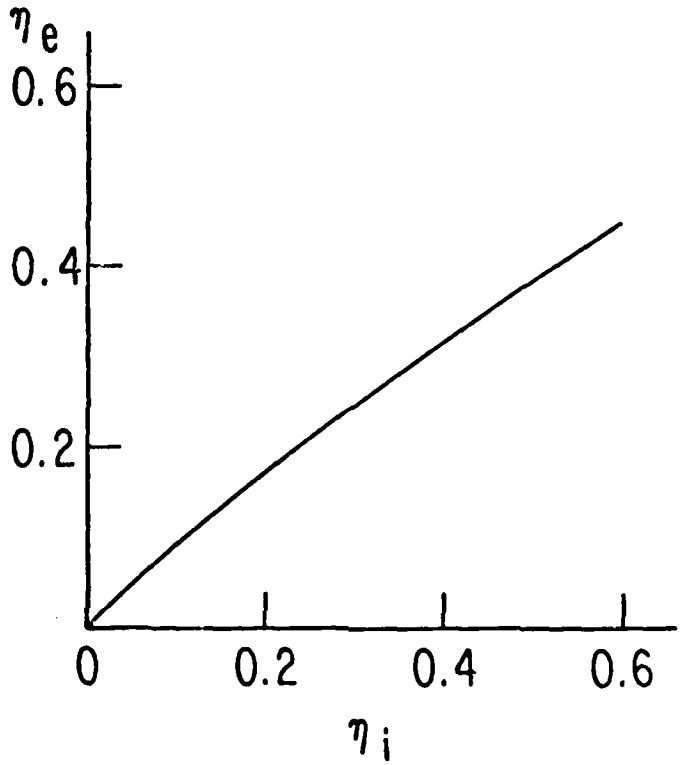

FIGURE 4.6

ELECTRONIC EFFICIENCY η_e AS A FUNCTION OF IDEAL EFFICIENCY η_i FOR THE MINIMUM POWER CONFIGURATION OF FIGURE 4.2.

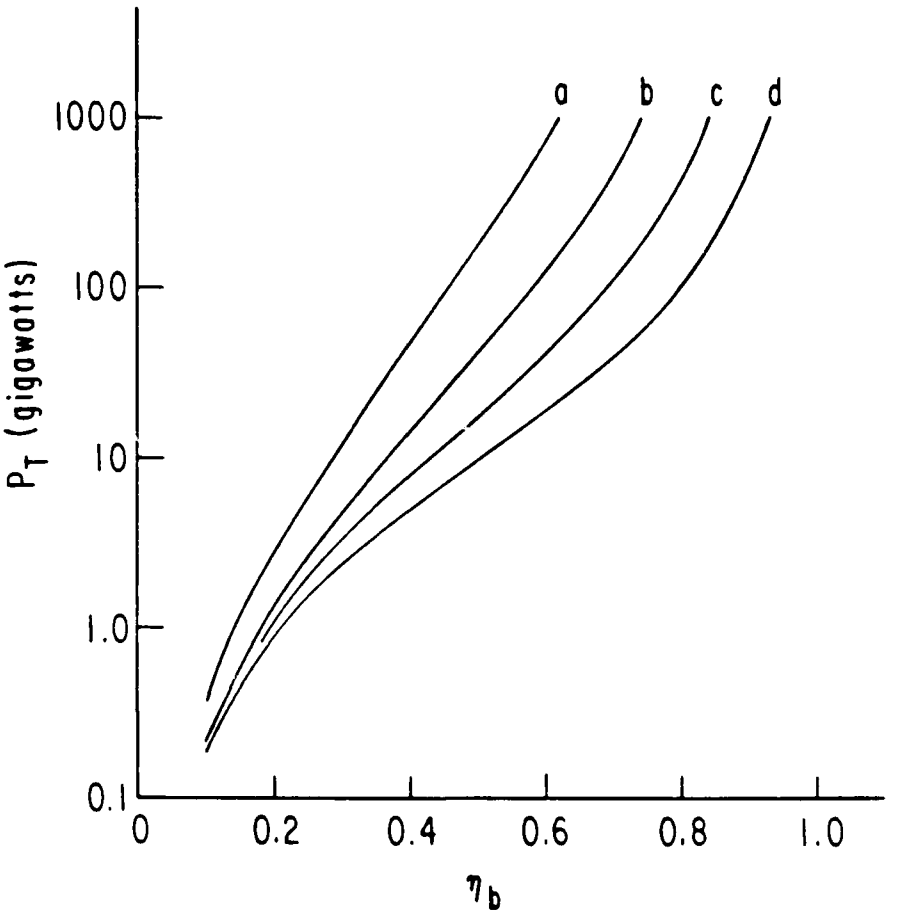

FIGURE 4.7

COMPARISON OF THRESHOLD POWERS AS FUNCTIONS OF η_b FOR VARIOUS CONSTANT ψ_r, CONSTANT a_s WIGGLER DESIGNS. THE FOUR CASES ARE:

a) Constant a_w/k_w

b) Constant a_w

c) Constant b_w

d) Constant k_w

detrapping increases, and its avoidance acquires more significance as a design consideration. It should be noted that in the case of an amplifier or heavily loaded oscillator, where a_s increases with z, detrapping tends to be avoided automatically, as discussed later in this section.

In all of the previous discussion we have imposed the requirement (largely to simplify the discussion) that ψ_r be z independent. One may ask whether this choice leads to an approximately optimized wiggler design. From the point of view of detrapping, it would be useful to have ψ_r decrease with z, to compensate for the decrease in a_w/k_w which seems to occur for the more optimum constant ψ_r designs. This is apparent from the behavior of $\alpha(\psi_r)$ [see Equations (4.13), (4.14) and (4.18)] shown in Fig. 2.6. On the other hand, from the point of view of initial capture, it would be best to have ψ_r have a very small, or even vanishing initial value. This can be seen from the plot of the trapping fraction, f_b, shown in Fig. 4.1. Thus to maximize trapping ψ_r should increase with z, while to avoid detrapping ψ_r should decrease with z. One can in principle increase a_w/k_w to overcome the effect of decreasing ψ_r and thus avoid detrapping, but experience with the constant ψ_r case suggests that this will not improve matters either. Hence the constant ψ_r, constant k_w design is probably not very far from an optimum one. Again in anticipation of the amplifier case, we note that an increase of a_s with z can eliminate the detrapping associated with an increase in ψ_r, so that an increase of ψ_r with z should have some advantages for an amplifier.

We conclude this discussion by listing the properties of a "standard" wiggler design, based upon the constant k_w case. It is certainly not unique and probably not optimal either, but it does provide a convenient point of reference for future discussion. We begin by specifying an idealized efficiency η_i, a signal frequency ω_s, and an electron beam radius r_e. The associated bucket efficiency, η_b, and resonant phase, ψ_r, are determined from η_i by Figure 4.2. For wiggler design parameters we then propose

$$k_w \cong \frac{1}{3r_e} \tag{4.19}$$

$$L \cong \frac{9}{8}\frac{\omega_s}{c} r_e^2 \tag{4.20}$$

$$a_w(z) = \frac{1 - \left(2\eta_b - \eta_b^2\right)(z/L)}{1-\eta_b} \tag{4.21}$$

$$B_w(z) = 1.7\, k_w a_w(z) \cong 1.7 \frac{a_w(z)}{3\, r_e(\text{cm})} \text{ Kilo Gauss} \tag{4.22}$$

the electron beam energy ε_e is given by

$$\varepsilon_e = mc^2\gamma_i \cong .51 \left[\frac{3}{2}\frac{\omega_s r_e}{c}\frac{2-2\eta_b+\eta_b^2}{(1-\eta_b)^2}\right]^{1/2} \text{ Mev} \tag{4.23}$$

The required peak beam current is given by

$$I_e = \frac{eP_m}{mc^2 \gamma_i \eta_e Q} \tag{4.24}$$

where Q is the "Q" of the optical resonator, and $\eta_e < \eta_i$, the electronic efficiency. Rewriting (4.24) yields

$$I_e = \frac{1}{Q(6\omega_s r_e/c)^{1/2}} \left(\frac{\eta_b^2 \csc^2 \psi_r}{\eta_e}\right) \frac{(2-\eta_b)^2}{(1-\eta_b)\left(2-2\eta_b+\eta_b^2\right)^{1/2}} \left(\frac{mc^3}{e}\right) \tag{4.25}$$

where

$$\left(\frac{mc^3}{e}\right) = 17.0 \text{ Kilo Amperes} \quad .$$

The degradations associated with the variation of the resonator mode over the electrons, as well as the effect of energy spread of the incident electrons have been neglected in the above. For assessing the effect of the latter we note the relation (using 4.8 and 2.56 together with the above).

$$\frac{\delta\gamma_{max}}{\gamma} = \frac{4\sqrt{3}}{3} \left(\frac{c\eta_b(2-\eta_b) \csc \psi_r}{\omega_s r_e \left(2-2\eta_b+\eta_b^2\right)}\right)^{1/2} \Gamma(\psi_r) \tag{4.26}$$

The electron beam radius which can be used is primarily determined by the electron beam emittance. It is shown in Appendix C that if one assumes ideal emittance scaling, then the beam radius must exceed a lower limit proportional to the emittance constant. Finally, we repeat that we have neglected the possiblity that some modification in the parametric dependencies may emerge if the omitted "σ" factors are taken into account.

It is instructive to illustrate the above expressions with a reasonable numerical example. Let us suppose we wish to construct a 1 micron oscillator. A preliminary perusal suggests that $\eta_i \approx .215$ might yield parameters achievable with current technology. Considerations bearing upon the choice of electron radius will be discussed in Appendix C, but for the moment we simply specify $r_e = 1.24$ mm. With these choices the following numbers emerge:

$\eta_e = .18$	$a_w = 1.75 - 1.18\ z/L$
$\eta_b = .43$	$B_w = 4.56 - 3.07\ z/L$ KG
$\psi_r = 32^o$	$E_e = 111$ Mev
$P_m = 21$ GW	$QI_e = 1100$ Amps.
$\lambda_w = 2.3$ cm	$\delta\gamma_{max}/\gamma = .014$
$L = 10.9$ m	

As indicated, the beam current, and accordingly the optical power generated (P_m/Q, of course), will depend upon the resonator Q which is chosen, and, on account of mirror losses, the optical power which emerges will be

reduced from that generated. Furthermore, we again emphasize that these are peak values. If the electron beam is provided by an RF linac, "peak" refers to values which obtain during a micropulse. Average values during a macropulse are reduced by a factor which typically lies between 25 and 100.

4.2 Operation with Amplifying Signal Amplitude

In discussing the behavior of the standard design the increase in the signal amplitude a_s was neglected. This neglect is justified for large values of Q. As one decreases Q we expect η_e to approach η_i more closely, but otherwise the basic formulas for the operation of the device are still expected to hold approximately despite the fact that a_s is increasing. The decrease in Q is likely to be associated with increased output coupling. This fact, together with the increase in η_e means that the extra beam power input associated with the increase in I_e is being more efficiently converted to signal power output.

These expectations are easily understood by making reference to Eq. (2.41), which we rewrite as

$$a_s \sin\psi_r \equiv -\frac{c\gamma_r}{\omega_s a_w}\frac{d\gamma_r}{dz} \tag{4.27}$$

The right hand side of this equation has already been determined by the standard design to be a constant. Associated with this design was an input value of a_s and an input value of ψ_r. However, if a_s increases, ψ_r simply decreases. Reference to Eq. (2.59) and Figure 2.6

tells us that the phase area of the bucket increases. Hence particles initially trapped remain trapped and apart from the small increase in energy of the untrapped particles, $\eta_e = \eta_i = \eta_b f_b$. Due to the fact that the bucket is actually widening, some initially untrapped particles may even become trapped, and η_e can exceed η_i . The important lesson to be learned is the fact that a more rapid than "planned" increase in a_s does no harm to the trapping and deceleration process. On the other hand if a_s increases less rapidly than planned, a reduction in phase area occurs which can lead to some detrapping. Indeed if a_s drops sufficiently below its planned value to require $\sin\psi_r > 1$,total detrapping takes place.

It should now be apparent that a simple way to design an amplifier is simply to remove the mirrors from the standard design and supply a beam current given by Eq. (4.25) with $1/Q$ replaced by $(G-1)$, where G is the power gain. The required input signal power is given by P_m .

In our discussion of high Q oscillators we established a quasi optimized connection between the minimum circulating power P_m and η_i . Clearly similar optimization could be desirable for an amplifier. The simple amplifier designed above makes no attempt to take a programmed increase of a_s into account in specifying its γ_r profile and hence is unlikely to be optimum in this respect. What we would wish to have is a procedure for designing the wiggler so as to maximize the efficiency for a specified power output and specified gain.

As a first example of a step in the desired direction we describe a procedure for choosing a_s (and hence γ_r) so as to maintain an

approximately constant ψ_r . In order to be specific we consider the constant k_w case. We then find from Eqs. (2.40) and (2.41), neglecting δk_s

$$a_w' = - \left(2k_w a_s(0) \sin \psi_r\right) \frac{a_s(z)}{a_s(0)} \tag{4.28}$$

Note that the coefficient in brackets is a constant. To relate $\frac{a_s(z)}{a_s(0)}$ to a_w we make use of Eq. (2.26), assuming that

$$\langle \gamma(0) \rangle - \langle \gamma(z) \rangle = \text{constant} \times \left(\gamma_r(0) - \gamma_r(z)\right) . \tag{4.29a}$$

This assumption is based upon the idea that the trapped electrons represent a constant fraction of the electrons, and that they give up energy at the rate $\frac{d\gamma_r}{dz}$. It yields the equation

$$\frac{a_s(z)}{a_s(0)} = \left[1 + (G-1) \frac{\mu(0)-\mu(z)}{\mu(0)-\mu(L)}\right]^{1/2} \tag{4.29b}$$

where G is again the power gain. Combining Eqs. (4.28) and (4.29) yields

$$\int_{a_w(L)}^{a_w(0)} \frac{da_w}{\left[1 + (G-1) \frac{\mu(0) - \sqrt{1 + a_w^2}}{\mu(0) - \mu(L)}\right]^{1/2}} = 2k_w L a_s(0) \sin \psi_r \tag{4.30}$$

The left hand side of Eq. (4.30) can be regarded as the analogue of the right hand side of Eq. (4.2), that is, as a quantity which in this instance

should be minimized with respect to $a_w(L)$ and $a_w(0)$ subject to the constraint $1 - \frac{\mu(L)}{\mu(0)} = \eta_b$. This condition then determines the appropriate values of $a_w(0)$ and $a_w(L)$ and hence $\mu(0)$ and $\mu(L)$. Subsequently $a_w(z)$ is determined from

$$\int_{a_w(z)}^{a_w(0)} \frac{da_w}{\left[1 + (G-1)\,\frac{\mu(0) - \sqrt{1 + a_w^2}}{\mu(0) - \mu(L)}\right]^{1/2}} = \frac{z}{L}\left(2k_w L a_s(0) \sin \psi_r\right) \tag{4.31}$$

As an example, we consider the case $\eta_b = .43$ and for simplicity neglect the final optimization. Instead we obtain $a_w(0)$ and $a_w(L)$ from Eq. (4.4), which holds for the G=1 case. For G=100, the value of the left hand side of Eq. (4.30) is found to be .203. This number for the right hand side of Eq. (4.30) should be compared to $a_w(0) - a_w(L) = 1.18$, which would be required by the simple amplifier design discussed previously in which a_w decreases linearly. Thus the improved wiggler profile permits a factor thirty reduction in the operating power level. The minimum of the left hand side of Eq.(4.30) is found to be very broad for G=100, so that the value obtained by choosing $a_w(0)$, $a_w(L)$ as noted above is within 1/2% of the minimum.

The predicted behavior of a_s is obtained from Eq. (4.29) by making use of $a_w(z)$ as given by Eq. (4.31). To complete this example we apply the standard procedure to the rest of the design. Hence we choose $\sin \psi_r$ from Figure 4.2 to obtain the value .53 and an η_i of .215. The

required optical input power is then 640 MW. Assuming an electronic efficiency equal to η_i and a gain of 100, we obtain a required electron beam power of 295 GW. Figure 4.8 shows the design behavior of a_w as given by Eq. (4.31) and a_s as given by Eq. (4.29) (curve d). It also shows the computed values of a_s and electronic efficiency as obtained from numerical simulation. The numerical simulation was based upon Eqs. (2.25) and (2.26), neglecting the δk_s terms, but explicitly carrying out the averages required for Eq. (2.26). Three cases are shown, corresponding to the design beam power, a somewhat higher power and a lower power. The design beam power does not quite yield the design performance. First we note that the expectation of the ideal electronic efficiency failed to take account of energy gain from the untrapped electrons. Second, Eq. (4.29a), the assumption of a constant ratio between $\gamma_r(0) - \gamma_r(z)$ and $\langle\gamma(0)\rangle - \langle\gamma(z)\rangle$, is clearly not satisfied at the input of the amplifier. The flat behavior of a_s at the input reflects the fact that bunching must take place before amplification can begin. We see that increasing the beam power improves the efficiency as well as providing more than the design gain. The reduced beam power example illustrates the effect of a smaller increase in a_s than was anticipated in the wiggler design. Equation (4.27) causes ψ_r to constantly increase, continually detrapping particles, until at $z/L \sim .8$, ψ_r has reached $\frac{\pi}{2}$. All particles are detrapped and amplification has ceased.

Because a_s is an increasing function of z it should be possible to allow ψ_r to increase with z without detrapping particles. One simply requires that the phase area J, given by

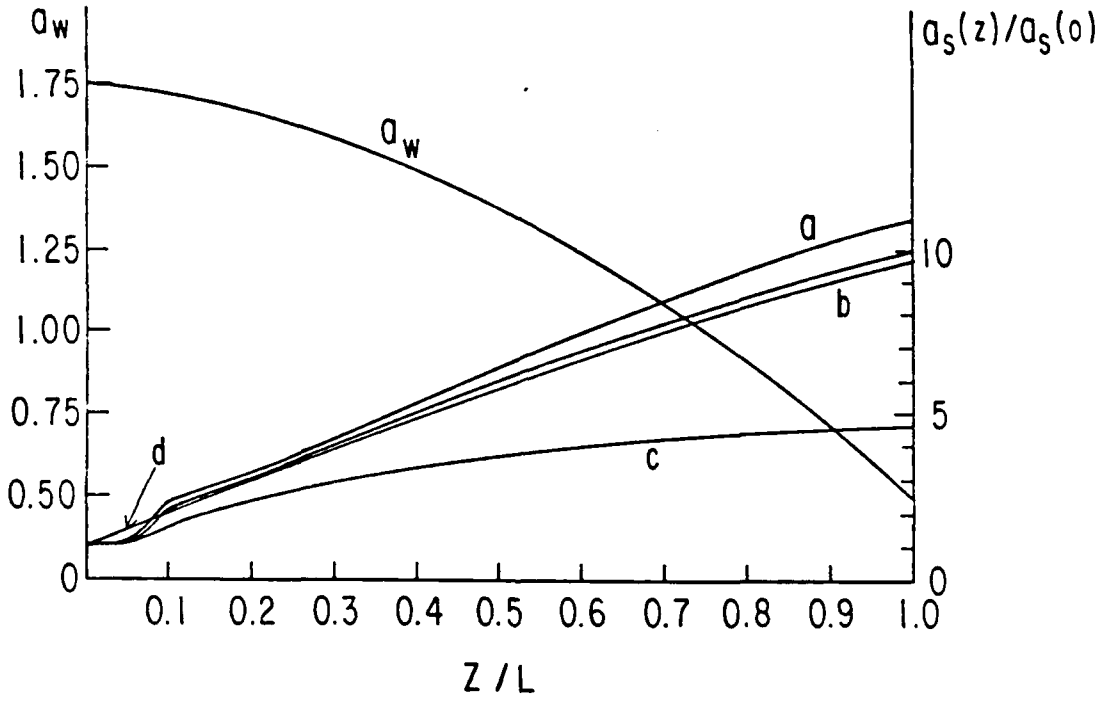

FIGURE 4.8

SIMULATED PERFORMANCE OF A MATCHED PROFILE AMPLIFIER.

	Peak Electron Beam Power	Electronic Efficiency
a)	350 GW	.214
b)	295 GW	.203
c)	145 GW	.091

Curve d shows the $a_s(z)/a_s(0)$ profile obtained using Eq. (4.29a).

Eq. (2.59), not decrease. Indeed, by choosing $\frac{d\gamma_r}{dz}$ to vanish at the input one can begin by trapping all particles, since ψ_r will initially be zero. Since a_s will at each z increase monotonically with increasing beam power, there will always be a critical beam power above which all particles remain trapped, so that $f_b = 1$ and $\eta_e = \eta_b$. Whether it is better to use the beam power to increase f_b to unity rather than to increase η_b is a question which we have not explored.

The amplifier length provides another quantity which can be varied as a part of an optimization procedure. In our discussion up to this point we have assumed the length to be given by Eq. (4.20), but there is, however, no compelling reason to limit the length in this way.[21] It can be argued that so long as the rate of amplification is sufficiently great to maintain a_s constant on the electron beam (i.e., to counter the effect of diffraction spreading) the device can in principle be arbitrarily long. It appears likely that δk_s can also play an important role in this situation. We have not, however, carried out a complete analysis of this super-long amplifier and will not discuss it further here.

In our discussion of the amplifier we have consistently neglected δk_s. It would of course be a straightforward matter to include it in carrying out simulations. It appears as an order $\frac{\delta k_s}{k_w}$ correction to Eqs. (2.24) and (2.25). Just as a local value of $a_s^2(z)$ is obtained from Eq. (2.26), a local value of δk_s can be obtained from Eq. (2.36). For the case illustrated by Figure 4.8 we consider that $\langle \cos \psi/\gamma \rangle = 0$ for the first five percent of the amplifier, so that δk_s is in fact zero

initially. For the region in which a_s increases approximately linearly it is likely that $\frac{\langle \cos \psi/\gamma \rangle}{\langle \sin \psi/\gamma \rangle} \approx 1$ so that $\delta k_s = \frac{a_s'}{a_s} \approx \frac{9}{(L + 9z)}$ and we estimate $\delta k_s < \frac{10}{L}$ everywhere. Thus $\frac{\delta k_s}{k_w} < .003$ everywhere, so that its neglect appears to be justified so long as transverse effects are ignored.

We conclude this section by pointing out the fact that the neglect of transverse effects appears to be especially suspect for the design and analysis of amplifiers. In the amplifier illustrated in Figure 4.8, and in the qualitative discussion of other designs that followed we have depended upon the predicted growth of a_s to maintain the electron traps. We have assumed in carrying out the design, and in the simulations, that there is no transverse variation in the signal amplitude. This certainly will not be the case in actuality. Suppose, for example, that the electron beam has a Gaussian profile. Then we may write for Eq. (2.37)

$$a_s' = \frac{\omega_p^2(0)}{2\omega_s c} a_w \langle \sin \psi/\gamma \rangle \exp\left(-r^2/r_e^2\right) \tag{4.32}$$

Where $\langle \sin \psi/\gamma \rangle$ should also be assumed to be r dependent. We also have Eq. (4.27), which implies that $a_s \sin \psi_r$ is r independent. Suppose the amplifier has been designed so that ψ_r remains constant in z at some value of $r = r_d$. For smaller values of r we expect a_s to increase more rapidly, ψ_r decreases and trapping is unaffected. For particles outside r_d, a_s increases less rapidly than programmed. Detrapping can be

expected to develop at larger r and progressively work its way into r_d. This could lead to a decrease of amplitude at r_d itself and hence a progressive erosion of the edge. A similar erosion may be expected to occur at the trailing edge of the pulse. Thus while electrons at the trailing edge can initially be trapped by the input signal, the failure of the signal to amplify at the rear edge will lead to a progressive detrapping that moves up the pulse. These considerations suggest that some of the advantages of sophisticated designs over the "simple" design (in which one depends upon the initial amplitude to maintain trapping throughout) may be substantially reduced.

The situation is further complicated by the fact that

$$\delta k_s = \frac{\omega_p^2(0)}{2\omega_s c} \frac{a_s'}{a_s(r,z)} \langle \cos \psi/\gamma \rangle \exp\left(-r^2/r_e^2\right) \tag{4.33}$$

The presence of this variation tends to focus light towards the center, reinforcing the tendencies discussed in the preceding paragraph. In the amplifier illustrated in Figure 4.8 we estimated $\delta k_s \sim \frac{9}{L + 9z}$ for $z > .1\ L$. According to Eq. (4.33) this value should be construed as refering to the center of the beam so long as the variation of a_s and $\langle \cos \psi/\gamma \rangle$ with r is neglected. Because δk_s decreases with z, the focusing tendency is largest near the beginning of the amplifier. To obtain a crude quantitative estimate we consider the problem to be one of propagation of rays in a lenselike medium, with index of refraction given by $\delta n = c\delta k_s/\omega_s$. According to the paraxial ray equation, we have

$$\frac{d^2 r(z)}{dz^2} = \frac{d\delta n}{dr} \tag{4.34}$$

where $r(z)$ is the ray coordinate. We confine our attention to the central portion and write

$$\frac{d\delta n}{dr} = -\frac{2r}{r_e^2}(\delta n)_{r=0} \equiv -\frac{2r}{r_e^2}\delta n_o \tag{4.35}$$

Taking advantage of the fact that $r_s dn_o/dz$ is small we obtain, for a ray emitted at $z = z_1$ with zero slope,

$$r(z) = r(z_1)\sqrt{\frac{\delta n_o(z_1)}{\delta n_o(z)}}\left[\cos\int_{z_1}^{z}\sqrt{2\delta n_o}\,dz/r_e + \left(\frac{\delta n_o' r_e}{(2\delta n_o)^{3/2}}\right)_{z_1}\sin\int_{z_1}^{z}\sqrt{2\delta n_o}\,dz/r_e\right] \tag{4.36}$$

For the amplifier of Fig. 4.8, using the above mentioned estimate of δk_s we find for $z_1 = .1\ L$ that focus takes place at $z = .71\ L$. This presumably overestimates the effect because we have neglected the fact that the focusing effect further increases a_s, thus reducing δk_s. (The factor $\langle\cos\psi/\gamma\rangle$ also increases, but the size of the increases is limited by the fact that $|\cos\psi| < 1$, and the increase in a_s is the dominant effect). Nevertheless this estimate suffices to indicate that the effect can be significant. We remark that Eq. (4.33) does not necessarily imply that δk_s is a maximum in the center as the increase in a_s can dominate

other effects. The presence of this factor in the denominator also indicates that a true self focusing instability does not exist. The effect clearly decreases when the gain is smaller, so that the net outcome could simply be a limit on useable gain. On the positive side, the focusing effect can also lead to some optical beam trapping, which could be helpful for devices with $L > kr_e^2$. Clearly the complex of issues raised here constitutes an important subject for further research.

As a final comment we note that for an oscillator,

$$\int_0^L \delta k \, dz \sim \frac{1}{2Q} \tag{4.37}$$

This should be compared to the total phase shift, $2 \tan^{-1} .5$, which occurs in the traverse of the wiggler due to diffraction. As a consequence, low Q oscillators may require some small optical correction to take into account both the effect and the fact that it may vary during buildup of oscillation. Apart from this possibility, the δk_s effect does not appear to affect oscillator operation.

5.0 ADIABATIC CAPTURE, DECELERATION, AND DECAPTURE

In this section we will treat the problem of capturing the electrons into a stationary bucket with a resonant energy equal to the mean electron energy, while at the same time minimizing the increase in the phase area occupied by the electrons. After capture the average phase angle of the electrons must be changed to a positive value, so that the electrons can be placed in the center of a moving bucket and subsequently decelerated. For a single pass device it will be only necessary to make sure that the phase area of the captured electrons is less than the area of the decelerating bucket. However, for a multiple pass system we want to *minimize the increase* in phase area occupied by the beam. After the beam has been decelerated the average phase angle of the electron is returned to zero and placed in a new stationary bucket with a resonant energy equal to the final mean electron energy. Finally the decapture is performed in such a manner as to achieve the small desired energy spread. The total purpose of all of these processes is to obtain a minimum increase in the energy spread while at the same time to reduce significantly the average electron energy.

To illustrate these processes we divide the wiggler into five regions: region one, with $0 < z < z_1$, is where the adiabatic capture occurs; region two, with $z_1 < z < z_2$, is where the average phase angle is increased; region three, with $z_2 < z < z_3$, is where the deceleration occurs; region four, with $z_3 < z < z_4$, is where the average phase angle

is decreased to zero; and region 5, with $z_4 < z < z_5$, is where the decapture occurs. The phase space occupied by the electrons during various stages of these processes is shown as the shaded area in Figs. (5.1a to 5.1h).

Region 1

In order to capture all of the electrons without increasing the phase area occupied by the electrons it is necessary to use a stationary bucket, i.e. $\psi_r = 0$, and to adiabatically increase the height of the bucket. From Eq. (2.51) we see that for $\psi_r = 0$ the bucket height $\delta\gamma_{max}$ is given by

$$\delta\gamma_{max} = \frac{2\gamma_r \sqrt{a_w a_s}}{\sqrt{1 + a_w^2}} \quad . \tag{5.1}$$

We want to start with $\delta\gamma_{max} = 0$ at $z = 0$ and increase $\delta\gamma_{max}$ with z while keeping $\psi_r = 0$. This may be accomplished by having a_w increase with z while demanding that k_w also increase with z to maintain the condition

$$k_w(z) = \frac{k_s}{2\gamma_r^2} \left[1 + a_w^2\right] \tag{5.2}$$

Since $\delta\gamma_{max}(0) = 0$ and γ_r is a constant, equal to $\gamma_r(0)$, we must have

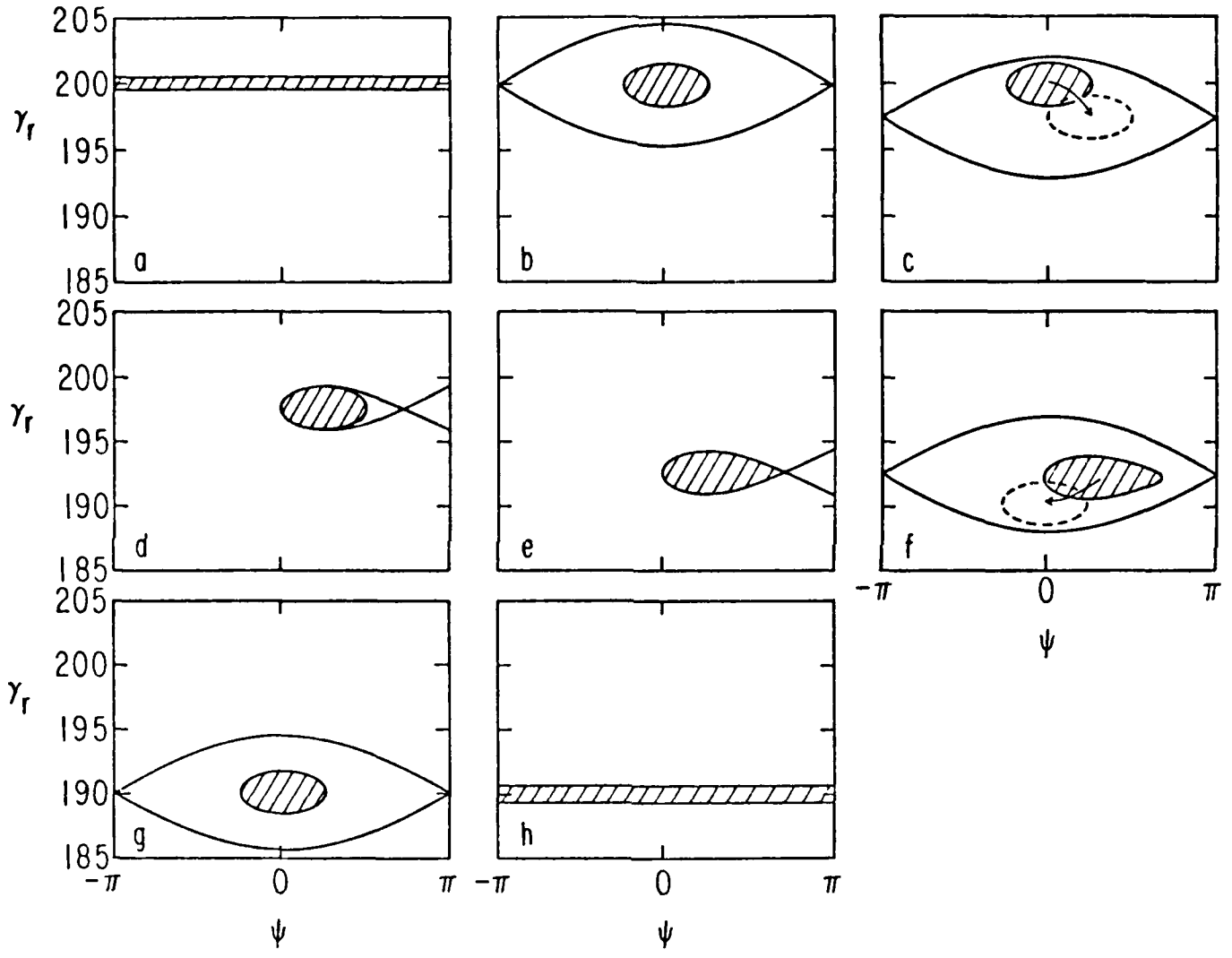

FIGURE 5.1(a)-(h)

SCHEMATIC BEHAVIOR OF THE γ, ψ PHASE SPACE DISTRIBUTION AS A FUNCTION OF 3 DURING AN ADIABATIC CAPTURE, DECELERATION, AND DECAPTURE PROCESS: (a.) INITIAL DISTRIBUTION. (b.) DURING CAPTURE. (c.) DURING INCREASE OF AVERAGE ψ. (d.) AND (e.) THE DECELERATION PROCESS. (f.) DURING DECREASE OF AVERAGE ψ. (g.) DURING DECAPTURE. (h.) AFTER DECAPTURE.

$$a_w(0) = 0 \quad \text{and} \quad k_w(0) = \frac{k_s}{2\gamma_r^2} \tag{5.3}$$

We combine Eqs. (5.1) and (5.2) and obtain

$$[\delta\gamma_{max}(z)]^4 = \frac{4k_s^2 a_s^2 [k_w(z) - k_w(0)]}{k_w^2(z) k_w(0)} \tag{5.4}$$

From Eq. (5.4) it follows that the maximum value of the bucket height occurs for a value $k_w(z) = 2k_w(0)$ corresponding to a value of $a_w(z)$ equal to one. It is desirable to have a large value for the final bucket height so we assume that region one of the wiggler is designed to increase both the magnetic field a_w and the wave number k_w to the final values:

$$k_w(z_1) = 2\, k_w(0) \tag{5.5}$$

$$a_w(z_1) = 1 \tag{5.6}$$

which yields a final bucket height

$$\delta\gamma_m(z_1) = \gamma_r \sqrt{2a_s} \tag{5.7}$$

Note that the final value of the fractional bucket height, $\frac{\delta\gamma_m(z_1)}{\gamma_r}$, is dependent upon only the field strength and the wavelength of the radiation. In order to capture all of the electrons in the bucket it is necessary for the initial energy spread in the beam before capture to be less than the final bucket area, i.e.

$$2\pi \left(\frac{\delta\gamma}{\gamma}\right)_{\text{initial}} < 8 \frac{\delta\gamma_m}{\gamma} \tag{5.8}$$

While Eqs. (5.5) and (5.6) give the final values for the wiggler wavelength and magnetic field necessary to achieve the maximum bucket area for capture, the exact speed and method of achieving these final values have yet to be determined. In order to satisfy the adiabatic condition, the change in k_w and a_w must be sufficiently slow. The exact number of phase oscillations that are needed for the adiabatic condition depends upon with what accuracy one needs the phase area to remain constant and will require computer studies for the motion of a large number of particles. However, as a rule of thumb the capture length must be long compared to the final phase oscillation period, i.e.

$$z_1 >> \frac{\pi\gamma_r^2}{k_s}\sqrt{\frac{2}{a_s}} \tag{5.9}$$

From Eq. (5.9) we see that it is desirable to have a low resonant energy and a high optical field in order to have a short capture length. The exact form of the change in k_w and a_w has only one constraint given by Eq. 5.2, so we are free to chose the simple form:

$$k_w(z) = k_w(0)\left[1 + \left(\frac{z}{z_1}\right)^{2\alpha}\right] \quad \text{, and} \tag{5.10}$$

$$a_w(z) = \left(\frac{z}{z_1}\right)^{\alpha} \tag{5.11}$$

with α a constant.

Region 2

In order to decelerate the electrons, after the adiabatic capture has been completed, it is necessary first to change the average phase of the electrons from zero to a positive value $\bar{\psi}(z_2)$. There are many possible programs for the variation of k_w and a_w that can be used to accomplish this change; as one example, we will describe one simple program below. From the preceding section we have shown that at the end of the adiabatic capture region ($z = z_1$) the values for the wiggler period, magnetic field and bucket height are given by Eqs. (5.5 to 5.7), and the average particle phase and energy are equal to $\bar{\psi}(z_1) = \psi_r(0) = 0$ and $\bar{\gamma}(z_1) = \gamma_r(0)$. Consider the case where the wiggler period and magnetic field are changed discontinuously at $z = z_1$ such that for $z > z_1$

$$k_w = k_w(z_1)\,[1 + f] \quad \text{and} \tag{5.12}$$

$$a_w = a_w(z_1) \tag{5.13}$$

with $f << 1$.

We can regard this as a discontinuous change in the definition of γ_r such that for $z > z_1$

$$\gamma_r = \gamma_r(0)\,[1 - f/2] \tag{5.14}$$

with ψ_r still equal to zero. For the case where the change in γ_r is less than the bucket height $\delta\gamma_m$ the center of the electron bunch will

proceed to perform synchrotron oscillations about the new value of γ_r (see Fig. 5.1c), with the maximum change in $\bar{\psi}$ occurring after one-quarter of a synchrotron oscillation period. If, on the other hand, the change in the value of γ_r is greater than the bucket height, the magnitude of the increase of $\bar{\psi}$ will not be limited (i.e. the electrons are detrapped). Because we want to prevent an increase in the phase area occupied by the bunch we need to change the phase and energy of all of the electrons in the bunch in a coherent manner. This can be achieved if all of the electrons in the bunch are near enough to the new bucket center to be in the linear region. In order to be able to accomplish this it is necessary that the phase area occupied by the bunch must be small compared to the bucket area and the change in the bucket center must be smaller than its height. This second condition yields

$$(f/2)\gamma_r < \delta\gamma_m \tag{5.15}$$

If the restriction of Eq. (5.15) is satisfied, the average values of ψ and γ are equal to the central values, and we find that after one-quarter of an oscillation $\bar{\psi}$ reaches its maximum value

$$\bar{\psi}_m = f \frac{\gamma_r}{\delta\gamma_m} \tag{5.16}$$

while the average energy of the bunch has changed by

$$\Delta\bar{\gamma} = - f/2\ \gamma_r(0) \tag{5.17}$$

Region 3

With the new values of $\bar{\psi}$ and $\bar{\gamma}$ it is now possible to use a tapered wiggler, as was discussed in detail in Section 4, to produce a decelerating bucket and to decrease the energy further. The energy of the bunch has already been decreased during the process of increasing $\bar{\psi}$ and if the desired energy extraction is sufficiently small it may be possible to skip the decelerating region entirely.

Region 4

In this region, with $z_3 < z < z_4$, we must reduce the average phase angle to zero in preparation for the decapture; as an example we choose a program similar to that used in region 2. That is we choose k_w and a_w such as to produce a stationary bucket with a resonant energy equal to $\bar{\gamma}(z_3)$ and allow the bunch to perform one-quarter of an oscillation so that $\bar{\psi}$ returns to zero (see Fig. 5.1f). The new average phase angle and energy at $z = z_4$ is given by

$$\bar{\psi}(z_4) = 0 \qquad \text{and} \tag{5.18}$$

$$\bar{\gamma}(z_4) = (1 - f/2)\ \bar{\gamma}(z_3) \tag{5.19}$$

Note that if major decelerating region 3 is eliminated the total energy change is

$$\Delta\gamma = \bar{\gamma}(z_4) - \bar{\gamma}(0) = - f\gamma_r \tag{5.20}$$

which corresponds to jumping the stationary bucket down in energy by $- f/2\ \gamma_r$ and allowing the bunch to perform one-half of a phase oscillation.

Region 5

In the fifth and final region, with $z_4 < z < z_5$, the electrons are debunched by allowing the magnetic field to decrease to zero. This process is the reverse of the capture process of region 1 and also must be done adiabatically in order to conserve the electron phase space density. It follows that the wiggler period must increase such that $\bar{\psi}$ remains zero and γ_r = constant . First the center of the bucket must be placed at a value of $\gamma_r = \bar{\gamma}(z_4)$ by a discontinuous change in the wiggler period and field such that for $z > z_4$

$$k_w(z) = (1 - f)\ k_w(z_4) \tag{5.21}$$

$$a_w(z) = a_w(z_4) \tag{5.22}$$

Next we must decrease the bucket area to zero to decapture the electrons; for simplicity we choose the reverse of the form chosen for the adiabatic capture in region 1, i.e. for $z_4 < z < z_5$

$$k_w(z) = \frac{k_w(z_4)}{2}\left[1 + \left(\frac{z_5 - z}{z_5 - z_4}\right)^{2\alpha}\right] \tag{5.23}$$

and

$$a_w(z) = \left(\frac{z_5 - z}{z_5 - z_4}\right)^{\alpha} \tag{5.24}$$

It is clear that an arbitrarily long wiggler magnet could in this way decelerate electrons while producing little energy spread. However, in order to determine whether or not the scheme is a promising one, further analysis is required. Especially, a more quantitative estimate is needed of the number of oscillations required in the adiabatic trapping and detrapping steps of the process. Furthermore, because of the additional length associated with these steps, a more severe side band instability problem (see Sec. 7) may be anticipated.

6.0 PHASE AREA DISPLACEMENT

In order that a large fraction of the electrons be decelerated and hence transfer energy into the optical field for the operational modes of the FEL described in the previous sections, it was necessary that the energy spread of the incoming electron beam be less than the maximum bucket height. In this Section we will discuss the method of phase area displacement[11] which can allow all of the electrons to be decelerated even when the initial energy spread (or effective energy spread when transverse emittance and magnetic field variation with beam size are included) is considerably larger than the bucket height. Phase area displacement refers to an operational mode in which an empty bucket is accelerated through the phase area of the beam with the result that the phase area occupied by the electrons is displaced downward in energy. Consider the case where the accelerating bucket starts with a resonant energy far below the energy of the electrons in the beam and is adiabatically moved through the beam until the final resonant energy is far above the electron's energy, as illustrated in Fig. 6.1. Note that for an accelerating bucket $\psi_r<0$. The final mean energy of the electrons is lowered by the phase area of the empty accelerating bucket divided by 2π , while the final energy spread of the beam is nearly equal to the initial energy spread, i.e.,

$$\langle\gamma(0)\rangle - \langle\gamma(L)\rangle = \frac{1}{2\pi} J \tag{6.1}$$

$$\Delta\gamma_f \sim \Delta\gamma_i \tag{6.2}$$

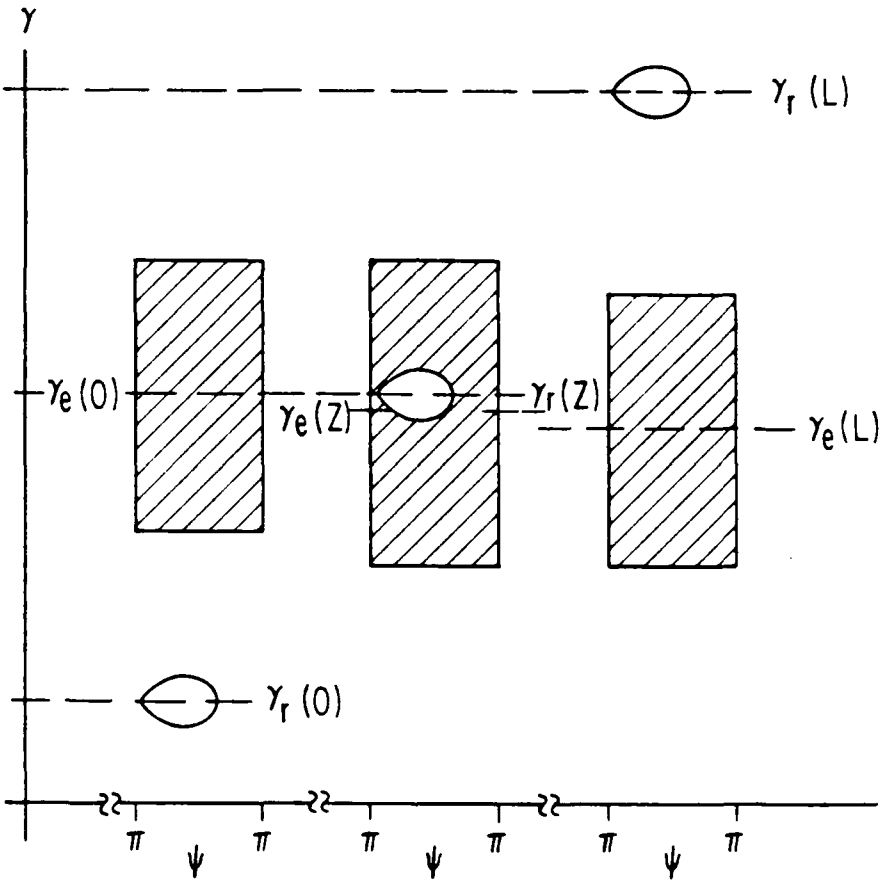

FIGURE 6.1

POSITION OF EMPTY BUCKET AND PHASE
AREA OF ELECTRONS AT VARIOUS POSITIONS
IN THE FEL.

where J is the area enclosed by the accelerating bucket and is given by Eq. (2.59). From Fig. 6.1 we see that the total change in γ_r must be much larger than the sum of the bucket height and the energy spread in the beam, i.e.

$$[\gamma_r(L) - \gamma_r(0)] \sim \gamma_r' L >> 2\,(\delta\gamma)_{max} + \Delta\gamma_{spread} \quad . \tag{6.3}$$

As long as both the adiabatic condition, which is discussed below, and the above condition are met, the energy spread of the beam is not greatly increased and the average energy loss of the electrons is independent of the initial energy spread. We note that the Hamiltonian for the particle motion as given by Eq. (2.44) is

$$H_4 = \frac{k_w}{\gamma_r}(\delta\gamma)^2 - \frac{\omega_s a_w a_s}{c\,\gamma_r}(\cos\psi + \psi \sin\psi_r) \quad . \tag{6.4}$$

It is convenient to use a transformation of the independent variable

$$du = \frac{2k_w}{\gamma_r}\,dz \quad , \tag{6.5}$$

to define a new Hamiltonian

$$H_5(\psi,\delta\gamma,u) = \frac{(\delta\gamma)^2}{2} - \Lambda\,(\cos\psi + \psi\sin\psi_r) \quad , \tag{6.6}$$

with

$$\Lambda = \left[\frac{\omega_s a_w a_s}{2 k_w c}\right] \quad . \tag{6.7}$$

If ψ_r is a constant, less than zero for an accelerating bucket, then for the wiggler design with $\frac{a_w}{k_w}$ = constant, the Hamiltonian is a constant of the motion; for simplicity we will specialize to this case to derive an analytical expression for the rms energy spread for the beam after passing through the FEL.

The equation for the rate of change in the synchronous energy in terms of u can be obtained from Eqs. (2.41) and (6.5)

$$\frac{d}{du}\gamma_r = -\Lambda \sin\psi_r \quad . \tag{6.8}$$

The rate of change for the total energy, $\gamma = (\delta\gamma + \gamma_r)$, follows directly from Hamilton's equation $\frac{d(\delta\gamma)}{du} = -\frac{\partial H_5}{\partial\psi}$ which when combined with Eq. (6.8) yields

$$\frac{d}{du}\gamma = -\Lambda \sin\psi \quad . \tag{6.9}$$

We can use the fact that H_5 is a constant of the motion along with Hamilton's equation $\frac{d\psi}{du} = \frac{\partial H_5}{\partial(\delta\gamma)}$ to obtain

$$\frac{d\psi}{du} = \delta\gamma \tag{6.10}$$

and

$$\delta\gamma = \mp\sqrt{2}\left|\bar{H} + \Lambda\left(\cos\psi + \psi\sin\psi_r\right)\right|^{1/2} \quad . \tag{6.11}$$

Thus the change in energy is given by

$$\Delta\gamma = -\frac{\Lambda}{\sqrt{2}} \int \frac{\mp (\sin\psi)\, d\psi}{\sqrt{\bar{H} + \Lambda(\cos\psi + \psi \sin \psi_r)}} \quad . \tag{6.12}$$

We are considering an electron which passes completely around the bucket, i.e., ψ starts at a large negative value ψ_1, reflects at ψ_f, and returns to a large negative value ψ_2 as shown in Fig. 6.2. We neglect the quantities which oscillate rapidly as ψ_1 and $\psi_2 \to -\infty$, neglect ψ_f compared to ψ_1 and ψ_2, and note that $\bar{H} = -\Lambda(\cos\psi_f + \psi_f \sin\psi_r)$ to find

$$\Delta\gamma = -\Lambda\sqrt{2} \int_{-\infty}^{\psi_f} \sin\psi_r d\psi \left[\frac{1}{\sqrt{\bar{H} + \Lambda(\cos\psi + \psi\sin\psi_r)}} - \frac{1}{\sqrt{\bar{H} + \Lambda(\cos\psi_f + \psi\sin\psi_r)}} \right]. \tag{6.13}$$

If we know the probability of an electron having a certain value of ψ_f then we can use Eq. (6.13) to calculate both the average energy change of electrons, $\overline{\Delta\gamma}$, and the final rms spread.

The evaluation of Eq. (6.13) is rather complicated and details are given in Appendix B. A further energy spread is expected from the fact that the bucket is of course not moved up from $-\infty$ to $+\infty$ but has a finite energy traverse

$$2\,\Delta\tilde{\gamma} = \gamma_r(L) - \gamma_r(0) \quad . \tag{6.14}$$

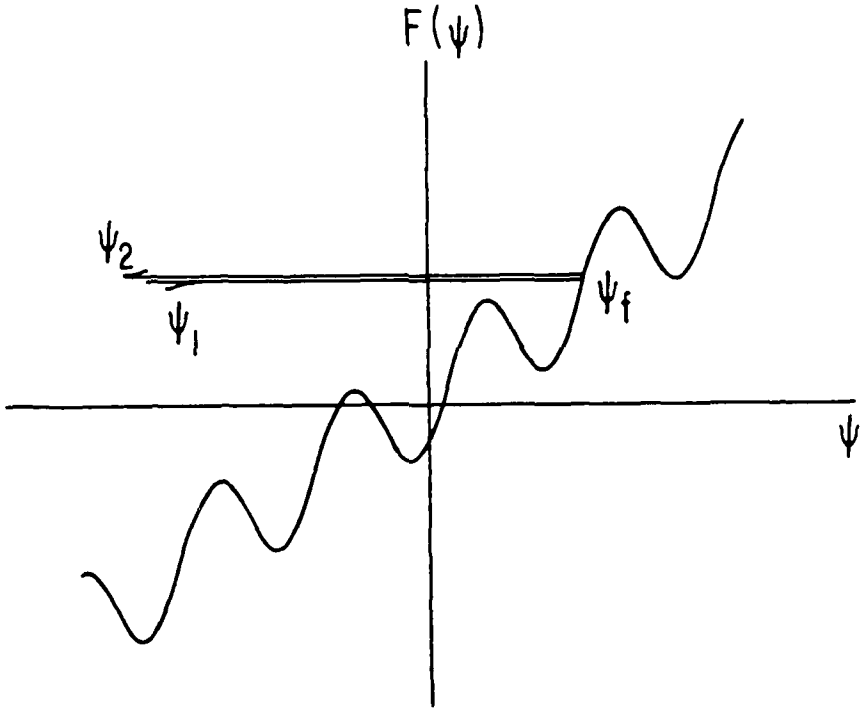

FIGURE 6.2

MOTION OF ELECTRON IN POTENTIAL
WELL OF AN ACCELERATING BUCKET

The additional energy spread due to the end points is uncorrelated with the spread due to the spread calculated above and the two spreads should be added in quadrature. This effect also is considered in Appendix B where it is shown that for $\psi_r << 1$, the average energy gain is given by

$$\overline{\Delta\gamma} = \frac{8}{\pi}\sqrt{\Lambda} \quad , \tag{6.15}$$

and the ratio of rms energy spread to energy gain is approximately given by

$$\frac{(\Delta\gamma)\text{rms}}{\overline{\Delta\gamma}} = \sqrt{\sin^2\psi_r + \frac{\pi^4}{(64)^2}\left(\frac{\overline{\Delta\gamma}}{\widetilde{\Delta\gamma}}\right)^2} \quad . \tag{6.16}$$

These equations are in good agreement with numerical calculations for small values of ψ_r .

For a reasonable wiggler it is not feasible to allow a very large value of $\widetilde{\Delta\gamma}$ or a very small value of ψ_r , and because of the approximations made in deriving the Hamiltonian H_4 it is necessary to numerically integrate the equations of motion, Eqs. (2.22 and 2.23), for a large number of electrons with various initial conditions. For the case where ψ_r is held constant a small fraction of the particles are often captured by the moving bucket and will have their energy increased, thereby significantly contributing to the increase in the energy spread of the final electron beam. Whether this trapping, which would not occur for a static Hamiltonian, is due to numerical errors or the small non-static

corrections to the Hamiltonian is not now completely clear. However it would probably be present due to small errors in any physical realization of the wiggler. The particles that may become captured are those which are near the unstable fixed point of the bucket when the bucket passes through the phase space of the beam. One method that may be used to prevent this capture is to increase the magnitude of the resonant phase angle ψ_r as the bucket is accelerated; this moves the unstable fixed point slightly, preventing the trapping of the electron. This results in electrons with larger energies being decelerated less than those at the lower energies producing an extra source of energy spread in the emerging beam. A balance between all of these effects as well as a desire to minimize the length of the wiggler requires computer simulation to arrive at a reasonable design.

While this method will allow a much larger entrance bandwidth and produce a relatively small additional energy spread as compared to a constant wiggler one must pay the price with a longer wiggler magnet. It also appears that the small signal gain of such a device behaves differently from that of the constant parameter FEL.[12] At this writing it does not appear to be out of the question that the phase area displacement wiggler has adequate characteristics to be used in a CW storage ring, although much more simulation is required and the start-up problem must be addressed.

7.0 INSTABILITIES

7.1 Introduction

We have been concerned in this paper primarily with free electron lasers operating at very high γ, and our principal interest has been the mode of operation in which the electrons are trapped in decelerating potential wells for a single pass through the wiggler. In this mode of operation collective effects should be small. In particular the relativistic longitudinal plasma frequency $\omega_{PL} = \left(\frac{4\pi ne^2}{m\gamma^3}\right)^{1/2}$ is small enough that $\int \omega_{PL} dt \ll 1$ for a pass through the wiggler. Thus we will concentrate our attention on instabilities which arise essentially from interactions of individual electrons with the electromagnetic field.

These are of two kinds. First there are problems arising from the transverse structure of the beam which occur because the effective refractive index depends on the density of trapped electrons. A qualitative discussion has been given in Section 4; a more complete quantitative treatment is in progress and will be published later.

A second type of interaction which can occur is the unstable generation of parasitic electromagnetic waves, i.e. waves with a different frequency from that of the signal which we are trying to grow. Such generation can be expected in any situation other than the simple linear

regime operated at the maximum of the signal gain curve. Thus in the "descending bucket" scheme, a highly non-linear mode of operation, the electrons are all effectively trapped and moving on the average at a common velocity. We might therefore worry that a wave of somewhat lower frequency than the signal wave, corresponding to a ponderomotive phase velocity $v = \frac{\omega_R}{k_R + k_w}$ which is slightly smaller than the bucket velocity, could be unstably amplified. In the remainder of this section we will show that such amplification does occur.

7.2 Linear Theory of Raman Instability

The problem which we will treat is that of the stability of an infinitesimal electromagnetic wave as it perturbs the equilibrium of electrons trapped in the ponderomotive buckets of the signal wave. In a single pass wiggler this equilibrium is not quite a static one. The potential wells may change slowly in shape and depth as the wiggler is traversed, the electron oscillation phase may not be quite random due to the trapping process at the entrance to the wiggler, and the wiggler is of course of finite length. In order to make the stability problem tractable we will idealize to a true static equilibrium. This would correspond physically to a constant parameter wiggler in which the electrons are uniformly accelerated by a DC (or resonant RF) longitudinal electric field of such a magnitude as to exactly balance the radiative loss to the signal wave. This equilibrium may be described by the Hamiltonian H_4 given in Eq. (2.44):

$$H_4 = \frac{k_w + \delta k_s}{\gamma_r} (\delta\gamma)^2 - \frac{\omega_s a_w a_s}{c\gamma_r} (\cos \psi + \psi \sin \psi_r) \qquad (7.1)$$

where we recall that γ_r is the resonant γ for particles in the well, k_w is the wiggler wave number, δk_s the modification of the signal wave number which may be lumped into k_w and will be subsequently ignored, a_w and a_s the non-dimensional vector potentials of the wiggler and signal fields, and the phase $\psi \equiv \int_0^z (k_w + k_s)\, dz - \omega_s t$. We recall that the canonical variables in Eq. (7.1) are $\delta\gamma$ and ψ . The independent variable is z .

For the static situation which we are considering all quantities except $\delta\gamma$ and ψ are constants and from Eq. (2.41) we see that the D.C. electric field necessary to maintain the static equilibrium is given by

$$\frac{eE}{mc^2} = \frac{a_w a_s \omega_s}{\gamma_r c} \sin \psi_r \, . \qquad (7.2)$$

We note further, from Eq. (2.41), that the rate at which a given electron is radiating into the signal wave depends on its phase and is given by: (in units of mc^2)

$$\dot{E}_s = \frac{a_s a_w \omega_s}{\gamma_r} \sin \psi \, . \qquad (7.3)$$

In order to eliminate unnecessary constants it is convenient to define $U^2 = \frac{2k_w \omega_s a_s a_w}{c\gamma_r^2} z^2$, and $p = \sqrt{\frac{2k_w c}{\omega_s a_s a_w}}\, \delta\gamma$. In these units the Hamiltonian becomes simply

$$H_5 = \frac{p^2}{2} - (\cos\ \psi + \psi \sin\ \psi_r) \tag{7.4}$$

where p and ψ are the new canonical momentum and coordinate effectively and U is the independent variable.

This is of course the Hamiltonian for the pendulum equation which we have discussed in Sect. 2 and 3 with a succession of potential wells as shown in Fig. 2.1. Electrons trapped in the potential well oscillate with frequency $\Omega\ (H_5)$. This frequency ranges from $\Omega = 0$ for particles at the top of the potential well to $\Omega = \sqrt{\cos\ \psi_r}$ for particles at the bottom. Thus $\Delta U = 2\pi$ corresponds to a synchrotron period, while a typical wiggler length would be of order $U \sim (a_s)^{-1/2}$ for an efficient single pass design. To specify the equilibrium we must give the distribution of electrons $f(p,\psi)$ in the potential well. In steady state we expect f to be independent of the phase of oscillation in the potential. It is therefore convenient to introduce action angle variables:

$$J(H_5) = \oint p\ d\psi = \oint d\psi'\ \sqrt{2(H_5 + \cos\ \psi' + \psi' \sin\ \psi_r)} \tag{7.5}$$

and

$$\phi(H_5,\psi) = \Omega \int_0^{\psi} \frac{d\psi'}{\sqrt{2(H_5 + \cos\ \psi' + \psi' \sin\ \psi_r)}} \tag{7.6}$$

with

$$\Omega(H_5) = 2\pi \left[\oint \frac{d\psi}{p}\right]^{-1} .$$

The symbol $\oint$ means a complete cycle of oscillation in the potential well. From Eq. (7.6) we see that ϕ varies between 0 and 2π in an oscillation period. The area in phase space is given by $\frac{1}{2\pi}\, dJ\, d\phi$ and the equilibrium distribution function is independent of ϕ. Thus we specify the equilibrium by giving:

$$f_o = f_o(J) \ . \tag{7.7}$$

The equations of motion of a particle are

$$\frac{dJ}{dU} = 0 \tag{7.8}$$

and

$$\frac{d\phi}{dU} = \Omega(J) \ . \tag{7.9}$$

Note that because of the well-known adiabatic properties of J, we might expect our results to be applicable also to slowly varying wigglers. For convenience we normalize

$$\int_o^{J_{max}} f_o(J)\, dJ = 1$$

The rate at which energy is given to the signal wave may be seen from Eq. (7.3) to be:

$$\frac{dE_s}{dz} = \frac{a_s a_w \omega_s}{c\gamma_r} \frac{1}{2\pi} \int\int f \sin \psi \, dJ \, d\phi \tag{7.10}$$

For the equilibrium distribution this is

$$\frac{dE_s}{dz} = \frac{a_s a_w \omega_s}{c\gamma_r} \sin \psi_r \tag{7.11}$$

since $\langle \sin \psi \rangle = \sin \psi_r$, (the bracket indicating a phase average i.e., $\langle A \rangle = \frac{1}{2\pi}\int A d\phi$) . Finally we note that the phase space above the potential well must be empty, i.e., the phase space density of untrapped electrons must be much smaller than that for trapped electrons which have been held together by the ponderomotive wave. Moreover we expect the distribution to be continuous, since various diffusive processes which we will discuss later are operative. Hence it is reasonable to impose the condition

$$f_o (J_{max}) = 0 \tag{7.12}$$

where J_{max} corresponds to the top of the well.

Next we consider the introduction of a small perturbing electromagnetic wave defined by a helical vector potential analogous to that given for the signal wave in Eq. (2.8)

$$\vec{A}_R = \varepsilon A_s \left[\hat{x} \cos (k_R z - \omega_R t) - y \sin (k_R z - \omega_R t)\right] . \tag{7.13}$$

Here ε specifies the relative strength of the perturbing wave. The Hamiltonian H_1 of Eq. (2.9) then becomes

$$H_1' = mc^2 \left\{ \mu^2 + \gamma^2 + 2a_w a_s \cos\psi + 2\,\epsilon\, a_w a_s \cos\psi_R \right\}^{1/2}$$

where the phase of the perturbing ponderomotive wave is given by

$$\psi_R \equiv (k_w + k_R)\, z - \omega_R t = k_w \left(1 - \frac{\omega_R}{\omega_s}\right) z + \frac{\omega_R}{\omega_s}\,\psi \qquad (7.14)$$

The development of Section 2 is easily modified to include both radiation fields, A_r and A_s, to yield the new Hamiltonian:

$$H_5' = \frac{p^2}{2} - (\cos\psi + \psi \sin\psi_r) - \epsilon \cos\psi_R\,, \qquad (7.15)$$

with, in these units, $\psi_R = \psi + \lambda U$. The canonical variables of course remain p and ψ. We will retain the angle action variables defined by Eqs. (7.5) and (7.6) although the evolution of p and ψ are now given by Hamilton's equations for (7.15).

In this expression we have neglected $\left(\frac{\omega_R}{\omega_s} - 1\right)\psi$ since $\left|\frac{\omega_R}{\omega_s} - 1\right| \ll 1$ and ψ remains bounded for trapped particles. Further,

$$\lambda \equiv \frac{1}{2}\sqrt{\frac{1 + a_w^2}{a_s a_w}}\left[1 - \frac{\omega_R}{\omega_s}\right]\,. \qquad (7.16)$$

(We note parenthetically that for $a_w \approx 1$, λ would be nearly constant even for a variable wiggler oscillator. For an amplifier, in which a_s is a strong function of z, λ may vary appreciably.)

Similarly following the developments in Section 2 we find that the energy given to the perturbing wave is analogous to that described by Eq. (7.10), i.e.

$$\frac{dE_R}{dz} = \epsilon \frac{a_s a_w \omega_s}{\gamma_r c} \frac{1}{2\pi} \int\int f \sin \psi_R \, dJ \, d\phi \tag{7.17}$$

Since f_o is independent of U the energy transfer given by Eq. (7.17) will be oscillatory in U, i.e., vanish on average, for the equilibrium distribution $f = f_o$. Hence it is necessary to proceed to the next order and determine f_1, the distribution function to first order in ϵ, the amplitude of the sideband.

Noting that the phase space element $2\pi \, dp d\psi \equiv dJ d\phi$, we can write the Liouville equation for the distribution function:

$$\frac{\partial f}{\partial U} + \frac{d\phi}{dU} \frac{\partial f}{\partial \phi} + \frac{dJ}{dU} \frac{\partial f}{\partial J} = 0 \quad .$$

Recalling that $\frac{\partial f_o}{\partial U} = \frac{\partial f_o}{\partial \phi} = 0$ the linearized Liouville equation is:

$$\frac{\partial f_1}{\partial U} + \Omega \frac{\partial f_1}{\partial \phi} + \left.\frac{dJ}{dU}\right|_1 \frac{\partial f_o}{\partial J} = 0 \tag{7.18}$$

It is thus necessary to find the rate of change of J caused by the perturbation.

From Eqs. (7.4), (7.5), (7.6) and (7.15), we have:

$$\frac{dJ}{dU} = \frac{2\pi}{\Omega}\frac{dH_5}{dU} = \frac{2\pi}{\Omega}\left[-\frac{\partial H_5}{\partial p}\frac{\partial H_5'}{\partial \psi} + \frac{\partial H_5}{\partial \psi}\frac{\partial H_5'}{\partial p}\right]$$

$$= -\frac{2\pi}{\Omega} p\epsilon \sin\psi_R = -2\pi\epsilon\frac{\partial \psi}{\partial \phi}\sin\psi_R$$

$$= 2\pi\epsilon\frac{\partial}{\partial \phi}\cos\psi_R \quad .$$

We may now substitute into Eq. (7.18)

$$f_1 = -\frac{2\pi\epsilon}{\Omega}\cos\psi_R \frac{\partial f_0}{\partial J} + \hat{f}_1$$

to see that $\hat{f}_1$ satisfies:

$$\frac{\partial \hat{f}_1}{\partial U} + \Omega\frac{\partial \hat{f}_1}{\partial \phi} + \epsilon\frac{2\pi\lambda}{\Omega}\sin\left(\psi(J,\phi) + \lambda U\right)\frac{\partial f_o}{\partial J} = 0 \quad . \qquad (7.19)$$

The first term in the above expression for f_1 will give no non-oscillatory contribution to $\frac{dE_R}{dz}$ as may be seen from Eq. (7.17) since $\cos\psi_R \sin\psi_R$ oscillates with frequency $2\lambda U$. Hence, only $\hat{f}_1$ contributes to energy transfer. We solve Eq. (7.19) by first substituting

$$\hat{f}_1 = f_+(J,\phi)\, e^{-i\lambda U} + c.c.$$

Further, writing $f_+ = e^{i\frac{\lambda}{\Omega}\phi}\chi$ it is easy to solve for

$$f_+ = -i\epsilon \frac{\pi\lambda}{\Omega^2} e^{i\frac{\lambda}{\Omega}\phi} \frac{\partial f_o}{\partial J} \int_{-\infty}^{\phi} d\phi' \, e^{-i\left(\psi' + \frac{\lambda}{\Omega}\phi'\right)} \tag{7.20}$$

The lower limit has been specified by the following argument, familiar in plasma physics. We must suppose the perturbation to be a growing wave i.e. λ has a small positive imaginary part. This makes the integral convergent. Moreover we see that $f_+ (\phi + 2\pi) = f_+ (\phi)$ as is required for a single-valued function. Hence Eq. (7.20) is the unique solution of Eq. (7.19). We may now find the energy transfer rate from Eq. (7.17).

$$\frac{dE_R}{dz} = \epsilon \frac{a_s a_w \omega_s}{\gamma_r c} \frac{1}{2\pi} \iint dJ \, d\phi \sin \psi_R \left[f_+ e^{-i\lambda U} + c.c. \right]$$

We are in fact concerned with that part of the radiated energy which is non-oscillatory in U, i.e.

$$\frac{dE_R}{dz} = -\epsilon^2 \frac{a_s a_w \omega_s}{\gamma_r c} \frac{\pi}{2} \lambda \int_0^{J_{max}} dJ \frac{1}{\Omega^2} \frac{\partial f_o}{\partial J} \left[\frac{1}{2\pi} \int_0^{2\pi} d\phi \, e^{i\left(\frac{\lambda}{\Omega}\phi + \psi\right)} \int_{-\infty}^{\phi} d\phi' \, e^{-i\left(\psi' + \frac{\lambda}{\Omega}\phi'\right)} + c.c. \right] \tag{7.21}$$

We may simplify the ϕ' integral in the following way. Note that ψ is a periodic function of ϕ so that the integrals for successive periods differ by factors of $e^{-i\lambda 2\pi/\Omega}$. Thus

$$I = \int_0^{2\pi} d\phi\, e^{i\left(\frac{\lambda}{\Omega}\phi + \psi\right)} \int_{-\infty}^{\phi} d\phi'\, e^{-i\left(\psi' + \frac{\lambda}{\Omega}\phi'\right)}$$

$$= \int_0^{2\pi} d\phi\, e^{i\left(\frac{\lambda}{\Omega}\phi + \psi\right)} \left[\sum_{n=0}^{\infty} e^{2\pi i n \frac{\lambda}{\Omega}} \int_0^{\phi} e^{-i\left(\psi' + \frac{\lambda}{\Omega}\phi'\right)} d\phi' \right.$$

$$\left. + \sum_{n=0}^{\infty} e^{2\pi i (n+1)\frac{\lambda}{\Omega}} \int_{\phi}^{2\pi} e^{-i\left(\psi' + \frac{\lambda}{\Omega}\phi'\right)} d\phi' \right]$$

We may exchange labels ϕ and ϕ' in the second term to obtain

$$I = \sum_{n=0}^{\infty} \int_0^{2\pi} d\phi \int_0^{\phi} d\phi' \left[e^{2\pi i n \frac{\lambda}{\Omega}} e^{-i\left(\psi' + \frac{\lambda}{\Omega}\phi'\right)} e^{i\left(\frac{\lambda}{\Omega}\phi + \psi\right)} \right.$$

$$\left. + e^{2\pi i (n+1)\frac{\lambda}{\Omega}} e^{-i\left(\psi + \frac{\lambda}{\Omega}\phi\right)} e^{i\left(\frac{\lambda}{\Omega}\phi' + \psi'\right)} \right]$$

Finally I must be added to its complex conjugate to yield

$$I = \sum_{n=-\infty}^{\infty} \int_0^{2\pi} d\phi \int_0^{\phi} d\phi'\, e^{2\pi i n \frac{\lambda}{\Omega}} \left\{ e^{-i\,\psi' - \left[\psi + \frac{\lambda}{\Omega}(\phi' - \phi)\right]} + e^{-i\left[\psi - \psi' + \frac{\lambda}{\Omega}(\phi - \phi')\right]} \right\}$$

However $\sum_{n=-\infty}^{\infty} e^{2\pi i n \frac{\lambda}{\Omega}} = \sum_{m=-\infty}^{\infty} \delta\left(\frac{\lambda}{\Omega} - m\right) = \sum_{m=-\infty}^{\infty} \Omega\delta(\lambda - m\Omega)$ where m is any

integer. We may again exchange ϕ and ϕ' in the second term to obtain finally,

$$I = \sum_{m=-\infty}^{\infty} \delta\left(\frac{\lambda}{\Omega} - m\right) \left| \int_0^{2\pi} d\phi \, e^{i\left(\psi + \frac{\lambda}{\Omega}\phi\right)} \right|^2 \quad . \tag{7.22}$$

This result may now be substituted into Eq. (7.21). However it is useful first to define the relative gain of the unstable wave to the signal gain. Thus,

$$G(\lambda) = \frac{1}{\epsilon^2 a_s^2} \frac{dE_R}{dz} \Big/ \frac{1}{a_s^2} \frac{dE_s}{dz} \, . \tag{7.23}$$

From Eqs. (7.11, 7.22 and 7.23) we have

$$G(\lambda) = -\sum_{m=-\infty}^{\infty} m \int_0^{J_{max}} dJ \left\{ \frac{\partial f_0}{\partial J} \, \delta(\lambda - m\Omega(J)) \left| \int_0^{2\pi} e^{i(\psi + m\phi)} \, d\phi \right|^2 \right\} \Big/ 4\sin\psi_r \tag{7.24}$$

Recall that we have normalized $\int f_0 \, dJ = 1$.

Equation (7.24) is our principal result. We note that in an amplifier G directly gives us the number of e-foldings of an unstable mode relative to the signal gain. In general it will turn out that G is only slightly larger than 1 and therefore the buildup from noise is not significant. Further we see from Eq. (7.16) that since in an amplifier a_s varies strongly with U , the resonant condition $\lambda = m\Omega$ is only met for a short time. We conclude that the instability is not important for an amplifier.

For an oscillator, however, where the optical waves are reflected many times we must require $G(\lambda) < 1$ if the external circuit is non-dispersive, i.e., if the external fractional attenuation of the signal and the sideband are equal. For $G > 1$ the sideband would grow when the signal is in steady state, and as we discuss in the following section, would presumably destroy the particle trapping. Hence an effective requirement for oscillator stability is $G(\lambda) < 1$ for all λ.

The form of Eq. (7.24) immediately suggests the physical interpretation of our results. Recall that the action J is analogous to the quantum level of the electron in the potential well. Thus the instability consists of a stimulated Raman scattering in which the signal wave ω_s decays into the sideband ω_R plus m "quanta" of particle oscillation. Since both this process and its inverse are possible, the net energy transfer depends on the derivative of the distribution function $\frac{\partial f_o}{\partial J}$. If $\frac{\partial f_o}{\partial J} < 0$, the usual case, it is waves with $\lambda > 0$, i.e., the lower sideband, which grow. When many waves of different frequencies λ are excited we may expect the particles to diffuse in the potential well leading eventually to detrapping as will be discussed later.

Equation (7.24) is of course a rather complicated one, with the gain depending in detail on the distribution fucntion. We have not quite been able to prove that it is impossible to make $G(\lambda) < 1$ for all λ. However the following sum rule indicates strongly that this is the case.

Consider

$$\Gamma = \int_0^\infty G\lambda \, d\lambda = -\sum_{m=0}^{\infty} \int dJ \, \frac{\partial f_o}{\partial J} \, m^2 \Omega \left| \int_0^{2\pi} d\phi \, e^{i(\psi + m\phi)} \right|^2 (4 \sin \psi_r)^{-1} \quad . \tag{7.25}$$

Now

$$\sum_{m=0}^{\infty} m^2 \left| \int_0^{2\pi} e^{i(\psi + m\phi)} d\phi \right|^2 = \sum_{m=0}^{\infty} \int_0^{2\pi} e^{i\psi} \frac{\partial}{\partial \phi} e^{im\phi} \, d\phi \int_0^{2\pi} e^{-i\psi'} \frac{\partial}{\partial \phi'} e^{-im\phi'} d\phi'$$

$$= \frac{1}{2} \sum_{m=-\infty}^{\infty} \int_0^{2\pi} d\phi \int_0^{2\pi} d\phi' \, \frac{\partial \psi}{\partial \phi} \, \frac{\partial \psi'}{\partial \phi'} \, e^{i(\psi - \psi')} \, e^{im(\phi - \phi')} = \pi \int_0^{2\pi} d\phi \left(\frac{\partial \psi}{\partial \phi} \right)^2$$

$$= \pi \oint \frac{\partial \psi}{\partial \phi} \, d\psi = \pi \, \frac{J}{\Omega} \quad .$$

In the last line we have used definitions (7.5) and (7.6). Substituting this result into Eq. (7.25) and integrating by parts on J while using the fact that $f_o(J_{max}) = 0$, we find that

$$\Gamma = \int_0^\infty G\lambda \, d\lambda = \frac{\pi}{4 \sin \psi_r} \, . \tag{7.26}$$

We may compare this to Γ_o , the value which we would have for a marginal case where $G \equiv 1$ from $\lambda = 0$ to $\lambda = \Omega_{max} = (\cos \psi_r)^{1/2}$ and zero for $\lambda > \Omega_{max}$. We see that

$$\frac{\Gamma}{\Gamma_o} = \frac{\pi}{\sin 2\psi_r} > 1 \qquad (7.27)$$

This result is not quite conclusive proof of instability since G is non-zero even for $\lambda > \Omega_{max}$ due to harmonic emission. However in practice these growth rates appear to be small, and are not enough to offset the numerical factor in Eq. (7.27). We would expect therefore that values of G somewhat greater than unity would typically be found. This is indeed true for all distributions we have looked at.

There is a particular distribution function f_o, of some physical interest, for which Eq. (7.24) simplifies somewhat. This distribution is given by

$$f_o = \frac{1}{J_{max}} \quad \text{for} \quad J < J_{max}$$

and

$$f_o = 0 \quad \text{for} \quad J > J_{max} . \qquad (7.28)$$

If electrons are introduced into the wiggler from a distribution which has some energy spread and is random in optical phase we would expect the phase space to be uniformly occupied as in Eq. (7.28). Such a distribution would also tend to arise from a slow diffusive process in which electrons were boiled off from the top of the well. One might also expect this distribution to be relatively favorable since the derivative of f_o is large only near the top of the well where the coupling to the radiation is weak.

Since the integrand of Eq. (7.24) is non-vanishing only for $J \sim J_{max}$ we may take the orbit integrals in Eq. (7.24) to be those for the particle at the top of the well i.e. in Eq. (7.5) we should put

$$H = H_M = \cos \psi_r - (\pi - \psi_r) \sin \psi_r \ .$$

It is useful to take advantage of periodicity to improve convergence of the orbit integral for particles near the top of the well. We may thus put

$$\int_0^{2\pi} e^{i(\psi - m\phi)} d\phi = \Omega \oint \left[e^{i\psi} + e^{-i\psi_r} \right] \frac{e^{-im\Omega \int_0^{\psi} d\psi' \left[2(H_M + \cos\psi' + \psi' \sin\psi_r) \right]^{-1/2}}}{\sqrt{2(H_M + \cos\psi + \psi \sin\psi_r)}} \, d\psi$$

$$= \Omega K(\lambda)$$

where

$$K(\lambda) = \oint \left[e^{i\psi} + e^{-i\psi_r} \right] \frac{e^{-i\lambda \int_0^{\psi} d\psi' \left[2(H_M + \cos\psi' + \psi' \sin\psi_r) \right]^{-1/2}}}{\sqrt{2(H_M + \cos\psi + \psi \sin\psi_r)}} \, d\psi \qquad (7.29)$$

is independent of J . Note that the subtraction we have performed makes the integrals smoothly convergent. Equation (7.24) then becomes

$$G(\lambda) = + \sum_m \int_0^{\Omega_{max}} d\Omega \frac{\partial f}{\partial \Omega} \delta(\lambda - m\Omega) \ \Omega^2 |K(\lambda)|^2 / 4 \sin \psi_r$$

$$= + \sum_{m=0}^{\infty} \Omega^2 \frac{\partial f}{\partial \Omega} \bigg|_{\Omega = \frac{\lambda}{m}} \quad \frac{|K(\lambda)|^2}{4 \sin \psi_r}$$

But $\Omega^2 \frac{\partial f}{\partial \Omega} = - \frac{\partial f}{\partial \frac{1}{\Omega}}$ and the sum over m may be converted to an integral $\lambda \, d(\frac{1}{\Omega})$. Hence we obtain the growth rate

$$G(\lambda) = \frac{\lambda |K(\lambda)|^2}{4 \sin \psi_r J_{max}} \tag{7.30}$$

We have evaluated Eq. (7.30) numerically and find that the growth rates indeed have the properties we have described. The results are illustrated in Fig. 7.1 for various ψ_r. Thus peak gains of about $G = 2$ occur, typically for values of $\lambda \sim .4 - .5$. The optimum value of ψ_r is seen to be around 30°. A significant feature of the results is that there is a range $\lambda < .1$ for which $G < 1$ even for a distribution in which the well is filled to the top. This implies that the growing sideband is separated by a finite frequency interval from the signal so that dispersive external optics may be applied to correct the modest parasitic excess growth.

From Eq. (7.16) we note that the unstable region is given by

$$.2 \sqrt{\frac{a_s a_w}{1 + a_w^2}} < \left[1 - \frac{\omega_R}{w_s} \right] < 2 \sqrt{\frac{a_s a_w}{1 + a_w^2}} \tag{7.31}$$

Here $a_w \sim 1$ and as a typical value is $a_s = 10^{-4}$, the unstable sideband extends in the range $10^{-2} > \frac{\Delta\omega}{\omega} > 10^{-3}$.

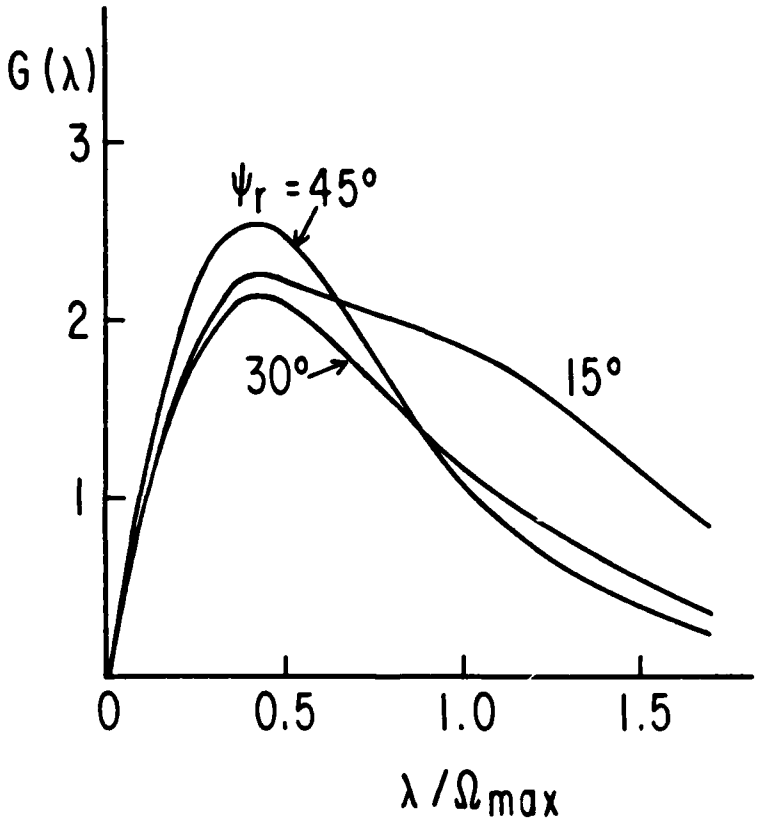

FIGURE 7.1

RELATIVE GAIN OF SIDEBAND COMPARED TO SIGNAL. $G(\lambda)$ IS DEFINED BY EQ. (7.30) AND PLOTTED AS A FUNCTION OF THE FREQUENCY SHIFT OF THE TEST WAVE FOR DIFFERENT VALUES OF ψ_r .

7.3 Discussion and Conclusions

In Section 7.2 we have shown that an idealized constant wiggler oscillator is linearly unstable against sideband generation. In this section we will describe briefly the results of some particle simulations and some nonlinear estimates.

In principle it appears attractive to do a 1-dimensional particle simulation, calculating particle orbits and interactions with the electromagnetic waves. We have in fact done some simulations of the pendulum equations (2.25) including the linearized equation for $\delta\psi$ resulting from the presence of the sideband. By integrating Eq. (7.24) by parts we see that the rate of energy transfer by a particle to the sideband field should be proportional to

$$\frac{dE}{dU} \sim \epsilon^2 \frac{\partial}{\partial J} \left\{ \delta(\lambda - m\Omega(J)) \left| \int_0^{2\pi} e^{i(\psi + m\phi)} d\phi \right|^2 \right\} . \qquad (7.38)$$

Here E is in units of the bucket height $\gamma\sqrt{a_s}$ and all other quantities are $O(1)$.

This result would evidently be a bit difficult to simulate! In fact the wigglers which were simulated were of finite length and variable properties. If we try to take the finite length into account by solving Eq. (7.19) over a finite interval in U the infinite sums leading to Eq. (7.22) are replaced by finite sums and we find that Eq. (7.38) is approximately modified (averaging over the initial phases of the particles or the sideband waves) by replacing

$$\delta(\lambda - m\Omega) \to \frac{1}{\pi} \frac{\sin(\lambda - m\Omega)U}{\lambda - m\Omega} \quad . \tag{7.39}$$

Variable wiggler profiles lead to λ depending on U as is seen from Eq. (7.16) and it should be so interpreted in the argument of the δ function in Eq. (7.38). We have not found a simple way to represent both effects simultaneously.

The results of the simulations so interpreted were in agreement with Eq. (7.38), and unstable over-all relative gains $G = 3\text{-}4$, consistent with the distributions studied, were observed. There was however one striking result which has not been quantitatively analyzed. Particles near the top of the well sometimes gained or lost large amounts of energy. This came about because such particles, as they are about to detrap, are in an unstable equilibrium perched at the top of the well, and strongly perturbed by the sideband. For such particles the assumption of many oscillation periods is clearly incorrect. The fluctuations of energy were large and of either sign and we have not determined whether such particles produce any net effect, either stabilizing or destabilizing. Very good statistics would be required to determine this, but on the basis of our limited simulations it seems unlikely that this effect is strong enough to modify our overall picture.

We pass now to a brief discussion of the non-linear behavior of the excited wave. We first consider the situation where only a single unstable mode is excited in addition to the signal. In this case we expect the wave to be stabilized by eventual detuning of resonant particles from

the wave as their energy is changed. We will not present here the lengthy calculation of this effect but will give a qualitative estimate based on Eqs. (7.38 and 7.39).

We imagine a sideband wave with amplitude ϵ interacting with an electron beam weak enough that the amplitude ϵ is unchanged during the interaction. After a certain distance U, which we wish to determine, the resonant electrons will become detuned and further transfer of energy to the wave will not occur. Integrating Eq. (7.38) with respect to U from 0 to U we find for a nearly resonant particle, i.e. a particle for which $(\lambda - m\Omega)U \sim O(1)$, an energy change at position U

$$\Delta E \sim \epsilon^2 \frac{\partial}{\partial J} \frac{\sin^2 \frac{(\lambda-m\Omega)U}{2}}{(\lambda-m\Omega)^2} \left| \int_0^{2\pi} e^{i(\psi-m\phi)} d\phi \right|^2 . \qquad (7.40)$$

This may be estimated by expanding the sine, and putting $(\lambda-m\Omega)U \sim 1$, while recalling that in our units all parameters are of order unity. Thus

$$\Delta E \sim \epsilon^2 U^3 .$$

However, detuning will occur for $\frac{\partial \Omega}{\partial E} \Delta E U \sim 1$, i.e. the resonant electrons will be detuned for $U \gtrsim \epsilon^{-1/2}$. The width of the resonance, i.e. the number of electrons involved at this point will be of order $U^{-1} \sim \epsilon^{1/2}$. Integrating Eq. (7.38) over J we see that the peak energy transfer rate $\Delta E' \sim \epsilon^2$ and the maximum energy transferred to the wave in an infinite length wiggler is then:

$$\Delta E_{sat} \sim \varepsilon^{3/2} \quad . \tag{7.41}$$

This contrasts with the signal wave growth which continues for the length of the wiggler. For good extraction, $\frac{\Delta\gamma}{\gamma} \sim O(1)$, this length is $\Delta U \sim a_s^{-1/2}$ as noted earlier. Hence the relative gain may be estimated by $G = \frac{1}{\varepsilon^2} \Delta E_{sat} a_s^{1/2} = \left(\frac{a_s}{\varepsilon}\right)^{1/2}$. Another way to see this is to note that over the distance in which it is amplified, $\varepsilon^{-1/2}$, the sideband growth rate is only slightly larger than that of the signal, while the latter continues to grow for the full length $a_s^{-1/2}$. Thus a single wave will saturate at a very low level $\varepsilon \sim a_s \sim 10^{-4}$, since above this level its growth is less than that of the signal for each pass of the wiggler.

Unfortunately there may be of order 10^9 optical wavelengths between mirrors, hence 10^7 possible unstable modes (even neglecting off-angle propagation). Under these circumstances even the relatively narrow resonances for the saturated single modes overlap and we can expect that the resonant detuning will not occur, since particles will simply move from one wave to the next as their energy changes. In these circumstances it seems appropriate to assume random phases for the waves, leading to a quasi-linear diffusion of the particles in the well. The quasi-linear diffusion equations may be obtained by carrying Eq. (7.19) to second order. Omitting the details of the derivation we find:

$$\frac{\partial f_o}{\partial U} = \sum_m m^2 \frac{\pi}{2} \frac{\partial}{\partial J} \varepsilon^2 (m\Omega) \left| \int_0^{2\pi} e^{i(\psi + m\phi)} d\phi \right|^2 \frac{\partial f_o}{\partial J} \tag{7.42}$$

Here we have normalized $\epsilon^2(\lambda)d\lambda$ as the energy in sideband waves between λ and $\lambda + d\lambda$ relative to the signal. Equation (7.42) is consistent with our physical picture of the instability, describing a Brownian motion of the electrons in the potential well as the Raman scattering proceeds. If we multiply Eq. (7.42) by J and integrate over a small interval we see that the rate of change in the number of action "quanta" in that interval is proportional to m times the rate of energy gain of the waves in that interval as given by Eq. (7.24). [Recall that $f_o\, dJ$ is the number of electrons.] The form of Eq. (7.42) can be simplified if we assume a flat sideband spectrum, i.e. put $\epsilon^2(\lambda) \equiv \epsilon^2$ for all λ. The sum on m can then be done as in the derivation of Eq. (7.26) to give

$$\frac{\partial f_o}{\partial U} = \epsilon^2 \frac{\pi^2}{2} \frac{\partial}{\partial J} \frac{J}{\Omega} \frac{\partial f_o}{\partial J} \quad . \tag{7.43}$$

This is a diffusion equation with diffusion coefficient of order ϵ^2. Hence a characteristic diffusion distance for detrapping to occur is $U \sim \epsilon^{-2}$. It follows that when the energy in the sidebands is greater than $a_s^{1/2}$ times the signal energy the buckets will be destroyed before the wiggler has been traversed. We have of course assumed random phases in the sideband waves, but any kind of phase locking which could restore stable buckets seems improbable.

In summary we find that the scheme of decelerating electrons trapped in potential wells is subject to a Raman sideband instability where the gain of the unstable wave is several times the signal gain. It seems probable that any mode of FEL operation which tries to suppress energy

spread, e.g., adiabatic trapping, gain expanders, etc. would be subject to similar instabilities, which are inherent to operation away from the peak of the linear gain curve.

We note finally that rather modest dispersive optics would be required to stabilize a high-Q-trapped-electron-oscillator. If the cavity Q were 50 it would have to be reduced to 20 for the sidebands. This could presumably be accomplished by incorporating a grazing incident diffraction grating in the optical system or by providing an etalon grating in the outer part of the mirrors. It would also be possible to introduce a gas or liquid with enough dispersion that the sideband pulses would arrive back out of phase with the electron micropulses, if breakdown could be avoided at high power.

8.0 CONCLUSION

In the preceding sections we have described and analyzed a number of techniques for making use of the properties of variable parameter wigglers to substantially improve the efficiency of energy extraction from the electrons. These techniques have the common feature of requiring the existence of substantial ponderomotive potential wells or "buckets" which are then manipulated so as to produce desirable properties. Because of this feature, they all require high optical peak power, either circulating in a resonator or emitted from an amplifier, and are thus intrinsically high peak power devices.

A number of potential problems have been identified for "filled" bucket devices. One of these especially applicable to oscillators is the potential instability to parasitic oscillations at frequencies displaced from the main frequency by an amount of the order of the frequency of particle oscillation in the trapping buckets. It appears that some frequency discrimination device such as a diffraction grating may be required to suppress these oscillations. The second, especially applicable to amplifiers, has to do with the effects of transverse variation. The amplification process may introduce growing inhomogeneity in the optical field arising both from inhomogeneity in the growth rate and transverse inhomogeneity in the induced non linear index of refraction. The assessment of this problem requires further work and clarification before one can judge its magnitude. More generally, the one dimensional character

of our analysis is a major deficiency. Serious attempts to design practical devices should be based upon an analysis which includes three dimensional effects more adequately.

Despite the above comments, it is our overall conclusion that the use of a variable parameter wiggler in a free electron laser to produce high power optical radiation at selectable frequency and reasonable efficiency is a quite promising prospect. The exact scheme that is the best one to use (or combination of various schemes) will depend upon the type of electron beam that is available as well as the type of use for the radiation. At the present time there are several groups that are pursuing the variable wiggler approach, and we have enjoyed greatly our interaction with them. It is a pleasure to thank C. Brau and R. Cooper of LASL; D. Prosnitz, and A. Szoke of LLL: S. Mani and J. Reilly of Schafer Associates; R. Center and J. Slater of MSNW; and P. Sprangle of NRL for sharing their preliminary results on the variable parameter wiggler with us. We especially wish to acknowledge the many insights gained from our collaborators, V. K. Neil and R. Novick, without whose help this paper could never have come into being.

APPENDIX A

THE RELATION BETWEEN ENERGY SPREAD AND ENERGY TRANSFER IN THE SMALL SIGNAL LIMIT

John Madey[12] has proved an important theorem which, in the small signal limit, relates the phase averaged energy spread to the phase averaged energy change experienced by an electron as it passes through the laser interaction region. The theorem states that

$$\langle \gamma_f - \gamma_i \rangle = \frac{1}{2} \frac{\partial}{\partial \gamma_i} \langle (\gamma_f - \gamma_i)^2 \rangle \qquad \text{(A-1)}$$

where $\langle\ \rangle$ denotes an average over entry phase and γ_i , γ_f denote initial and final values respectively. γ_i is taken to be fixed so that it is γ_f which is dependent upon the entry phase before the average is carried out. The left hand side is obviously the phase averaged energy change, δE_L (measured, of course, in units of mc^2). The phase averaged energy spread, ΔE_s , is given by

$$\Delta E_s^2 \equiv \langle \gamma_f^2 \rangle - \langle \gamma_f \rangle^2 = \langle (\gamma_f - \gamma_i)^2 \rangle - \langle (\gamma_f - \gamma_i) \rangle^2 \ .$$

We shall see that $\langle (\gamma_f - \gamma_i) \rangle^2 / \langle (\gamma_f - \gamma_i)^2 \rangle$ vanishes in the small signal limit (indeed, it is implied by Eq. (A-1)) so that (A-1) may also be written

$$\delta E_L = \frac{1}{2} \frac{\partial}{\partial E_i} \Delta E_s^2 \qquad \text{(A-2)}$$

Both Eqs. (A-1) and (A-2) are valid only in the small signal limit.

The importance of the theorem in the discussion of the energy spread problem in storage rings has been indicated in section 3. The proof given by Madey contains a number of unnecessary approximations and restrictions which complicate the exposition and limit the generality of the result. It therefore seems worthwhile to present our modified version of his proof here. We shall see that the derivation of (A-1) is not significantly more complicated than the evaluation $\langle \gamma_f - \gamma_i \rangle$ in specific cases, so that one can take advantage of Eq. (A-1) to obtain $\langle \gamma_f - \gamma_i \rangle$ from the much simpler evaluation of $\langle (\gamma_f - \gamma_i)^2 \rangle$.

For simplicity we make the (almost certainly) unnecessary assumption that the transverse canonical momentum is both conserved and vanishing. As described in Section 2, the motion of an electron through the wiggler magnet is, under these conditions, described by the Hamiltonian

$$H = mc^2\gamma = mc^2 \left[\mu^2(z) + \left(\frac{P_z}{mc}\right)^2 - 2a_w(z)a_s(z)\cos \psi(z,t)\right]^{1/2} \qquad \text{(A-3)}$$

where we have introduced the dimensionless vector potentials $a = \frac{eA}{mc^2}$ and

$$\mu^2(z) = 1 + a_w^2(z) + a_s^2(z) \qquad \text{(A-4)}$$

$$\psi = \int (k_w + k_s)\, dz' - \omega_s t + \phi \tag{A-5}$$

a_w and a_s are the vector potential amplitudes of circularly polarized wiggler and optical fields respectively. We shall assume that a particle enters at $z = 0$, $t = 0$ and exits at $z = L$. The phase ϕ then represents the random phase of the optical field at which the particle enters. From Hamilton's equations one easily shows that

$$\frac{d\gamma}{dz} = - \frac{\omega_s a_w a_s \sin \psi}{c \sqrt{\gamma^2 - \mu^2 + 2a_w a_s \cos \psi}} \tag{A-6}$$

and

$$\beta \equiv \frac{v_z}{c} = \sqrt{1 - \frac{\mu^2}{\gamma^2} + \frac{2a_w a_s}{\gamma^2} \cos \psi} \tag{A-7}$$

For a more detailed discussion of the equations of motion, the reader is referred to Section 2.

We are now in a position to undertake the derivation of Eq. (A-1). First write

$$\gamma = \gamma_i + \gamma_1 + \gamma_2 + \cdots \tag{A-8}$$

where γ_1 is first order in a_s, γ_2 second order, etc.

From (A-6) we have

$$\gamma(z) - \gamma_1 = -\frac{\omega_s}{c}\int_0^z \frac{a_w(z')a_s(z')\sin\psi\,(z',t(z'))dz'}{\sqrt{\gamma^2(z') - \mu^2(z') + 2a_w(z')\,a_s(z')\cos\psi\,(z',t(z'))}} \tag{A-9}$$

where

$$t(z) = \frac{1}{c}\int_0^z \frac{dz'}{\beta(z')} \tag{A-10}$$

$$= t_o + t_1 + \ldots \tag{A-11}$$

and t_o, t_1, etc. also refer to zero, first, etc. order in a_s. We have immediately

$$\gamma_1(z) = -\frac{\omega_s}{c}\int_0^z \frac{a'_w a'_s \sin\psi'_o dz'}{\sqrt{\gamma_1^2 - \mu_o'^2}} \tag{A-12}$$

where $\psi'_o \equiv \psi(z',t_o(z'))$, $\mu_o^2 = 1 + a_w^2$, and in general, the primes indicate that the argument is z' (and double primes, that the argument is z''). Using

$$\langle \sin\psi'_o \rangle = 0 \tag{A-13}$$

and

$$\langle \sin \psi_o' \sin \psi_o'' \rangle = \frac{1}{2} \cos (\psi_o' - \psi_o'') \tag{A-14}$$

yields

$$\langle \gamma_1 \rangle = 0 \tag{A-15}$$

and, to lowest nonvanishing order (second in a_s), using $\langle (\gamma_i - \gamma_f)^2 \rangle = \langle \gamma_1^2 \rangle_{z=L}$, also yields

$$\langle (\gamma_i - \gamma_f)^2 \rangle = \frac{\omega_s^2}{2c^2} \int_o^L dz \int_o^L dz' \frac{a_w' a_s'}{\sqrt{\gamma_i^2 - \mu_o'^2}} \frac{a_w'' a_s''}{\sqrt{\gamma_i^2 - \mu_o''^2}} \cos(\psi_o' - \psi_o'') \tag{A-16}$$

Expanding Eq. (A-9) one obtains

$$\gamma_2 = -\frac{\omega_s}{c} \int_o^z \left[\frac{\partial}{\partial \gamma_i} \left(\frac{a_w' a_s'}{\sqrt{\gamma_i^2 - \mu_o'^2}} \right) \gamma_1' \sin \psi_o' - \frac{\omega_s a_w' a_s'}{\sqrt{\gamma_i^2 - \mu_o'^2}} t_1' \cos \psi_o' \, dz' \right]$$

$$+ \frac{\omega_s}{c} \int_o^z \frac{a_w' a_s'^2}{(\gamma_i^2 - \mu_o'^2)^{3/2}} \sin \psi_o' \cos \psi_o' \, dz' \tag{A-17}$$

We write $\tilde{\gamma}_2$ for the first line of Eq. (A-17) and note that since

$$\langle \sin \psi_o' \cos \psi_o' \rangle = 0, \quad \langle \gamma_2 \rangle = \langle \tilde{\gamma}_2 \rangle .$$

Next, expanding Eq. (A-10), and using Eq. (A-7) yields

$$t_o(z') = \frac{1}{c}\int_o^{z'} \frac{dz_o''}{\beta_o''} \tag{A-18}$$

$$\beta_o = \sqrt{1 - \frac{\mu_o^2}{\gamma_i^2}} \tag{A-19}$$

and writing $t_1 = t_{1a} + t_{1b}$

$$t_{1a} = \frac{1}{c}\int_o^{z} \gamma_1'' \frac{\partial}{\partial \gamma_i}\frac{1}{\beta_o''}\, dz'' \tag{A-20}$$

$$t_{1b} = \frac{1}{c}\int_o^{z} \frac{\partial}{\partial \gamma_i}\left(\frac{a_w' a_s'}{\sqrt{\gamma_i^2 - \mu_o'^2}}\right) \cos\psi_o'\, dz' \tag{A-21}$$

In writing Eq. (A-21), we have, in anticipation of what is to follow, made use of the identity

$$\frac{d}{d\varepsilon}\left(1 - \frac{\mu_o^2}{\gamma_i^2} + \frac{2\varepsilon}{\gamma_i^2}\right)^{-1/2}\Bigg|_{\varepsilon=0} = \frac{d}{d\gamma_i}\frac{1}{\sqrt{\gamma_i^2 - \mu_o^2}} \tag{A-22}$$

Substituting Eq. (A-12) in Eq. (A-20) and interchanging the order of integration we obtain

$$t_{1a} = -\frac{\omega_s}{c^2}\int_0^z dz' \frac{a'_w a'_s \sin\psi'_o}{\sqrt{\gamma_i^2 - \mu_o'^2}} \int_{z'}^z dz'' \frac{\partial}{\partial\gamma_i}\frac{1}{\beta''_o}$$

$$= -\frac{\omega_s}{c}\int_0^z dz' \frac{a'_w a'_s \sin\psi'_o}{\sqrt{\gamma_i^2 - \mu_o'^2}} \frac{\partial}{\partial\gamma_i}\left(t_o(z) - t_o(z')\right) \qquad \text{(A-23)}$$

Now substitute Eqs. (A-12), (A-21) and (A-23) into Eq. (A-17) to obtain

$$\tilde{\gamma}_2 = \frac{\omega_s^2}{c^2}\int_0^z dz' \int_0^{z'} dz'' \left[\frac{\partial}{\partial\gamma_i}\left(\frac{a'_w a'_s}{\sqrt{\gamma_i^2 - \mu_o'^2}}\right)\frac{a''_w a''_s}{\sqrt{\gamma_i^2 - \mu_o''^2}} \sin\psi'_o \sin\psi''_o\right.$$

$$+ \frac{a'_w a'_s}{\sqrt{\gamma_i^2 - \mu_o'^2}} \frac{\partial}{\partial\gamma_i}\left(\frac{a''_w a''_s}{\sqrt{\gamma_i^2 - \mu_o''^2}}\right) \cos\psi'_o \cos\psi''_o$$

$$\left. - \frac{a'_w a'_s}{\sqrt{\gamma_i^2 - \mu_o'^2}} \frac{a''_w a''_s}{\sqrt{\gamma_i^2 - \mu_o''^2}} \cos\psi'_o \sin\psi''_o \omega_s \frac{\partial}{\partial\gamma_i}\left(t'_o - t''_o\right)\right]$$

(A-24)

Then phase averaging and supplementing Eq. (A-14) with

$$\langle\cos\psi'_o \cos\psi''_o\rangle = \frac{1}{2}\cos\left(\psi'_o - \psi''_o\right) \qquad \text{(A-25)}$$

$$\langle\cos\psi'_o \sin\psi''_o\rangle = -\frac{1}{2}\sin\left(\psi'_o - \psi''_o\right) \qquad \text{(A-26)}$$

yields, to lowest nonvanishing order (second in a_s)

$$\langle \gamma_f - \gamma_i \rangle = \langle \tilde{\gamma}_2 \rangle_{z=L}$$

$$= \frac{\omega_s^2}{2c^2} \frac{\partial}{\partial \gamma_i} \int_0^L dz' \int_0^{z'} dz'' \frac{a_w' a_s'}{\sqrt{\gamma_i^2 - \mu_o'^2}} \frac{a_w'' a_s''}{\sqrt{\gamma_o^2 - \mu_o''^2}} \cos(\psi_o' - \psi_o'') \tag{A-27}$$

$$= \frac{1}{2} \frac{\partial}{\partial \gamma_i} \langle (\gamma_f - \gamma_i)^2 \rangle \tag{A-28}$$

In going from Eq. (A-27) to Eq. (A-28) we have made use of Eq. (A-16) and of the symmetry in (z', z'') of the integrand of Eq. (A-27). Eq. (A-28) and Eq. (A-1) are the same so the proof is now complete.

It should be added that an identical theorem holds for the Yariv, Shih[22] device. The proof is similar but simpler.

Madey has also derived Eq. (A-1) by means of a quantum mechanical argument in which stimulated and spontaneous emissions are related to one another and to Eq. (A-1). In a similar spirit, we offer an even simpler proof based upon the principle of detailed balance. Let $P(\gamma_1, \gamma_2)$ be the probability density in γ_2 that an electron which enters at $\gamma = \gamma_1$ leaves with $\gamma = \gamma_2$. The principle of detailed balance states that

$$P(\gamma_1, \gamma_2) = P(\gamma_2, \gamma_1) \, . \tag{A-29}$$

Assuming that the wiggler magnet with optical field satisfies Eq. (A-29), we have, with $\Delta\gamma = \gamma_2 - \gamma_1$,

$$P(\gamma_1, \gamma_1 + \Delta\gamma) = P(\gamma_1 + \Delta\gamma, \gamma_1 + \Delta\gamma - \Delta\gamma)$$

$$= P(\gamma_1, \gamma_1 - \Delta\gamma) + \left(\frac{\partial}{\partial\gamma_1}\right)_{\Delta\gamma} P\ (\gamma_1, \gamma_1 - \Delta\gamma)\ \Delta\gamma \qquad \text{(A-30)}$$

Eq. (A-30) holding only in the small signal limit. Now multiplying Eq. (A-30) by $\Delta\gamma$, integrating over $\Delta\gamma$, and using

$$\langle(\gamma_f - \gamma_i)\rangle = \int P(\gamma_1, \gamma_1 + \Delta\gamma)\Delta\gamma\ \ d(\Delta\gamma) = -\int P(\gamma_1, \gamma_1 - \Delta\gamma)\Delta\gamma\ \ d(\Delta\gamma)$$

and

$$\int\left(\frac{\partial P}{\partial\gamma_1}\right)_{\Delta\gamma}\ (\Delta\gamma)^2 d(\Delta\gamma) = \frac{\partial}{\partial\gamma_1}\int P(\gamma_1, \gamma_1 - \Delta\gamma)\ (\Delta\gamma)^2\ \ d(\Delta\gamma)$$

$$= \frac{\partial}{\partial\gamma_1}\langle(\gamma_f - \gamma_i)^2\rangle$$

we obtain Eq. (A-1) again.

It is perhaps worth emphasizing that Eq. (A-1) demonstrates that for finite wigglers in the small signal limit, zero energy spread implies zero energy transfer. To see this we note that Eq. (A-16) may be written in the form

$$\langle(\gamma_f - \gamma_i)^2\rangle = \frac{\omega_s^2}{2c^2}\ F^*F \qquad \text{(A-31)}$$

with

$$F = \int_0^L dz \; \frac{a_w a_s}{\sqrt{\gamma_1^2 - \mu_o^2}} \exp i\psi_o \tag{A-32}$$

The vanishing of $\langle(\gamma_f - \gamma_i)^2\rangle$ therefore implies that F vanishes. For finite L, $\frac{\partial F}{\partial \gamma_i}$ cannot be singular so $\frac{\partial}{\partial \gamma_i}\langle(\gamma_f - \gamma_i)^2\rangle$ must vanish as well.

As a simple example of the application of (A-1) we consider the case of a variable parameter wiggler. Equation (A-5) specialized to zeroth order yields

$$\frac{d\psi_o}{dz} = k_w - \frac{\omega_s \mu^2}{2\gamma^2 c} \tag{A-33}$$

and for simplicity we consider the case studied by Brau[23]

$$k_w = k_{wo} + k_w' z \tag{A-34}$$

with a_w, a_s, μ constant and $\sqrt{\gamma_i^2 - \mu_o^2} \tilde{=} \gamma_i$. Because of Eq. (A-31) we may choose the integration constant arbitrarily in determining ψ_o from Eq. (A-33). Choosing this constant conveniently, we obtain

$$\langle(\gamma_f - \gamma_i)^2\rangle = \frac{\omega_s^2 a_w^2 a_s^2}{2c^2\gamma_i^2} F_1 F_1^* \tag{A-36}$$

where

$$F_1 = \int_0^L dz \exp i \frac{k'_w}{2} (z - z_o)^2 \qquad \text{(A-37)}$$

with

$$z_o = \left(\frac{\omega_s \mu^2}{2\gamma_1^2 c} - k_{w_o} \right) / k'_w \qquad \text{(A-38)}$$

The point z_o corresponds to $d\psi_o/dz$ as given by Eq. (A-33). It is, of course, the phase matching point for given ω_s, γ_1 when it occurs within the wiggler. It is apparent from Eq. (A-37) that the dependence on z_o is identical to that which occurs for the single slit Fresnel intensity problem, where z_o is the displacement of the observation point from and parallel to the slit edge and k_w/k'_w its distance from the slit plane. The constant wiggler corresponds to the Fraunhofer limit and hence to the case $k'_w L^2 \lesssim 1$. To express F_1 in terms of standard Fresnel integrals we define

$$F_2(y) = \frac{y}{|y|} \int_0^{|y|} \exp i \frac{k'_w}{2} z^2 \, dz = \sqrt{\pi/k'_w} \left[C\left(y \sqrt{k'_w/\pi}\right) + iS\left(y \sqrt{k'_w/\pi}\right) \right] \qquad \text{(A-39)}$$

Then

$$F_1 = F_2(z_o) + F_2(L - z_o) \qquad \text{(A-40)}$$

and Eq. (A-1) yields immediately

$$\langle \gamma_f - \gamma_o \rangle \approx \frac{\omega_s^2 a_w^2 a_s^2}{2c^2\gamma_i^2} \frac{dz_o}{d\gamma_i} \mathrm{Re}\left(\frac{dF_1^*}{dz_o} F_1\right) \qquad \text{(A-41)}$$

$$= \frac{\omega_s^3 a_w^2 a_s^2 \mu^2}{2c^3\gamma_i^5 k_w'} \mathrm{Re}\left\{\left[e^{-i\frac{k_w'}{2}(L - z_o)^2} - e^{-i\frac{k_w'}{2} z_o^2}\right] \cdot \left(F_2(z_o) + F_2(L - z_o)\right)\right\}$$

Equation (A-41) reveals the energy transfer to be a rapidly oscillating function of z_o. While its derivation is simple, the discussion of its behavior is complicated. For z_o well within the wiggler, $F_2(z_o) + F_2(L - z_o) \approx \frac{(1 + i)}{2}\sqrt{\frac{\pi}{k_w'}}$ and hence

$$\mathrm{Re}\ \frac{dF_1^*}{dz_o} F_1 \approx \sqrt{\frac{\pi}{2k_w'}}\left(\cos\left(\frac{k_w'}{2}(L - z_o)^2 - \frac{\pi}{4}\right) - \cos\left(\frac{k_w'}{2} z_o^2 - \frac{\pi}{4}\right)\right).$$

$$= \sqrt{\frac{2\pi}{k_w'}} \sin k_w' L z_1 \sin\left(\frac{k_w'}{2}\left(\frac{L^2}{4} + z_1^2\right) - \frac{\pi}{4}\right)$$

where $z_1 = z_o - L/2$ is the distance of z_o from the wiggler center. The energy transfer is seen to oscillate symmetrically about zero with decreasing period and non decreasing amplitude as z_o moves towards the center of the wiggler. An energy spread in the incident beam induces an

average in z_o over a range $\delta z_o \approx \frac{2k_w}{k'_w} \frac{\delta\gamma_i}{\gamma_i}$. For typical values of $\frac{\delta\gamma_i}{\gamma_i}$ and the other parameters the average extends over several periods (~ 5) near the center. For such a beam the oscillations will decrease strongly in amplitude as one moves towards the center.

The situation near one side of the wiggler is different. For z_o negative or $\approx$ zero we write

$$\frac{dF_1^*}{dz_o} F_1 = -\left[\left(F_2(z_o) + F_2(L - z_o)\right) e^{-i\frac{k'_w}{2} z_o^2}\right]\left[1 - e^{i\frac{k'_w}{2}(z_o^2 - (L - z_o)^2)}\right]$$

The first factor in square brackets is non oscillatory in the range considered. The second factor is even more rapidly oscillating than before but with average value equal to 1. Again an energy spread will strongly damp the oscillations. We therefore omit the oscillating term to obtain

$$\mathrm{Re}\ \frac{dF_1^*}{dz_o} F_1 = -\left(\sqrt{\pi/k'_w}\right) g\left(-z_o\sqrt{k'_w/\pi}\right)$$

where

$$g(x) \equiv \left[\frac{1}{2} - C(x)\right] \cos\frac{\pi}{2}x^2 + \left[\frac{1}{2} - S(x)\right] \sin\frac{\pi}{2}x^2$$

$$\approx \frac{1}{2 + 4.142x + 3.492x^2 + 6.670x^3} \quad \text{for } x > 0 .$$

For $x < 0$, g reaches a peak of ~ 1.3 at $x \sim -.74$ and then commences to oscillate at non decreasing amplitude and decreasing period, being $\sim \sqrt{2} \sin\left(\frac{\pi}{2}x^2 + \frac{\pi}{4}\right)$ for $|x|$ large. The situation at $z_o > L$ or $\approx L$ is similar, but with the sign of the effect reversed. A qualitative picture of the behavior as a function of $\langle \gamma_1 \rangle$ that results after energy averaging is shown in Fig. A-1.

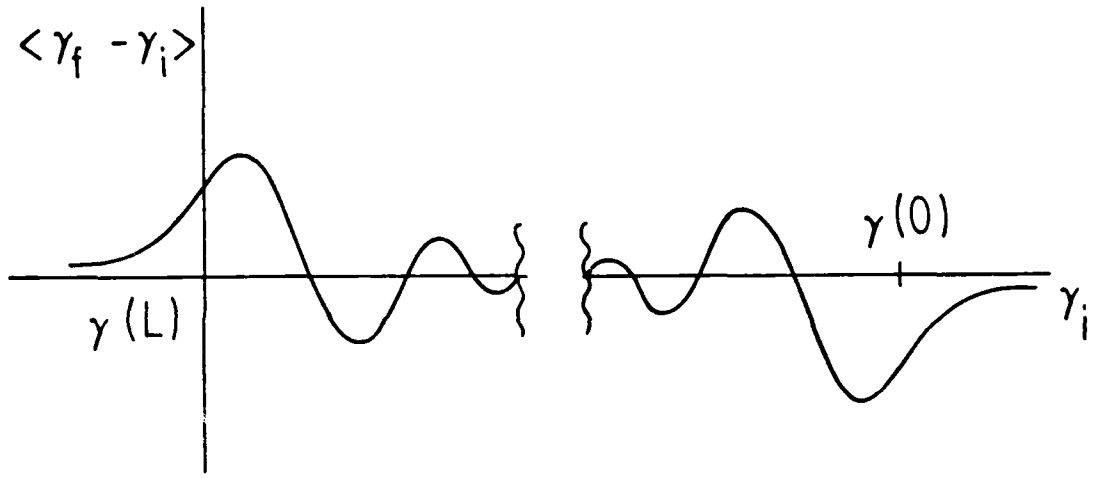

FIGURE A-1

QUALITATIVE PICTURE OF THE ELECTRON ENERGY TRANSMIT FUNCTION IN THE SMALL SIGNAL LIMIT FOR A VARIABLE PARAMETER WIGGLER.

APPENDIX B

EVALUATION OF PHASE AREA DISPLACEMENT ENERGY TRANSFER AND ENERGY SPREAD

We may obtain a formal result for $\Delta\gamma$ by rewriting Eq. (6.13)

$$\Delta\gamma = -\frac{2\sqrt{2}}{\sqrt{\pi}}\sqrt{\Lambda}\sin\psi_r \int_{-\infty}^{\psi_f} d\psi \int_0^{\infty} d\lambda \left\{ e^{-\lambda^2\left[H + (\cos\psi + \psi\sin\psi_r)\right]} - e^{-\lambda^2\left[H + (\cos\psi_f + \psi\sin\psi_r\right]} \right\} \tag{B-1}$$

where here $H = -\cos\psi_f - \psi_f\sin\psi_r$, and we focus our attention upon the turning point ψ_f which lies between the minimum at ψ_r and maximum at $\pi-\psi_r$ as shown in Fig. 6.2. The range of ψ_f within these limits is given by $\psi_1 < \psi_f < \pi-\psi_r$, where ψ_1 satisfies

$$\cos\psi_1 + \psi_1\sin\psi_r = \cos(\pi + \psi_r) - (\pi + \psi_r)\sin\psi_r$$

and is given by $\psi_l = (\pi - \sqrt{4\pi|\psi_r|} - \psi_r)$ for small $|\psi_r|$. Since ψ_r is negative here, we find it convenient to write $\psi_r = -|\psi_r|$ and replace ψ_f by $\psi_f' \equiv \psi_f - \pi$, so that $-\sqrt{4\pi|\psi_r|} < \psi_f' - |\psi_r| < 0$. Making these changes and also shifting the variable of integration by π we obtain

$$\Delta\gamma = 2\sqrt{2\Lambda/\pi}\,\sin|\psi_r| \int_{-\infty}^{\psi_f'} d\psi \int_0^{\infty} d\lambda \Big\{ \exp\,\lambda^2[\cos\,\psi - \cos\,\psi_f' + (\psi - \psi_f')\,\sin|\psi_r|] - \exp[\lambda^2(\psi - \psi_f')\,\sin|\psi_r|] \Big\} \tag{B-2}$$

Next we write

$$\int_{-\infty}^{\psi_f'} \exp\,\lambda^2(\cos\psi + \psi\,\sin|\psi_r|)\,d\psi = \sum_{n=0}^{\infty} \int_{\psi_f' - 2\pi(n+1)}^{\psi_f' - 2\pi n} \exp\,\lambda^2(\cos\,\psi + \psi\,\sin|\psi_r|)d\psi$$

$$= \int_{\psi_f' - 2\pi}^{\psi_f'} d\psi\,\exp\,\lambda^2(\cos\,\psi + \psi\,\sin|\psi_r|) \sum_{n=0}^{\infty} [\exp(-2\pi\lambda^2\sin|\psi_r|)]^n$$

$$= \frac{\exp(\pi\lambda^2\sin|\psi_r|)}{2\,\sinh(\pi\lambda^2\sin|\psi_r|)} \int_{\psi_f' - 2\pi}^{\psi_f'} \exp\,\lambda^2(\cos\,\psi + \psi\,\sin|\psi_r|)\,d\psi \tag{B-3}$$

and

$$\int_{\psi_f'-2\pi}^{\psi_f'} \exp\ \lambda^2(\cos\ \psi + \psi\ \sin|\psi_r|)d\psi = \int_{-\pi}^{\psi_f'} \exp\ \lambda^2(\cos\ \psi + \psi\ \sin|\psi_r|)d\psi$$

$$+ \exp(-2\pi\lambda^2\sin|\psi_r|) \int_{\psi_f'}^{\pi} \exp\ \lambda^2(\cos\ \psi + \psi\ \sin|\psi_r|)\ d\psi$$

(B-4)

Substituting (B-4) into (B-3) and (B-3) into (B-2) we obtain

$$\Delta\gamma = 2\sqrt{2\Lambda/\pi}\ \sin|\psi_r| \int_0^{\infty} d\lambda\ e^{-\lambda^2\cos\ \psi_f'} \left\{ \frac{1}{2\ \sinh(\pi\lambda^2\sin|\psi_r|)} \right.$$

$$\left[e^{-\pi\lambda^2\sin|\psi_r|} \int_{\psi_f'}^{\pi} e^{-\lambda^2\sin|\psi_r|(\psi_f' - \psi)}\ e^{\lambda^2\cos\ \psi}\ d\psi \right.$$

$$\left. \left. + e^{\pi\lambda^2\sin|\psi_r|} \int_{-\pi}^{\psi_f'} e^{-\lambda^2\sin|\psi_r|(\psi_f'-\psi)}\ e^{\lambda^2\cos\ \psi}\ d\psi \right] - \frac{e^{\lambda^2\cos\ \psi_f'}}{\lambda^2\sin|\psi_r'|} \right\}$$

(B-5)

which we rewrite as

$$\Delta\gamma = 2\sqrt{2\Lambda/\pi}\,\sin|\psi_r|\int_0^\infty d\lambda\, e^{-\lambda^2\cos\,\psi_f'}\left\{\frac{1}{2\sinh\,\pi\lambda^2(\sin|\psi_r|)}\right.$$

$$\left[\cosh(\pi\lambda^2\,\sin|\psi_r|)\int_{-\pi}^{\pi} e^{-\lambda^2\sin|\psi_r|(\psi_f'-\psi)}\; e^{\lambda^2\cos\,\psi}\, d\psi\right]$$

$$\left. + \sinh(\pi\lambda^2\,\sin|\psi_r|)\left[\int_{-\pi}^{\psi_f'} - \int_{\psi_f'}^{\pi} d\psi\, e^{-\lambda^2\sin|\psi_r|(\psi_f'-\psi)}\; e^{\lambda^2\cos\,\psi}\right] - \frac{e^{\lambda^2\cos\,\psi_f'}}{\lambda^2\sin|\psi_r|}\right\}$$

(B-6)

This is of course a bit complicated. However we may perform the integral over ψ in the limit $\psi_f'^2, |\psi_r| \to 0$ to yield, after some manipulation,

$$\Delta\gamma = 2\sqrt{2\Lambda/\pi}\;|\psi_r|\int_0^\infty d\lambda\left[-\frac{1}{\lambda^2|\psi_r|} + \left\{I_o(\lambda^2)\; e^{-\lambda^2}\; e^{\frac{\lambda^2}{2}(\psi_f'-|\psi_r|)^2}\left[\pi[\coth\,\pi\lambda^2|\psi_r|-1]\right.\right.\right.$$

$$\left.\left.\left. + \sqrt{2\pi}\int_\beta^\infty e^{-x^2/2}\, dx\right]\right\}\right] \qquad \text{(B-7)}$$

where $\beta \equiv \lambda|\psi_f' - |\psi_r||$ and I_o is the usual Bessel function of imaginary argument. This is still too hard to do exactly. Splitting it into ranges we have for the integrand if

$$\frac{1}{|\psi_f' - |\psi_r||} > \lambda$$

$$-\frac{1}{\lambda^2 |\psi_r|} + \left[I_o(\lambda^2)\ e^{-\lambda^2} \left\{ 1 + \frac{\lambda^2}{2} (\psi_f' - |\psi_r|)^2 \right\} \left(\pi \coth \pi\lambda^2 |\psi_r| - \sqrt{2\pi}\ \lambda\ |\psi_f' - |\psi_r|| \right) \right]$$

and if $\lambda > \frac{1}{|\psi_f' - \psi_r||}$

$$I_o(\lambda^2)\ e^{-\lambda^2}\ e^{\frac{\lambda^2}{2}(\psi_f' - |\psi_r|)^2} \left[2\pi\ e^{-2\pi\lambda^2 |\psi_r|} - \frac{\sqrt{2\pi}\ e^{-\frac{\lambda^2}{2}(\psi_f' - |\psi_r|)^2}}{\lambda |\psi_f' - |\psi_r||} \right] - \frac{1}{\lambda^2 |\psi_r|} \tag{B-8}$$

The integrations may be done approximately to yield

$$\Delta\gamma = 2\sqrt{2\Lambda/\pi} \left[\int_0^\infty d\lambda\ \frac{[I_o(\lambda^2)\ e^{-\lambda^2} - 1]}{\lambda^2} + \frac{1}{2\sqrt{2\pi}} (\psi_f' - |\psi_r|)^2\ \ell n\ \frac{1}{\sqrt{\sin |\psi_r|}} \right.$$

$$\left. + |\psi_r| \sqrt{\frac{\pi}{2}}\ \ell n\ \frac{\sqrt{4\pi |\psi_r|}}{|\psi_f' - |\psi_r||} + \sqrt{\frac{\pi}{2}}\ |\psi_r|\, Ei\left(\frac{4\pi |\psi_r|}{(\psi_f' - |\psi_r|)^2} - 1 \right) \right] \tag{B-9}$$

with Ei(z) the exponential integral. We observe that

$$\int_0^\infty d\lambda\ \frac{e^{-\lambda^2} I_o(\lambda^2) - 1}{\lambda^2} = -2\sqrt{2/\pi}$$

Note that the result diverges unless $-\sqrt{4\pi|\psi_r|} < \psi_f' - |\psi_r| < 0$ which is the allowable range for turning. The derivation is correct only in the limit of very small $|\psi_r|$. The logarithmic terms are exact but errors of order $(\ell n|\psi_r|)^{-1}$ are to be expected. We have somewhat arbitrarily chosen them so that the leading term goes to zero for $\sin|\psi_r| = 1$.

Noting that the range of $\psi_f' - |\psi_r|$ is from $-\sqrt{4\pi|\psi_r|}$ to 0, we put $(\psi_f' - |\psi_r|) = -\sqrt{4\pi\psi_r}\,\chi$. Then as a rough approximation we have with $0 < \chi < 1$,

$$\Delta\gamma = \frac{8}{\pi}\sqrt{\Lambda}\left\{-1 + \frac{\pi\psi_r}{4}\left[\chi^2\,|\ell n\,\sin|\psi_r|| + |\ell n\,\chi| + \ell n\,|1-\chi|\right]\right\} \qquad \text{(B-10)}$$

and doing the averages over $2\chi d\chi$ we find the r.m.s. spread

$$\frac{\Delta\gamma_{rms}}{\bar{\Delta\gamma}} = \frac{\left[\overline{(\Delta\gamma)^2} - (\bar{\Delta\gamma})^2\right]^{1/2}}{\bar{\Delta\gamma}} = \frac{\pi}{4}\sin|\psi_r|\sqrt{\left(4 - \frac{\pi^2}{3}\right) + \frac{1}{3}\,|\ell n\,\sin|\psi_r|| + \frac{1}{12}\,|\ell n\,\sin|\psi_r||^2} \qquad \text{(B-11)}$$

Note that $\bar{\Delta\gamma} = -\frac{8}{\pi}\sqrt{\Lambda}$ is exactly what is obtained in the $|\psi_r| = 0$ limit by taking the phase space displacement at the bump as expected. The terms proportional to $|\ell n\,\chi|$ and $\ell n|1-\chi|$ in Eq. (B-10) arise of course from particles which just graze the top of the reflecting wells.

A further energy spread is to be expected from the fact that the bucket is of course not moved up from $-\infty$ to $+\infty$ but has a finite energy traverse $2\Delta\tilde{\gamma}$. Thus in Eq. (6.12) if we look at the end point contributions to $\Delta\gamma$ we see that we may expect a spread from the two end points

$$\Delta\gamma = \frac{\cos\psi \Lambda \sqrt{2}}{\Delta\tilde{\gamma}} .$$

Eliminating Λ by using Eq. (B-8) we find for the r.m.s. contribution to end-loss

$$\frac{\Delta\gamma_{rms}}{\overline{\Delta\gamma}} = \frac{\pi^2}{64} \frac{\overline{\Delta\gamma}}{\Delta\tilde{\gamma}} . \qquad \text{(B-12)}$$

The spreads (B-11) and (B-12) are presumably statistically independent so they should be added on in the r.m.s. sense. For small resonant angles we may approximate the slowly varying terms in Eq. (B-11) and combine it with Eq. (B-12) to give a simple formula for the ratio of spread to gain

$$\frac{\Delta\gamma_{rms}}{\overline{\Delta\gamma}} = \sqrt{\sin^2\psi_r + \frac{\pi^4}{(64)^2}\left(\frac{\overline{\Delta\gamma}}{\Delta\tilde{\gamma}}\right)^2} \qquad \text{(B-13)}$$

APPENDIX C

THE LIMITATION ON ELECTRON BEAM RADIUS IMPOSED BY EMITTANCE

All of the discussion in the main body of this paper has been carried out under the assumption, $P_\perp = 0$. Any real electron beam will, however, have a distribution of transverse velocities, so that at best one can only expect $P_\perp/P_z$ to be small. While we are not prepared to discuss the effects of this spread completely, there is one important effect which can be readily estimated and which provides a basis for estimating the magnitude of spread which can be tolerated. This effect is the spread in the axial velocity v_z which a spread in $P_\perp$ implies for a monoenergetic beam.

We assume an azimuthally symmetric beam. The phase area in x , $\frac{dx}{dz}$ which contains the beam is equal to that in y , $\frac{dy}{dz}$ and is denoted by $\pi\varepsilon$. The quantity ε is referred to as the beam emittance. We therefore take

$$P_\perp = \varepsilon \frac{P_z}{r_e} \tag{C-1}$$

as an appropriate measure of the variation in $P_\perp$ (r_e is the electron beam radius as in Section 4). We take

$$\gamma = \left[1 + \left(\frac{P_z}{mc}\right)^2 + \left(\frac{e}{} w - \frac{P_\perp}{mc}\right)^2\right] 1/2 \tag{C-2}$$

to be fixed, so that the deviation of P_z oscillates with the wiggler period. Since this period is short compared to the synchrotron period, it is appropriate to average. Hence we obtain (assuming $\beta_z \sim 1$)

$$\frac{\langle \delta P_z \rangle}{P_z} = \frac{\langle \delta \beta_z \rangle}{\beta} = 1/2 \left(\frac{P_\perp}{\gamma mc} \right)^2 . \tag{C-3}$$

We require

$$\langle \delta \beta_z \rangle < \frac{d\beta_z}{d\gamma} \cdot \delta\gamma_{max} = \frac{\mu^2}{\gamma^3} \delta\gamma_{max} \tag{C-4}$$

where $\delta\gamma_{max}$ is the bucket height defined by Equation (2.56). Combining these relations yields the inequality

$$r_e > \frac{\gamma}{\mu \sqrt{2 \frac{\delta\gamma_{max}}{\gamma}}} \varepsilon \tag{C-5}$$

For linear accelerators the following relation has some theoretical and considerable experimental support[24]

$$\varepsilon = \frac{K}{\gamma\beta} \bar{I}_e^{1/2} \tag{C-6}$$

where K is referred to as the emittance constant. $\bar{I}_e$ is the peak electron beam current averaged over a macropulse. Hence we obtain

$$r_e > \frac{\bar{I}_e^{1/2}}{\mu \sqrt{2 \frac{\delta\gamma_{max}}{\gamma}}} K . \tag{C-7}$$

All of the factors which appear in Equation (C-7) can be related to the "standard design" parameters discussed in Section 4. Thus using Equations (4.25) and (4.26) we obtain

$$r_e > 1/4 \left[\frac{\sqrt{2}\ \eta_b^{3/2}\ (2-\eta_b)^{5/2}\ \csc^{3/2}\psi_r}{\eta_e(1-\eta_b)\ (2-2\eta_b+\eta_b^2)\ \Gamma} \right]^{1/2}$$

$$\cdot \left(\frac{\bar{I}_e}{QI_e} \right)^{1/2} \left(\frac{mc^3}{e} \right)^{1/2} \cdot K \qquad \text{(C-8)}$$

which, for the numerical example following Eq.(4-26), takes the form

$$r_e > 1.28 \left(\frac{\bar{I}_e}{QI_e} \right)^{1/2} \left(\frac{mc^3}{e} \right)^{1/2} K \qquad \text{(C-9)}$$

Since I_e refers to the peak current in a micropulse, the factor $\bar{I}_e/I_e$ varies from 1/25 to 1/100, depending upon design. A typical "good" value for K is .3 cm - $(kA)^{-1/2}$. Assuming this value for K we see that the choice r_e = 1.24 mm used in the numerical examples satisfies C-9 for $\bar{I}_e/QI_e < 1/163$.

In the case of amplifiers, the peak current required is so large that it is probably necessary to use an induction accelerator instead of an RF linac. Then the factor $\bar{I}_e/I_e$ is simply unity. In addition Q is of course also unity. Actual numbers depend upon gain required and wiggler

profile design details, but for our example of Figure 4.8, we find $r_e > 5.6$ K cm . Reference to Equation (4.20) suggests that an order of magnitude reduction in K would greatly enhance the practicality of amplifier applications.

It should be mentioned that emittance also affects the beam transport problem[24]. Furthermore, to the extent that one depends upon the wiggler to provide focussing, there is a connection between emittance and the wiggler factor σ_w (Eq. 4.10a)[24,25]. These considerations have not been taken into account in deriving Eq. (C-8).

APPENDIX D

NEGLECT OF SPACE CHARGE FORCE

In this appendix we estimate the importance of space charge forces in the discussion of longitudinal motion. We do not consider transverse space charge effects.

The ponderamotive force on an electron has a z derivative given by

$$K_p = \frac{a_w a_s}{\gamma} m\omega_s^2 \cos\psi_r \tag{D-1}$$

at the bottom of the bucket. K_p may be thought of as the bucket spring constant. The negative spring constant arising from space charge forces at the bottom of the well is given (approximately) by

$$K_{sc} = 2\pi f_b e\rho_e = \frac{2f_b I_e e}{r_e^2 c} \tag{D-2}$$

where ρ_e is the electron beam charge density and f_b is the trapped fraction. Hence

$$\frac{K_{sc}}{K_p} = \frac{2f_b I_e \gamma e}{cm\omega_s^2 a_w a_s r_e^2 \cos\psi_r} \tag{D-3}$$

We consider space charge forces to be unimportant when this ratio is small.

From 2.40 and 2.41 in the standard model

$$a_s = \frac{\eta_b(2-\eta_b)}{2k_w L(1-\eta_b)\sin\psi_r} \tag{D-4}$$

From 4.24 and 4.11 (taking $\eta_e \approx f_b \eta_b$)

$$I_e = \frac{1}{2} \frac{mc^3}{e} \frac{\eta_b}{f_b} \frac{(2-\eta_b)^2}{(1-\eta_b)^2 \sin^2\psi_r Q\gamma_i} \tag{D-5}$$

and from 4.4 at $z = L$, where $\left(K_{sc}/K_p\right)$ is largest,

$$\frac{a_w}{\gamma} = \frac{1}{\gamma_i} \tag{D-6}$$

Combining the above relations in the standard model we obtain,

$$\frac{K_{sc}}{K_p} = \frac{9}{8Q\gamma_i^2} \frac{(2-2\eta_b+\eta_b^2)\ (2-\eta_b)}{(1-\eta_b)^3 \sin\psi_r \cos\psi_r} \tag{D-7}$$

For the values of γ_i which we have in mind, this is always a very small number. For the numerical example given after Eq. 4.26,

$$K_{sc} / K_p = 5.8 \times 10^{-4} / Q \ .$$

For the case of an amplifier the Q factor is of course missing. The space charge effect is relatively strongest at the input end because the ponderamotive force is weakest there. The numerical factors depend upon design details. For the amplifier of Figure 4-8 we find

$$\frac{K_{sc}}{K_p} \approx \frac{200}{\gamma_i^2} \qquad \text{(D-8)}$$

so that space charge effects can be significant for smaller values of γ_i .

APPENDIX E

THE OPTICAL KLYSTRON

In order to improve the efficiency of the constant parameter FEL in storage ring operation it is logical to think of bunching the electrons before sending them through the wiggler. One could speculate that by properly choosing the phase of the modulation, energy spread could be greatly reduced[14]. To study this we consider a system of two wiggler magnets (a velocity buncher and a radiator) separated by a long drift space (Fig. E.1).

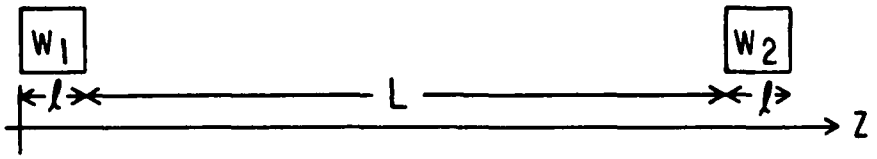

Fig. E.1 Schematic Representative of Optical Klystron Configuration

This is a special soluble case of a variable wiggler, where bunching becomes large. The electron motion is given by Eq. (2.44)

$$\frac{d\psi}{dz} = -A(z)\delta\gamma \qquad \text{(E-1)}$$

$$\frac{d\delta\gamma}{dz} = C(z) \sin \psi \ . \qquad \text{(E-2)}$$

Here A and C are defined in the main text. For our case, since $\ell \ll L$, we may take $A = 0$ for $z < \ell$, and $z > \ell + L$, and $A = \text{const}$ in the drift space. We take $C = C_1$ in the first magnet and $C = C_2$ in the second. Consider an electron with $\delta\gamma = \delta\gamma_o$, $\psi = \psi_o$ at $z = 0$. Then at $z = \ell$

$$\psi = \psi_o, \quad \delta\gamma = \delta\gamma_o + C_1 \ell \sin \psi_o$$

at $z = \ell + L$

$$\psi = \psi_o - A \left[\delta\gamma_o + C_1 \ell \sin \psi_o\right] L + \chi ,$$

where we have allowed for a phase shift χ in the second magnet and

$$\delta\gamma = \delta\gamma_o + C_1 \ell \sin \psi_o$$

and finally at $z = L + 2\ell$

$$\delta\gamma = \delta\gamma_o + C_1 \ell \sin \psi_o + C_2 \ell \sin\left[\psi_o + \chi - AL\left(\delta\gamma_o + C_1 \ell \sin \psi_o\right)\right]$$

$$= \delta\gamma_o + C_1 \ell \sin \psi_o + C_2 \ell \sum_{n=-\infty}^{\infty} J_n(AC_1 L \ell) \sin\left[\psi_o + \chi - AL\delta\gamma_o - n\psi_o\right], \tag{E-3}$$

with J_n being the n^{th} order Bessel function.

We may now average over initial phase ψ_o to obtain

$$\left\langle \delta\gamma - \delta\gamma_o \right\rangle = C_2 \ell J_1(AC_1 L\ell) \sin(\chi - AL\delta\gamma_o) \qquad \text{(E-4)}$$

and

$$\left\langle (\delta\gamma - \delta\gamma_o)^2 \right\rangle = \frac{1}{2} C_1^2 \ell^2 + \frac{1}{2} C_2^2 \ell^2 \left[1 - \cos 2(\chi - AL\delta\gamma_o) J_2(2AC_1 L\ell)\right]$$

$$+ C_1 C_2 \ell^2 \cos(\chi - AL\delta\gamma_o) \left\{ J_o(AC_1 L\ell) - J_2(AC_1 L\ell) \right\}$$

(E-5)

If we now minimize the ratio $\dfrac{\left\langle (\delta\gamma - \delta\gamma_o)^2 \right\rangle}{\left\langle \delta\gamma - \delta\gamma_o \right\rangle^2}$ with respect to C_2/C_1 holding other factors fixed we have:

$$\frac{\left\langle (\delta\gamma - \delta\gamma_o)^2 \right\rangle}{\left\langle (\delta\gamma - \delta\gamma_o) \right\rangle^2} = \frac{1}{2} \left[\frac{1 - \cos 2(\chi - AL\delta\gamma_o) J_2(2AC_1 L\ell) - \cos^2(\chi - AL\delta\gamma_o) \left[J_o - J_2\right]^2}{J_1^2 \sin^2(\chi - AL\delta\gamma_o)} \right]$$

$$= \frac{1}{2} \left[\frac{1 - J_2(2\beta) - \left(J_o(\beta) - J_2(\beta)\right)^2}{J_1^2(\beta) \sin^2(\chi - AL\delta\gamma_o)} + \frac{2J_2(2\beta) + \left(J_o(\beta) - J_2(\beta)\right)^2}{J_1^2(\beta)} \right]$$

with $\beta = AC_1 L\ell$

Since $1 - J_2(2\beta) - \left[J_o(\beta) - J_2(\beta)\right]^2 > 0$, the optimum value for the phase will be such that $\sin(\chi - AL\delta\gamma_o) = 1$, i.e. $C_1/C_2 = 0$. Hence, finally for the optimum energy $\delta\gamma_o$, the ratio of spread to gain is

given by:

$$\frac{\left\langle (\delta\gamma - \delta\gamma_o)^2 \right\rangle}{\left\langle (\delta\gamma - \delta\gamma_o) \right\rangle^2} = \frac{1}{2}\left[\frac{1 + J_2(2\beta)}{J_1^2(\beta)}\right]. \qquad \text{(E-6)}$$

The ratio is optimal for $\beta = 2.2$ where $\frac{\left\langle (\delta\gamma - \delta\gamma_o)^2 \right\rangle}{\left\langle (\delta\gamma - \delta\gamma_o) \right\rangle^2} = 2$. This, at first sight, may appear advantageous for finite β operation. However we may note that for small values of β the moments given by Eq. (E-4) obey the Madey theorem:

$$\left\langle (\delta\gamma - \delta\gamma_o) \right\rangle = \frac{1}{2}\frac{\partial}{\partial\gamma_o}\left\langle (\delta\gamma - \delta\gamma_o)^2 \right\rangle$$

while as β is increased the bandwidth $\sim \frac{1}{AL} \sim \frac{C_1 \ell}{\beta}$ also becomes very small. For storage ring operation the ratio, bandwidth x mean energy loss/(energy spread)^2, optimised with respect to C_2/C_1 for $\delta\gamma_o$ at the peak gain point $(\sin (x - A\ell\delta\gamma_o) = -1)$, is presumably more relevant. The optimised ratio is found to be $\approx J_1(\beta) / \beta$ so that low β operation is in fact preferable. Similarly, use of the Fokker-Planck equation to determine a steady state solution from Eqs. (A-4) and (A-5) shows that even for large β , the steady state is characterized by an emitted power which is a small fraction of synchrotron radiation (and a decreasing function of β). However, that is only an indicative result, not a conclusive one since for large β , the Fokker-Planck equation is not valid as higher derivatives $\frac{\partial n_f}{\partial \gamma_o^n}$ become important as the bandwidth becomes small. Pending a presumably numerical solution of the integral equation for the distribution function

in a storage ring at large β, we can only say that the outlook is not promising. In particular the result (E-6) shows that it is not possible, even for a δ-function input, to completely eliminate energy spread.

REFERENCES AND FOOTNOTES

1. J.M.J. Madey, H.A. Schwettman, and W.M. Fairbank, IEEE Trans. Nucl. Sci 20, p. 280, (1973).

2. R.M. Phillips, I.R.E. Trans. on Electron Devices, Vol. 7, p. 231, (1960).

3. L.R. Elias, W.M. Fairbank, J.M.J. Madey, H.A. Schwettman, and T.I. Smith, Phys. Rev. Lett. 36, 717, (1976); D.A.G. Deacon, L.R. Elias, J.M.J. Madey, G.J. Ramian, H.A. Schwettman, and T.I. Smith, Phys. Rev. Lett., 38, 892, (1977).

4. There is a great deal of literature on the equations of motion for electrons in the constant parameter FEL. For example, see Proceedings of Telluride Conf. and references therein. Physics of Quantum Electronics, Vol. 5, (Addision-Wesley, Reading, Mass., 1978).

5. The use of a Hamiltonian to describe the phase motion of the electrons in the constant parameter wiggler is described by A. Bambini and A. Renieri, Lett. Nuovo Cimento, 21, 399, (1978).

6. T.I. Smith, J.M.J. Madey, L.R. Elias, D.A.G. Deacon, "Reducing the Sensitivity of Free Electron Laser to Electron Energy," to be published in Appl. Phy. Lett. (1979).

7. D.A.G. Deacon, "Theory of the Isochronous Storage Ring Laser," Ph.D. thesis, Stanford University (Stanford, CA), June 1979.

8. K.R. Symon and A.M. Sessler; CERN Symposium 1956, 1, pp 44-58.

9. A somewhat different type of analysis has been used by J.G. Meeker, J.E. Rowe I.R.E. Trans on Electron Devices Vol., 257 (1962) in tapering the RF circuit velocity for traveling-wave amplifiers.

10. The possibility of decelerating trapped electrons was discussed by R.B. Palmer in J. Appl. Phys. Vol. 43, 7, (1972); however, it was not appreciated that a change in the radiation field, by itself, is insufficient to decrease the resonant energy of the electrons.

11. D.A. Swenson; Int. Conf. of High Energy Acc., 1961 (BNL), p 187.

12. J.M.J. Madey, Nuovo Cimento, 50B, 64, (1979).

13. N.A. Vinokurov and A.N. Skrinskii, "Oscillator Klystron in the Optical Band using Relativistic Electrons", Institute of Nuclear Physics Preprint 77-59, Novosibirsk, 1977.

14. P. Meystre, G.T. Moore, M.O. Scully, and F.A. Hopf, Optics Comm., 29, 87-90, (1979).

15. The field produced by the higher harmonics is small because the higher harmonics are not phase matched. That is to say their phase velocity differs from c by too large an amount. The current will in general contain Fourier components of the general form

$$A_{ns}(z)\begin{matrix}\cos\\ \sin\end{matrix}(n\psi \mp \int k_w dz), \text{ for which } (\omega/c - k)_n = (n \mp 1)k_w - n\delta k_s .$$

Thus, a single term (n-1, with n = 1) dominates so long as $\delta k_s << k_w$.

16. More explicitly one might take for an adiabaticity condition $|\gamma_r'| << (2\pi/Z)\ \delta\gamma_{max}$, or, using Eqs. (2.50, 2.51 & 2.40), we find

$$|\gamma_r'| << 2\frac{\omega_s a_s a_w}{c\gamma_r}\sqrt{\cos^2\psi_r - (\frac{\pi}{2}\,\mathrm{sgn}\psi_r - \psi_r)\cos\psi_r\,\sin\psi_r}$$

This is seen to be consistent with Eq. (2.41) for sufficiently small ψ_r . Numerical simulation to be described later suggests that for smoothly varying wigglers with approximately constant ψ_r that Eq. (2.41) is, in fact, sufficient for adiabatic behavior.

17. A. Renieri, "The Free Electron Laser: The Storage Ring Operation", Report 77.33, CNEN - Centro di Frascati, Edizioni Scientifiche C.P. 65, 00044, Frascati, Rome, Italy (1977).

18. D.A.G. Deacon, and J.M.J. Madey, Applied Physics, 19, 295, (1979).

19. L.R. Elias, J.M.J. Madey, and T.I. Smith, "One Dimensional Monte Carlo Analysis of a Free Electron Laser in a Storage Ring", Stanford High Energy Physics Laboratory Report HEPL 824 (1978), Submitted to Applied Physics.

20. In comparing different wiggler profiles in the context of the above discussion, it is the maximum value of k_w which should be the same for the configurations being compared. For the three cases being considered here this occurs at $z = L$.

21. This was first pointed out by S. Mani (private communication).

22. A. Yariv and C. Shih, Optics Comm., 24, 233, (1978).

23. C.A. Brau, "Small Signal Gain of Free Electron Lasers with Nonuniform Wigglers," IEEE J. Quant. Electron. (in press).

24. V.K. Neil, Emittance and Transport of Electron Beams in a Free Electron Laser, SRI Technical Report JSR-79-10, SRI International, (1979).

25. J. Slater, private communication.

DISTRIBUTION LIST

ORGANIZATION	NO. OF COPIES
Dr. Tony Armstrong SAI, Inc. P.O. Box 2351 La Jolla, CA 92038	1
Dr. Robert Behringer ONR 1030 E. Green Pasadena, CA 91106	1
Dr. Arden Bement Deputy Under Secretary of Defense for R&AT Room 3E114, The Pentagon Washington, D.C. 20301	2
Maj. Rettig P. Benedict, USAF DARPA/STO 1400 Wilson Boulevard Arlington, VA 22209	1
Dr. Michael Berry Photon Chemistry Department Allied Chemical Corporation Morristown, NJ 07960	1
Dr. Charles Brau Applied Photochemistry Division Los Alamos Scientific Laboratory P.O. Box 1663, M.S. - 817 Los Alamos, NM 87545	1
Dr. Fred Burskirk Physics Department Naval Postgraduate School Monterey, CA 93940	1
Dr. Gregory Canavan Director, Office of Inertial Fusion, U.S. DOE M.S. C404 Washington, D.C. 20545	1
Dr. C. D. Cantrell T-DOT, MS210 Los Alamos Scientific Lab Los Alamos, NM 87545	1
Dr. Maria Caponi TRW, Building R-1, Room 1070 One Space Park Redondo Beach, CA 90278	1
Dr. Weng Chow Optical Sciences Center University of Arizona Tucson, AZ 85721	1
Dr. Leslie Cohen Code 6650 Naval Research Lab Washington, D.C. 20395	1
Dr. Peter Clark TRW, Building R-1, Room 1096 One Space Park Redondo Beach, CA 90278	1
Dr. Robert Clark P.O. Box 1925 Washington, D.C. 20013	1
Dr. William Colson Rice University P.O. Box 1892 Space Physics Houston, TX 77001	1
Dr. William Colson Physics Department Stanford University Stanford, CA 94305	1
Dr. Richard Cooper Los Alamos Scientific Laboratory P.O. Box 1663 Los Alamos, NM 87545	1
Cmdr. Robert Cronin NFOIO Detachment, Suitland 4301 Suitland Road Washington, D.C. 20390	1
Dr. John Dawson Physics Department University of California Los Angeles, CA 90024	1

ORGANIZATION	NO. OF COPIES
Dr. David Deacon Physics Department Stanford University Stanford, CA 94305	1
Defense Documentation Center Cameron Station Alexandria, VA 22314	12
Dr. Francesco De Martini Instituto de Fiscia "G. Marconi" Univ. Piazzo delle Science, 5 ROMA00185 ITALY	1
Dr. Luis R. Elias Quantum Institute University of California Santa Barbara, CA 93106	1
Dr. David D. Elliott SRI International 333 Ravenswood Avenue Menlo Park, CA 94025	1
Dr. Norval Fortson Department of Physics University of Washington Seattle, WA 98195	1
Director National Security Agency Fort Meade, MD 20755 ATTN: Mr. Richard Foss, A42	2
Dr. Robert Fossum, Director DARPA 1400 Wilson Boulevard Arlington, VA 22209	2
Dr. Edward A. Frieman Director, Office of Energy Research, U.S.DOE M.S. 6E084 Washington, D.C. 20585	1
Dr. George Gamota OUSDRE (R&AT) Room 3D1067, The Pentagon Washington, D.C. 20301	3
Dr. Richard L. Garwin IBM, TJWatson Research Center P.O. Box 218 Yorktown Heights, NY 10598	1
Dr. Edward T. Gerry, President W.J. Schafer Associates, Inc. 1901 N. Fort Myer Drive Arlington, VA 22209	1
Dr. Avraham Gover Tel Aviv University Fac. of Engineering Tel Aviv, ISRAEL	1
Mr. Donald L. Haas, Director DARPA/STO 1400 Wilson Boulevard Arlington, VA 22209	1
Dr. P. Hammerling La Jolla Institute P.O. Box 1434 La Jolla, 1CA 92038	1
Director National Security Agency Fort Meade, MD 20755 ATTN: Mr. Thomas Handel, A243	1
Dr. William Happer 560 Riverside Drive New York City, NY 10027	1
Dr. Robert J. Hermann Assistant Secretary of the Air Force (RD&L) Room 4E856, The Pentagon Washington, D.C. 20330	1
Dr. Rod Hiddleston KMS Fusion Ann Arbor, MI 48106	1
Dr. R. Hofland Aerospace Corp. P.O. Box 92957 Los Angeles, CA 90009	1

ORGANIZATION	NO. OF COPIES
Dr. Fred Hopf University of Arizona Tucson, AZ 85721	1
Dr. Benjamin Huberman Associate Director, OSTP Room 476, Old Executive Office Bldg. Washington, D.C. 20506	1
Dr. S. F. Jacobs Optical Sciences Center University of Arizona Tucson, AZ 85721	1
Mr. Eugene Kopf Principal Deputy Assistant Secretary of the Air Force (RD&L) Room 4E964, The Pentagon Washington,D.C. 20330	1
Dr. Tom Kuper Optical Sciences Center University of Arizona Tuscon, AZ 85721	1
Dr. Thomas Kwan Los Alamos Scientific Lab MS608 Los Alamos, NM 87545	1
Dr. Willis Lamb Optical Sciences Center University of Arizona Tucson, AZ 85721	1
Mr. Mike Lavan BMDATC-O ATTN: ATC-O P.O. Box 1500 Huntsville, ALA 35807	1
Dr. John D. Lawson Rutherford High Energy Lab Chilton Didcot, Oxon OX11 OOX ENGLAND	1
Mr. Ray Leadabrand SRI International 333 Ravenswood Avenue Menlo Park, CA 94025	1
Mr. Barry Leven NISC/Code 20 4301 Suitland Road Washington, D.C. 20390	1
Dr. Donald M. LeVine SRI International 1611 N. Kent Street Arlington, VA 22209	3
Dr. A. Lewis Licht Department of Physics U. of Chicago, Circle Campus Box 4348 Chicago, IL 60680	1
Dr. Anthony T. Lin University of California Los Angeles, CA 90024	1
Dr. B.A. Lippmann Physics International San Leandro, CA 94577	1
Director National Security Agency Fort Meade, MD 20755 ATTN: Mr. Robert Madden, R/SA	2
Dr. John Madey Physics Department Stanford University Stanford, CA 94305	1
Dr. Joseph Mangano ARPA 1400 Wilson Boulevard Arlington, VA 22209	1
Dr. S. A. Mani W.J. Schafer Associates, Inc. 10 Lakeside Office Park Wakefield, MA 01880	1

ORGANIZATION	NO. OF COPIES
Dr. Mike Mann Hughes Aircraft Co. Laser Systems Div. Culver City, CA	1
Dr. T. C. Marshall Applied Physics Department Columbia Univerisity New York, NY 10027	1
Mr. John Meson DARPA 1400 Wilson Boulevard Arlington, VA 22209	1
Dr. Pierre Meystre Projektgruppe fur Laserfor-schung Max Planck Gesellschaft Garching, MUNICH AUSTRIA	1
Dr. Gerald T. Moore Optical Sciences Center University of Arizona Tucson, AZ 85721	1
Dr. Philip Morton Stanford Linear Accelerator Center P.O. Box 4349 Stanford, CA 94305	1
Dr. Jesper Munch TRW Space Park Redondo Beach, CA 90278	1
Dr. George Neil TRW One Space Park Redondo Beach, CA 90278	1
Dr. Kelvin Neil Lawrence Livermore Laboratory Code L-321, P.O. Box 808 Livermore, CA 94550	1
Dr. Brian Newnam, MS 564 Los Alamos Scientific Lab P.O. Box 1663 Los Alamos, NM 87545	1
Dr. Richard H. Pantell Stanford University Stanford, CA 94305	1
Dr. Claudio Parazzoli Hughes Aircraft Company Building 6, MS/C-129 Centinela & Teale Streets Culver City, CA 90230	1
Dr. Robert K. Parker Naval Research Lab Code 6742 Washington, D.C. 20375	1
Dr. Richard M. Patrick AVCO Everett Research Lab, Inc. 2385 Revere Beach Parkway Everett, MA 02149	1
Dr. Claudio Pellegrini Brookhaven National Laboratory Associated Universities, Inc. Upton, L.I., New York 11973	1
The Honorable William Perry Under Secretary of Defense (R&E) Office of the Secretary of Defense Room 3E1006, The Pentagon Washington, D.C. 20301	1
Dr. Alan Pike DARPA/STO 1400 Wilson Boulevard Arlington, VA 22209	1
Dr. Hersch Pilloff Code 421 Office of Naval Research Arlington, VA 22217	1

ORGANIZATION	NO. OF COPIES
Dr. Charles Planner Rutherford High Energy Lab Chilton Didcot, Oxon, OX11 OOX, ENGLAND	1
Dr. Michal Poole Daresbury Nuclear Physics Lab Daresbury, Warrington Cheshire WA4 4AD ENGLAND	1
Dr. Don Prosnitz Lawrence Livermore Lab Livermore, CA	1
Dr. D. A. Reilly Avco Everett Research Lab Everett, MA	1
Dr. James P. Reilly W.J. Schafer Associates, Inc. 10 Lakeside Office Park Wakefield, MA 01880	1
Dr. A. Renieri C.N.E.N. Div. Nuove Attivita Dentro di Frascatti Frascatti, Rome ITALY	1
Dr. Daniel N. Rogovin SAI P.O. Box 2351 La Jolla, CA 92038	1
Dr. Michael Rosenbluh MIT - Magnet Lab Cambridge, MA 02139	1
Dr. Marshall N. Rosenbluth Institute for Advanced Study Princeton, NJ 08540	1
Dr. Eugene Ruane P.O. Box 1925 Washington, D.C. 20013	2
Dr. Antonio Sanchez MIT/Lincoln Laboratory Room B231 P.O. Box 73 Lexington, MA 02173	1
Dr. L.A. Lewis Licht Department of Physics U. of Illinois, Chicago Circle Box 4348 Chicago, IL 60680	1
Dr. Howard Schlossberg AFOSR Bolling AFB Washington, D.C. 20332	1
Dr. Stanley Schneider Rotodyne Corporation 26628 Fond Du Lac Road Palos Verdes Peninsula, CA	1
Dr. Marlan O. Scully Optical Science Center University of Arizona Tucson, Arizona 85721	1
Dr. Nat Seeman Code 6656 Naval Research Lab Washington, D.C. 20375	1
Dr. Steven Segel KMS Fusion 3621 S. State Street P.O. Box 1567 Ann Arbor, MI 48106	1
Dr. Robert Sepucha DARPA/STO 1400 Wilson Boulevard Arlington, VA 22209	1
Dr. A. M. Sessler Lawrence Berkeley Laboratory University of California 1 Cyclotron Road Berkeley, CA 94720	1

ORGANIZATION	NO. OF COPIES
Dr. Earl D. Shaw Bell Labs 600 Mountain Avenue Murray Hill, NJ 07974	1
Dr. Chan-Ching Shih Physics Department, Code 116-81 California Institute of Technology Pasadena, CA 91125	1
Dr. Jack Slater Mathematical Sciences, NW P. O. Box 1887 Bellevue, WA 98009	1
Dr. Kenneth Smith Physical Dynamics, Inc. P.O. Box 556 La Jolla, CA 92038	1
Mr. Todd Smith Hansen Labs Stanford University Stanford, CA 94305	1
Dr. Joel A. Snow Senior Technical Advisor Office of Energy Research, U.S. DOE, M.S. E084 Washington, D.C. 20585	1
Dr. Richard Spitzer Stanford Linear Accelerator Center P.O. Box 4347 Stanford, CA 94305	1
Dr. Philip Sprangle Plasma Physics Division Naval Research Laboratory Washington, D.C. 20375	1
Mrs. Alma Spring DARPA/Administration 1400 Wilson Boulevard Arlington, VA 22209	1

ORGANIZATION	NO. OF COPIES
SRI/MP Reports Area G037 333 Ravenswood Avenue Menlo Park, CA 94025 ATTN: D. Leitner	2
Dr. Abraham Szoke Lawrence Livermore Laboratoroy MS/L-470, P.O. Box 808 Livermore, CA 94550	1
Dr. Cha-Mei Tang Naval Research Lab Code 6740 Plasma Physics Division Washington, D.C.	1
Dr. Milan Tekula Avco Everett Research Lab 2385 Revere Beach Parkway Everett, MA	1
Dr. John E. Walsh Department of Physics Dartmouth College Hanover, NH 03755	1
Ms. Bettie Wilcox Lawrence Livermore Laboratory ATTN: Tech. Info. Dep't. L-3 P. O. Box 808 Livermore, CA 94550	1
Dr. A. Yariv California Institute of Tech. Pasadena, CA 91125	1
Dr. W. W. Zachary Code 66035 Naval Research Lab Washington, D.C. 20375	1